

LA--981

Copy 3 of [REDACTED]

C.3

CIC-14 REPORT COLLECTION
REPRODUCTION
COPY

LOS ALAMOS SCIENTIFIC LABORATORY

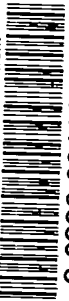
OF THE

UNIVERSITY OF CALIFORNIA

CONTRACT W-7405-ENG. 36 WITH

U. S. ATOMIC ENERGY COMMISSION

LOS ALAMOS NATIONAL LABORATORY



3 9338 00414 6493

CIC-14 REPORT COLLECTION
**REPRODUCTION
COPY**

LA-981



November 15, 1949

This document contains 152 pages

DIFFERENTIAL CROSS SECTION OF THE REACTION
 $\text{He}^3(d,p)\text{He}^4$ AT 10.2 MEV BOMBARDING ENERGY
AND SEARCH FOR EXCITED STATE IN He^4

by

J. C. Allred



Physics General



TABLE OF CONTENTS

CHAPTER	PAGE
I. INTRODUCTION	1
II. THE CROSS SECTION FORMULA	7
III. PHOTOGRAPHIC TECHNIQUE	16
IV. GAS HANDLING	37
V. GAS TARGETS	46
VI. EXPERIMENTAL PROCEDURE	56
VII. DIFFERENTIAL CROSS SECTION OF THE REACTION $\text{He}^3(d,p)\text{He}^4$	98
VIII. RESULTS OF SEARCH FOR EXCITED STATE IN He^4 . . .	113
 APPENDICES	
I. COLLISION MECHANICS OF NUCLEAR REACTIONS	121
II. DERIVATION OF CRITCHFIELD FORMULA	134
III. CORRECTION FOR SLIT PENETRATION	139
IV. FABRICATION OF MULTIPLATE CAMERA	144
 BIBLIOGRAPHY	149
 VITA	151

CHAPTER I
INTRODUCTION

Many aspects of an investigation of the reaction $\text{He}^3(d,p)\text{He}^4$ are of interest in nuclear physics. One of these is the fact that until very recently He^3 and tritium were not available in sufficient quantity to permit the observation of a bombardment of these gases in a gas target. A second is that the reaction involves a small number of nucleons, and such reactions are always of interest to theoretical physicists. A third point of interest is the extremely high Q of this reaction, and it is this high (18.4 Mev) Q which makes it possible to search for excited levels of high energy in the He^4 nucleus which may result from the above interaction.

A determination of the energy variation of the total cross section of the reaction $D(\text{He}^3, \text{He}^4)\text{H}^1$ was reported by the Purdue cyclotron group in 1943.¹ In this work air reduction He was introduced at the arc source of the cyclotron, which was tuned to accelerate He^3 . The target was deuterium gas. A determination of the total cross section was made using an ionization technique which detected the

1

C. P. Baker, M. G. Holloway, L. D. P. King, and R. E. Schreiber, LAMS-2, June, 1943.

He^4 particles. The value reported for the total cross section in the energy region 0.3 Mev to 1.0 Mev is of the order of 0.5 barns, the maximum cross section of 0.8 barns occurring at a bombarding energy of 0.65 Mev.

Subsequently the authors discovered an error in the geometry of their apparatus which gave a slightly larger value for the cross section at lower energies; however, the cross section at this energy remains substantially of the order of one barn. The only other measurement which has been reported on this reaction is a recent one by Hatton and Preston,² who bombarded a heavy ice target using He gas enriched in He^3 to 4×10^{-3} by a thermal diffusion process. These investigators observed the long range protons from the reaction $\text{He}^3(d,p)\text{He}^4$ at bombarding energies of the order of 100 KV, using a Cockcroft-Walton accelerator. The total cross section at 160 Kev bombarding energy is given as one tenth of that for the D-D reaction at the same energy. They reported no low energy protons which might indicate an excited state in He^4 . However, the energy available to excite the He^4 nucleus in their experiment is essentially that due to the Q of the reaction. Their investigation was thus limited to a lower energy region for the excited state in He^4 than the one proposed here.

²

J. Hatton and G. Preston, Nature, 164, 143 (July 23, 1949)

The possible existence of at least one excited level of the compound He^4 nucleus was demonstrated on theoretical grounds as early as 1936.³ Previously, Crane, Delsasso, Fowler, and Lauritsen had suggested four energy levels for the He^4 nucleus, based on their observations of the gamma-radiation from the reactions:



Bethe and Bacher⁶ have evaluated the literature to 1936 and have calculated the probable existence of three excited states, a 1P state, 16 Mev, and two 3P states, the energy of

³
E. Feenberg, Phys. Rev. 49, 328 (1936).

⁴
Crane, Delsasso, Fowler, and Lauritsen, Phys. Rev. 48, 100 (1935).

⁵
Crane, Delsasso, Fowler, and Lauritsen, Phys. Rev. 48, 125 (1935).

⁶
H. A. Bethe and R. F. Bacher, Rev. Mod. Phys. 8, 147 (1936).

the lower being about 10 Mev. More recently, Goldstein⁷ has shown in a theoretical paper that there should be a 1S state of the compound He^4 excited nucleus having an excitation energy of about 20.5 Mev.

This figure is based partially on the value of the cross section of the $He^3(n,p)H^3$ reaction obtained by Coon and Nobles.⁸ Their results show $\sigma = 5040 \pm 200 \times 10^{-24} \text{ cm}^2$ for thermal neutrons. From the above results it appears that there may exist a resonance for this reaction for a negative neutron energy. That is, although this cross section follows the $1/v$ law,⁹ the coefficient is so large as to indicate the proximity of a resonance. Since the energy difference between the nuclear masses $He^3 + n^1$ and He^4 is 20.55 Mev, it is likely that if this negative energy resonance exists, it is due to the formation of the excited He^4 nucleus. In any case, this mass difference sets an approximate upper limit for the energy of an excited state. The excitation energy required to cause the total disintegration of the He^4 nucleus is 28.2 Mev.

7

L. Goldstein, Declassified Los Alamos Report LADC-539, Dec. 1947.

8

J. H. Coon and R. A. Nobles, Phys. Rev. 75, 1358 (1949).

9

L. D. P. King and L. Goldstein, Phys. Rev. 75, 1366 (1949).

It has been pointed out by Goldstein⁷ that the above reasoning concerning the proximity of a resonance is strengthened by the experimental evidence of other kindred reactions. These are:

<u>Reaction</u>	<u>σ barns</u>
$\text{Li}^6 (n, \text{He}^4) \text{H}^3$	900
$\text{B}^{10} (n, \text{He}^4) \text{Li}^7$	3000

In both of these reactions the cross section is very large for thermal neutrons and both obey the $1/v$ law in this region. Further, for both reactions there exist well established excited states for the compound nuclei. Hence, it is not unreasonable to deduce from this evidence that there may exist a resonance in the He^4 nucleus.

It can therefore be seen that although the existence of excited states in the He^4 nucleus has not been definitely established, there seems to be general agreement as to the probable existence of such an excited state or states in the neighborhood of 15 to 20 Mev. The reaction $\text{He}^3(d,p)\text{He}^4$ offers an obvious and direct method for investigating the existence of such excited states in the energy region of interest.

If such an excited state exists, and if selection rules permit the reaction to go in such a manner as to leave an excited He^4 nucleus as one of the reaction products, there should appear in addition to the main group of high energy

protons a proton group of much lower energy. A search for this group of low energy protons can thus serve either to establish the existence of an excited state in the compound He^4 nucleus or to set an upper limit for the possible energy of this excited state, as determined by the lower limit of energy of the lowest energy group of protons which can be detected.

Thus, the purpose of this experiment was to determine the differential cross section of the reaction $\text{He}^3(d,p)\text{He}^4$ and to investigate the possibility of the existence of an excited state in the He^4 nucleus by the method outlined above.

CHAPTER II

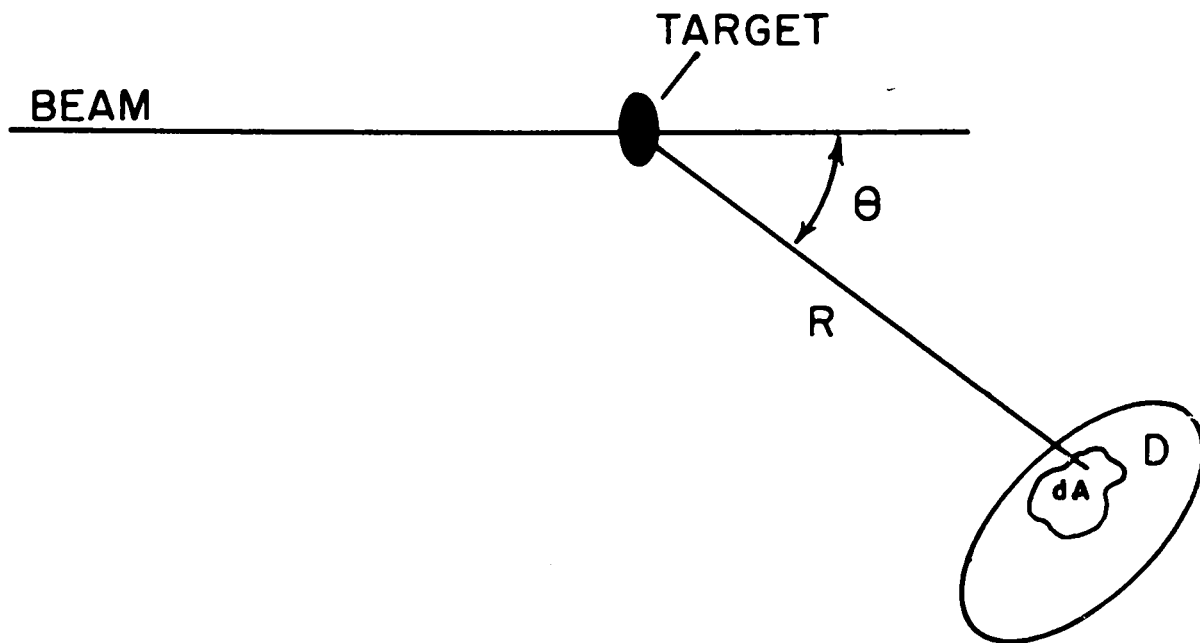
THE CROSS SECTION FORMULA

Of the measurements which may be made on a nuclear scattering or reaction experiment, one of the most fundamental is a measurement of the angular distribution of the reaction particles. In order to describe this angular distribution in terms of absolute quantities, it is convenient to introduce a quantity called the differential cross section per unit solid angle, often abbreviated to differential cross section. Fundamentally, the term cross section refers to the effective geometrical cross section which a target nucleus presents to a bombarding beam for the occurrence of a given process. The dimension of cross section is area, customarily expressed in barns. (1 barn = 10^{-24} cm²).

Before defining the term differential cross section per unit solid angle let us first consider the meaning of the term total cross section for a given nuclear process. Suppose we have a beam of particles of particle density N particles/cm³ moving with a velocity v cm/sec. Let this beam of particles be incident on a target, say a foil, containing n_1 particles/cm². Then the total number of reactions occurring per unit time for the reaction under consideration will be given by $Y = Nvn_1\sigma$ where σ represents the total cross section for the process involved and Y is the number of reaction particles produced per second by the particular process. It should be noted that

Nv represents the flux of the beam particles at the target. Here σ is the total cross section per atom and $n_1 \sigma$ represents the fraction of incident flux which will produce the reaction as the beam strikes the target. That is, the number of reactions produced per unit time is proportional to the flux by the quantity $n_1 \sigma$. If then one wishes to measure the total cross section for a certain nuclear process, the quantities which must be determined are the total flux on the target, the number of scattering centers per unit area, and the total number of reaction particles produced. It is customary to consider the integrated flux and the integrated yield rather than the flux per unit time or the yield per unit time. Thus, we may understand by Y the total number of reaction particles produced and alternatively by N the total number of particles which strike the target during the time of observation.

In the measurement of a differential cross section per unit solid angle one observes a reaction at a given angle to the beam, say θ (see Figure 1). Here one observes with a detector D the number of reaction particles produced at the point of bombardment which leave the target at an angle θ with the beam and pass through the solid angle subtended by the detector at the source. Differentiating the equation $Y = Nn_1 \sigma$ with respect to the solid angle Ω one obtains



GENERALIZED TARGET-DETECTOR GEOMETRY

FIG. 1

$$\frac{dY}{d\Omega} = Nn_1 \frac{d\sigma}{d\Omega}$$

In order, then, to determine the differential cross section per unit solid angle for a reaction one must measure the element of yield dY which passes through the solid angle $d\Omega$ subtended by the detector at the reaction center. For the situation illustrated this solid angle is dA/R^2 and the equation becomes

$$dY = Nn_1 \frac{d\sigma}{d\Omega} \frac{dA}{R^2}$$

In the case of bombardment of a gas target the situation is only slightly different. Let us assume, as is the case for most scattering experiments, that the incident beam is diaphragmed in such a manner that it is a circular cylinder passing through a length of target gas l , the radius of this circular cylinder being small compared to the distance from the reaction volume to the detector. The element of yield observed at the angle θ then is given by the equation

$$dY = Nn_0 l \sigma(\theta) d\Omega$$

where $\sigma(\theta)$ is the differential cross section per unit solid

angle at the angle of observation θ , N is the total number of particles passing through the reaction volume, n_0 is the number of particles per unit volume of the gas being bombarded, ℓ is the length of the reaction volume, and $d\Omega$ is the angle subtended by the detector at the reaction center. This treatment amounts to considering the reaction volume as a line source of reaction particles. Thus, the number of particles per unit area is $n_0 \ell$ and the equation is exactly analagous to the one above describing a reaction in which the target is a foil.

In the geometry of this experiment the error introduced by such a simplification is negligible. To show this let us consider a circular beam of radius K as the source of reaction particles, and let the distance from the detector to the center of the beam be R . Then the average solid angle subtended by the detector from the extreme far edge to the extreme near edge of the beam is

$$\bar{\Omega} = \frac{\int_{R - \frac{K}{\sin\theta}}^{R + \frac{K}{\sin\theta}} \frac{A dr}{r^2}}{\int_{R - \frac{K}{\sin\theta}}^{R + \frac{K}{\sin\theta}} dr}$$

$$\bar{\Omega} = \frac{A}{R^2 \left(1 - \frac{K^2}{R^2 \sin^2 \theta} \right)}$$

If we compute the solid angle using R as the effective distance from the beam to the detector we have

$$\Omega = \frac{A}{R^2}$$

and

$$\frac{\Omega}{\Omega} = 1 - \frac{K^2}{R^2 \sin^2 \theta}$$

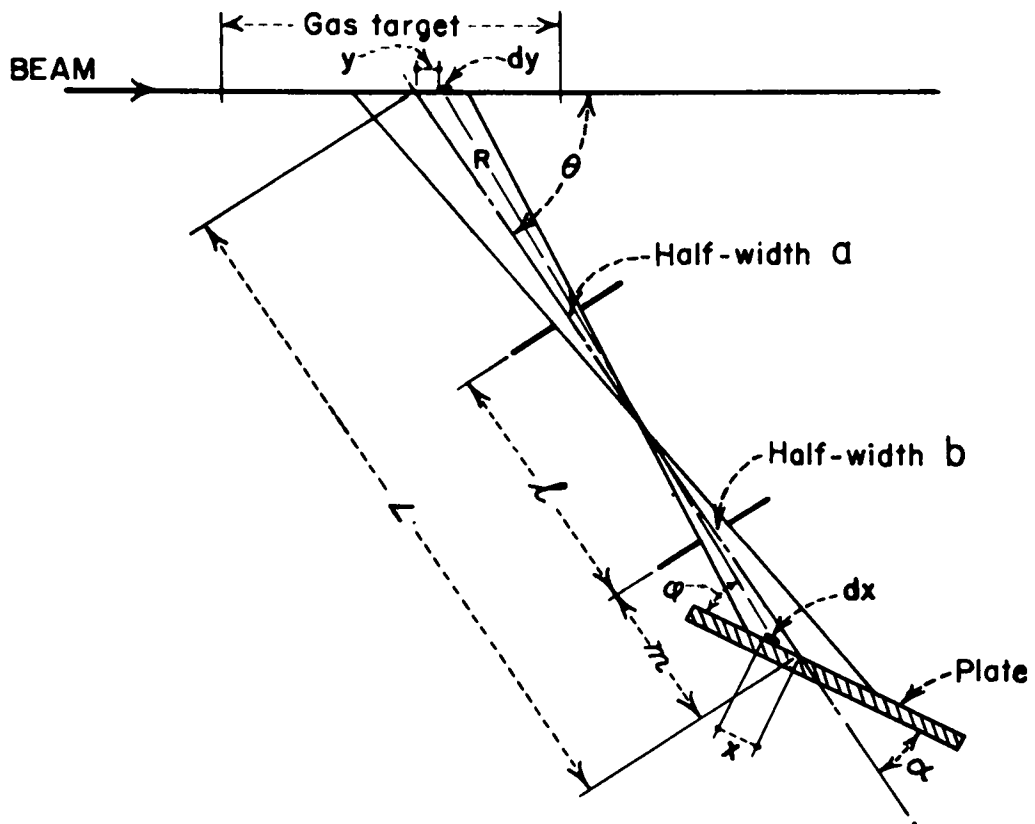
Then if $\frac{K}{R \sin \theta} = 0.1$, the correction is only 1 per cent.

Actually, for this experiment, the maximum value of

$$\frac{K}{R \sin \theta} = 0.04 \text{ and } \frac{K^2}{R^2 \sin^2 \theta} = 1.6 \times 10^{-3}, \text{ a negligible}$$

correction, especially when we note that the correction here is exaggerated due to the fact that the variation in R is greatest across the axis of the beam. That is, this approximation assumes that the beam is rectangular whereas it is actually circular, and the variation in R is smaller than that indicated by the above calculation.

If now we place collimating slits between the reaction volume and the detector (see Figure 2) it becomes apparent that each element of the reaction volume is not equally effective in producing counts at the detector. Let the detector be, as shown, a photographic plate, inclined at an angle α to the line joining the center of the plate and the center of the reaction volume. Let R be the path of a reaction particle which produces a track on the



SLIT SYSTEM GEOMETRY

FIG. 2

photographic plate, y the distance from the reaction center to the point of origin of the particle, and x the distance from the center of the plate to the point at which the reaction particle strikes the plate. Then let ϕ be the angle between R and the photographic plate. If one counts the number of tracks appearing in a swath of width w and length dx on the plate it can be seen that the effective element of area of the detector is $w dx \sin \phi$ and that the element of solid angle which the detector subtends at the point y is $w dx \sin \phi / R^2$. dy is the length which is effective in producing tracks on the plate in the area $w dx$. It is clear that the number of particles/cm² in the element of reaction volume is given by $n_0 dy$. Thus, the second differential element of yield d^2Y is given by

$$\begin{aligned} d^2Y &= N \sigma(\theta) n_0 dy d\Omega \\ &= N \sigma(\theta) n_0 dy \frac{w dx \sin \phi}{R^2} \end{aligned}$$

The yield, then, is given by

$$Y = N \sigma(0) n_0 \iint dy \frac{w dx \sin \phi}{R^2}$$

and for this particular geometry it becomes necessary to compute the quantity I given by

$$I = \iint \frac{w \, dx \, dy \, \sin \phi}{R^2}$$

Dr. C. L. Critchfield, Professor of Physics at the University of Minnesota and consultant to the Los Alamos Scientific Laboratory, has developed an elegant evaluation for the quantity I. This evaluation is given in Appendix II. The result is

$$I = \frac{4abw}{Ll \sin \theta} \left(1 - \frac{d^2 + b^2}{2l^2} - \frac{Pd^2 + Qb^2}{3l^2} \cot \alpha + \frac{P^2 d^2 + Q^2 b^2}{3l^2} \right)$$

$$P = \frac{m(\cot \alpha - \cot \theta)}{L}$$

$$Q = \frac{(m+l)(\cot \alpha - \cot \theta)}{L}$$

and the geometrical dimensions are as shown in Figure 2. Hence in order to measure a differential cross section one must determine the number of tracks appearing on a photographic plate in a swath of width w, the total number of particles in the incident beam which pass through the target volume, the number of particles of the target gas per unit volume, and the factor I from the dimensions of the experimental geometry.

CHAPTER III
PHOTOGRAPHIC TECHNIQUE

The use of photographic plates for the detection of charged particles as a tool in nuclear physics is possibly as old as any of the present systems of particle detection. Discovered in 1896 by Becquerel, developed to some extent early in this century, the possibilities of the effect of ionizing particles on photographic emulsions have nonetheless not been widely recognized as a useful research technique until comparatively recently.

That this is true is certainly not due to a lack of effort on the part of early workers in the photographic technique. Rather, the limitation of the development of the technique has been due to a lack of suitable nuclear emulsions. It has been, in fact, only very recently that a wide range of types of nuclear emulsions has become available for use in the various types of experiments which may be done with photographic plates.

The first quantitative measurements of the effect of ionizing particles on photographic emulsions were made by Kinoshita¹⁰ in 1910. Kinoshita used alpha particles from natural radioactive substances to bombard certain special emulsions with increased silver halide content. His work

¹⁰
S. Kinoshita, Proc. Roy. Soc. 83A, 432 (1910).

led to a theory of the action of ionizing particles on silver halide grains which, though not entirely accurate, is surprisingly similar to the explanation accepted today. Reinganum¹¹ was the first to observe actual tracks produced by alpha particles in an emulsion. By present standards these were hardly tracks, since they were composed of rather widely separated developed grains of silver. Nonetheless, these grains showed sufficient orientation to be identifiable as having been produced by the alpha particles which were used to bombard the plate. Further work with photographic plates was seriously hampered until about 1930 by two factors. These were, first, that the silver halide concentration in the emulsion was so low as to cause difficulty in distinguishing tracks, and, second, that the emulsions available were so thin that the entire length of a track could ordinarily not be observed completely in the emulsion. The first difficulty was overcome by the preparation of photographic emulsions containing about eight times as much silver bromide as is ordinarily used in standard photographic plates. The second difficulty was more serious, due to the fact that thick emulsions have a tendency to peel away from the base material on which they are coated during processing and that the technique of development is considerably more

11

M. Reinganum, Physik. Zeits. 12, 1076 (1911).

complicated for thick emulsions. Both of these difficulties have been largely overcome by the development of improved bonding and developing techniques.

Excellent discussions of the history and various uses of the photographic techniques have been given by Shapiro¹² and Webb.¹³ Powell and Occhialini¹⁴ in their book give examples of the various applications for which the technique has been used with some excellent illustrations of the tracks which are observed.

Photographic plates designed for various specific applications are now available commercially from the Ilford Company and Kodak, Ltd. in England and the Eastman Kodak Company in America. Emulsion thicknesses range from 25 microns to 200 microns. The emulsion is ordinarily coated on a standard 1 inch x 3 inch glass microscope slide and consists of silver bromide crystals uniformly dispersed in gelatin. Depending upon the type of emulsion, the silver bromide concentration varies from 65 per cent to 85 per cent of the weight of the

¹²
M. M. Shapiro, Rev. Mod. Phys. 13, 58 (1941).

¹³
J. H. Webb, Phys. Rev. 74, 511 (1948).

¹⁴
C. F. Powell and G. P. S. Occhialini, Nuclear Physics in Photographs.

emulsion. The size of the AgBr grains is controlled and varies from about 0.1 to 0.4 microns, depending upon the purpose of the emulsion, the smaller grain size being used to detect particles of greater specific ionization, such as fission fragments. By a proper choice of grain size it is also possible to obtain emulsions which will distinguish between different particles, as for instance between protons and alpha particles, by the grain density which the particles produce in the emulsion.

As an ionizing particle proceeds through the emulsion it imparts its energy progressively to electrons in the individual AgBr crystals. Some of these electrons receive enough energy to be raised to the conduction band of the AgBr crystals and move freely about within the crystal. When one of these electrons encounters a so-called sensitivity speck, by which is meant an impurity in or deformation of the crystal, the electron is captured at that point. An electron so captured produces an electrostatic field and attracts positive silver ions to it. If this process is carried on sufficiently within a crystal, enough clumps of the silver ions are produced to catalyze the reduction of the entire AgBr grain to metallic silver under the action of a suitable reducing agent. Since this process is repeated many times during the progress of the charged particle through the emulsion, the track of the particle after

development will be observed as a line of silver grains, the grain spacing being dependent on the rate of energy loss of the particle. After reduction of the AgBr grains by the developer the plate is cleared by the action of a suitable fixer, which dissolves and removes the unaffected AgBr in the emulsion. The removal of the unaffected AgBr causes a reduction in the thickness of the plate of about 50 per cent.

The range energy relation for protons, deuterons, and alpha particles in Eastman photographic emulsions has been calculated by Webb,¹³ assuming a stopping power of 1800 for photographic emulsion relative to air. Independently, Lattes, Fowler, and Cuer¹⁵ have measured the range energy relation for protons and alpha particles in the Ilford emulsions. The variation of stopping power in different types of emulsions is very slight. A convenient rule of thumb is that the range of a given particle in emulsion expressed in microns is five times its range in air in centimeters.

Charged particle detectors can be grouped into two general classes. One class is characterized by the counter-type detector, in which the passage of a charged particle initiates an electrical pulse which is amplified and recorded on a scaling circuit. The second group, which includes photographic plates and cloud chambers, is characterized by the

15

C. M. G. Lattes, D. H. Fowler, and P. Cuer, *Nature*, 159, 301 (March 1, 1947).

fact that the particle is observed directly, at least in the sense that one can observe the path of the particle by virtue of the ionization produced during its passage through the detector. Such is not always the case for a counter mechanism, inasmuch as it may be necessary for the charged particle to expend only a small portion of its total range in order to initiate counting.

There is no fundamental clash between the two systems of detection. The fact is that the two methods complement each other, and the overlap in their applications often makes it advisable that important experiments be done both ways. Since nuclear scattering experiments comprise one of the fields in which the two overlap, and since the great bulk of nuclear scattering experiments are done with counter techniques, it seems appropriate to consider the reasons for utilizing the photographic technique in this particular experiment.

A photographic plate is essentially a cloud chamber which is continuously sensitive to charged particles. In addition, its high stopping power makes it equivalent to a cloud chamber of practically infinite extent. The plate is extremely compact, however, and requires none of the accessories needed to operate a cloud chamber. The compactness of the plate permits the use of a great many plates simultaneously to observe a nuclear reaction or a scattering

process. This is probably the greatest single advantage of photographic plates over counter-type detectors in nuclear scattering. In addition, the power supplies, amplifiers, discriminators, and scalers ordinarily used with a counter circuit are eliminated. The inherent perverseness of electronic circuits makes this a not inconsiderable advantage.

The photographic plate detector represents a sort of coincidence detector in space. By this is meant that when the position of the source of charged particles is known relative to the plate, one can determine from the geometry of the experiment the direction in which the tracks should proceed within the plate. The criterion as to whether or not a track should be counted can be established in terms of defined horizontal and vertical directions on the plate and the necessity that the track of a charged particle start on the surface of the emulsion. Proper utilization of these facts permits the elimination of improper counting of background tracks which may appear in the plate.

The fact that data may be taken at many angles simultaneously permits a tremendous saving in the running time of the accelerator which is being used to produce the projectile nuclei. There are two distinct advantages involved here. For one, variations in the behavior of the accelerator, of which energy variation and beam direction variation are probably the most serious, are minimized.

Secondly, the monetary saving is quite significant when one considers the expenditure of money necessary to maintain and operate an accelerator such as a cyclotron.

Measurement of the length of tracks in photographic emulsion permits a determination of the energy spectrum of the products of a disintegration. Such an analysis can provide data on possible excited states involved in a given reaction. In addition a range analysis permits correction of the observed yield from a reaction for certain experimental factors such as slit penetration and impurities in the gas which is being bombarded. Of not inconsequential importance is the general fact that photographic plate detectors provide a new and independent means of doing important nuclear scattering experiments.

There is another point, peculiar to this particular experiment, which practically demands the use of photographic plates as detectors. This is that the target gases bombarded, He^3 and H^3 , are both extremely rare and valuable isotopes. Since the probability of the loss of the target gas is at least a linear function of the time that the gas is kept in the target, the use of a counter to detect the reaction particles might have been prohibitive in terms of time and the consequent risk of loss. Also the fact that photographic plates provide a permanent record of the experiment permits further study at any time with no equipment other than the exposed plates and a microscope.

Opposed to these advantages of the photographic technique are some equally obvious disadvantages resulting from the use of the method. Primary among these is the fact that the results of an experiment are not immediately available, since the processing of plates with 200 micron emulsions takes at least 12 hours and the analysis of a set of plates takes a much longer time. This is partially counterbalanced by the simplicity of the mechanism for detection of the charged particles. However, it still remains a serious disadvantage from the standpoint of obtaining immediate results. A second disadvantage is that proper analysis of a single photographic plate is a fairly tedious job and requires considerable time, about three 8 hour days on the average for the experiment under consideration. At the Los Alamos Scientific Laboratory a staff of technicians trained in nuclear microscopy is available for the analysis of plates. This, of course, is not true of most nuclear research laboratories, possibly explaining the reluctance of many workers to engage in research using photographic emulsions as particle detectors. Still another limitation, which is not apparent in the present experiment, is the fact that photographic plate detectors provide no time resolution in the counting of particles. This prohibits their use in time coincidence experiments, for instance, or in any experiment where one needs a time scale.

As has been pointed out in Chapter II, the determination

of an absolute cross section necessitates the measurement of the solid angle subtended by the detector at the reaction center. This measurement would be a difficult one if some means of collimation were not provided, since the charged particles are allowed to enter the surface of the plate at a grazing angle of the order of 10° . The number of tracks falling in a given area of the plate could, of course, be counted, but it would be necessary to have an accurate knowledge of the angle between the plate and the path of the reaction particles in order that this area could be projected to a plane perpendicular to the path of the reaction particles. Such a method is inherently susceptible to inaccuracy since the sine of this angle would then appear in the formula for the cross section as a linear function and, besides, the surface of the emulsion is not entirely flat. It is therefore desirable, if possible, to make the measurement of the solid angle subtended by the photographic plate at the reaction center independent, or nearly so, of the angle between the path of the reaction particles and the photographic plate surface.

A very early prototype of the camera used in the present experiment was constructed by Powell, May, Chadwick, and Pickavance¹⁶ for use in their investigation of the excited states of stable nuclei. This camera was a cylindrical

¹⁶

C. F. Powell, A. N. May, J. Chadwick, and T. G. Pickavance, *Nature* 145, 893 (1940).

tube with a slot 3 mm wide cut in one side. A bombarding beam was caused to pass through this cylindrical tube and strike the target gas inside the tube. A long photographic plate was placed parallel to the axis of the tube at a distance of 1 cm. from the tube. This method recorded all of the data from a particular experiment on a single long plate. However, it had the disadvantage that both the solid angle subtended by the plate and the amount of the target volume which could be seen by the plate at a particular angle were critically dependent on a knowledge of the angle which the reaction particles made with the plate as well as a measurement of the area on which tracks were counted.

At about the same time Wilkins and Kuerti¹⁷ at the University of Rochester constructed a camera with which they could simultaneously observe reaction particles at various laboratory angles produced when a central foil was bombarded by a cyclotron beam. This camera was quite similar in appearance to the one used in the present experiment. Again, collimation was provided by a single slit, in this case a ring surrounding the foil with pinholes in it through which the reaction particles could pass.

The experimental difficulties presented by the necessity for accurate knowledge of the position of the plate have been

¹⁷

T. R. Wilkins, J. App. Phys. 11, 35 (1940).

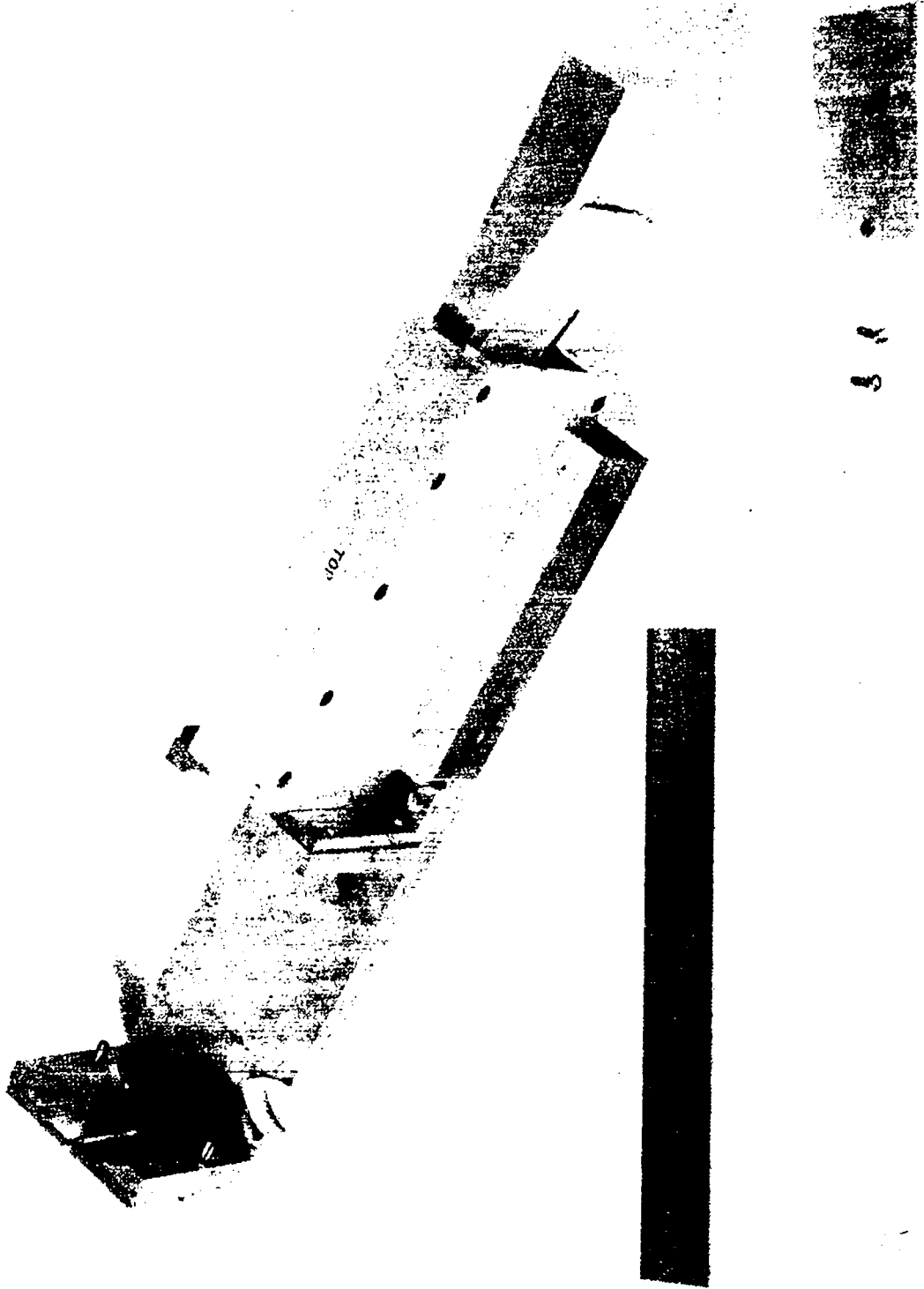
overcome through a method developed at this laboratory.¹⁸ This technique utilizes a second slit, together with the accurate measurement of the width of a swath in which tracks are counted taken lengthwise down the plate, to define the solid angle. The experimental set-up is essentially that shown in Figure 2.

Figure 3 shows a single plate nuclear camera together with the slit assembly constructed for it. This camera was used, together with other similar cameras, in the preliminary investigation of the differential cross section for the reaction $\text{He}^3(d,p)\text{He}^4$. The slit systems were designed specifically to be used in conjunction with the 90° gas target (see Chapter V). In this camera a single photographic plate is clamped securely at a fixed angle on the wedge shaped dural block which slides into the camera body. This sliding wedge is made to very close tolerances in order that the position of the plate inside the camera can be determined accurately by appropriate measurements. The two slits are located on the assembly with dowel pins and were cut on a milling machine in such a way that a line through their centers strikes a point $2/3$ of the way from the back end of the photographic plate to the front end of

18

L. Rosen, F. K. Tallmadge, and J. H. Williams
Phys. Rev. 76, 1283 (1949).

Figure 3
Single Plate Nuclear Camera



the plate. This insures that only a negligible fraction of the reaction particles which are scattered from an absorber at the front of the camera (not visible in photograph) will miss the surface of the plate after they are scattered.

The multiplate camera,¹⁹ shown in Figures 4 and 5, is in principle identical to the single plate camera assembly. It is essentially a compact arrangement of 69 single plate cameras with some added refinements. The beam of projectile particles passes centrally through the camera in the direction from the small brass tube towards the larger one. The small tube acts as a collimating assembly to determine the direction of the bombarding beam with respect to the slits in the camera. Inside this tube are four circular diaphragms. Proceeding in the direction of the beam through the collimating tube there is first a gold diaphragm with a $3/16$ inch reamed hole which permits passage of the beam. The second diaphragm is an anti-scattering diaphragm which removes parts of the beam scattered by the edges of the first slit and the outer window, its diameter being $1/4$ inch. The third diaphragm is again a $3/16$ inch diameter reamed hole, and the fourth still another $1/4$ inch anti-scattering diaphragm.

19

This camera was developed through the combined efforts of L. Rosen, F. K. Tallmadge, J. H. Williams, and the author. A description of its design and fabrication will be submitted for publication.

Figure 4
Multiplate Camera

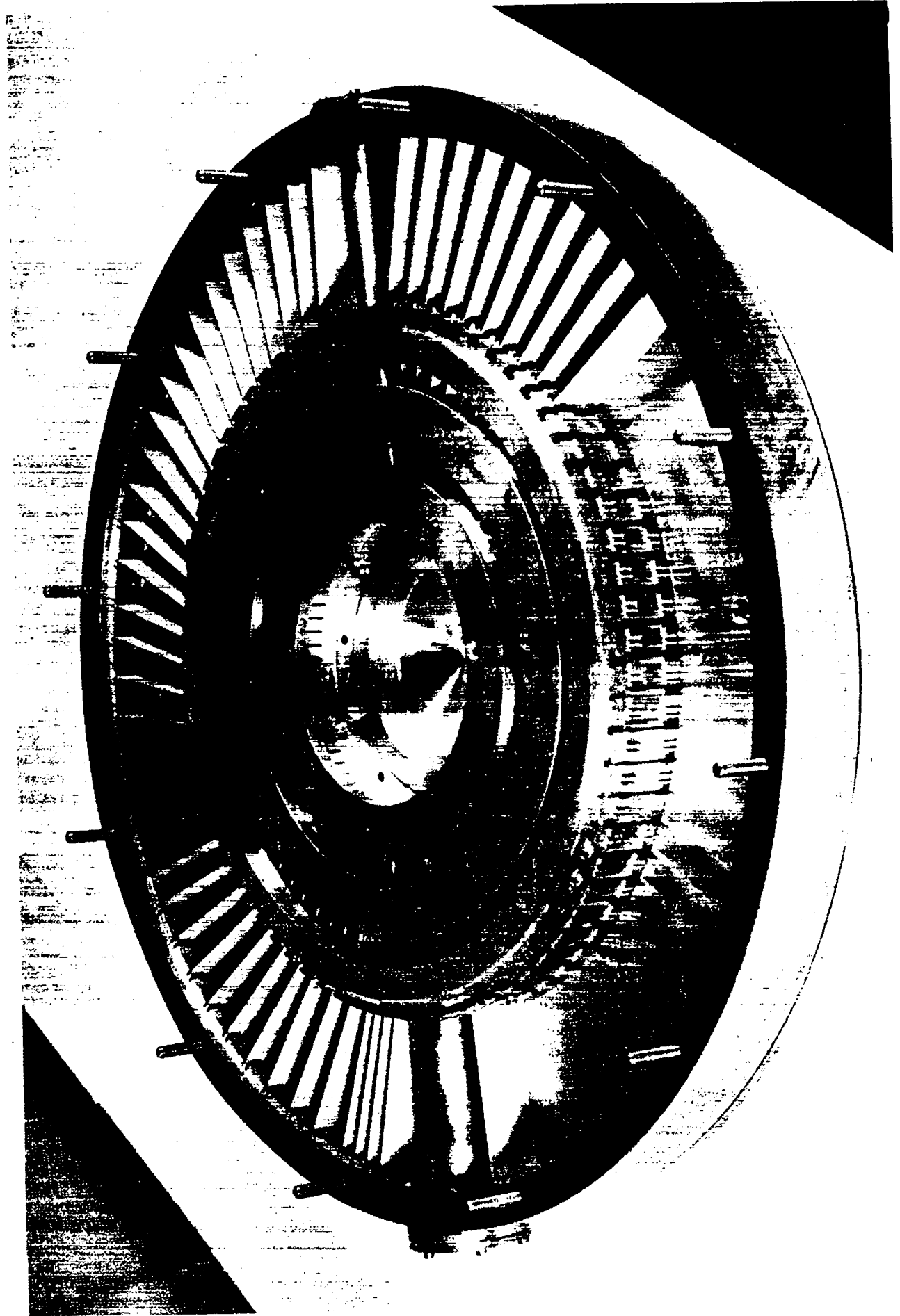
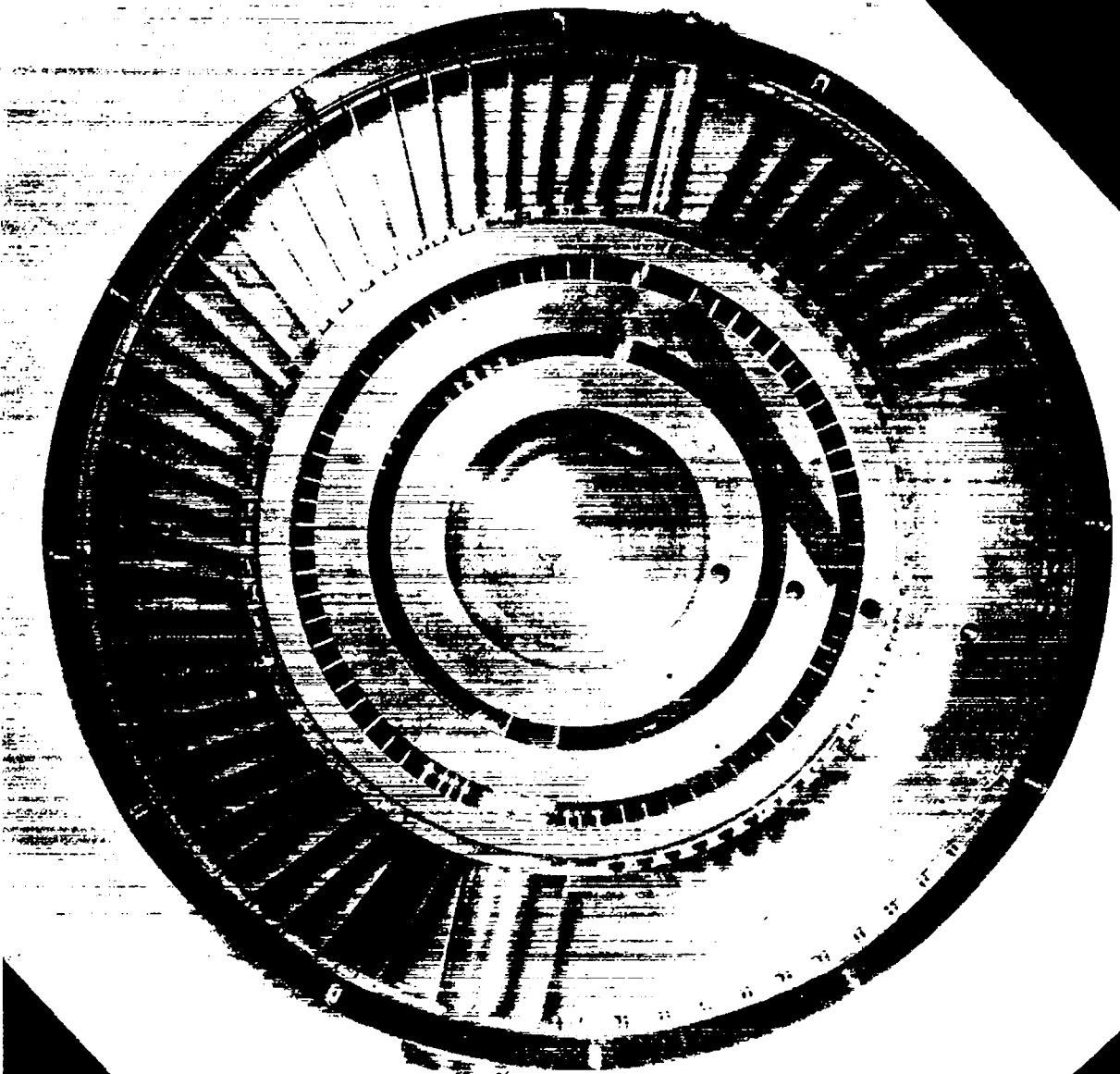


Figure 5
Multiplate Camera



The large exit tube is provided in order that the beam may spread inside the camera without striking the walls. The slit assemblies are constructed in three rings, in each of which slits have been cut such that a line through the centers of the three slits strikes a given photographic plate at a distance about $2/3$ of the way from the outer edge of the plate to the inner edge of the plate. Again this is to insure that only a small fraction of particles scattered by foils placed in front of the plate will miss the plate. It may be noted that two sets of slots are provided for locating each plate in order that the angle of the plate relative to the beam of reaction particles defined by the slits can be varied to one of two definite angles. Just inside the inner end of each plate a slot is cut in order that foils of suitable air equivalence can be placed in front of the photographic plate if this is desired. Except for the extreme forward angle plates the angular spacing between plates is 5° . In the case of three forward angle plates on one side and four on the other the spacing between plates is 2.5° . The addition of an extra 2.5° plate on one side permits staggering of the angles in order that data may be taken at 2.5° intervals in the laboratory system. Of the three slit rings, the inner and outer produce the actual collimation of the beam of reaction particles, while the center ring serves merely as a set of anti-scattering

slits which absorbs particles scattered from the edges of the slits in the inner ring.

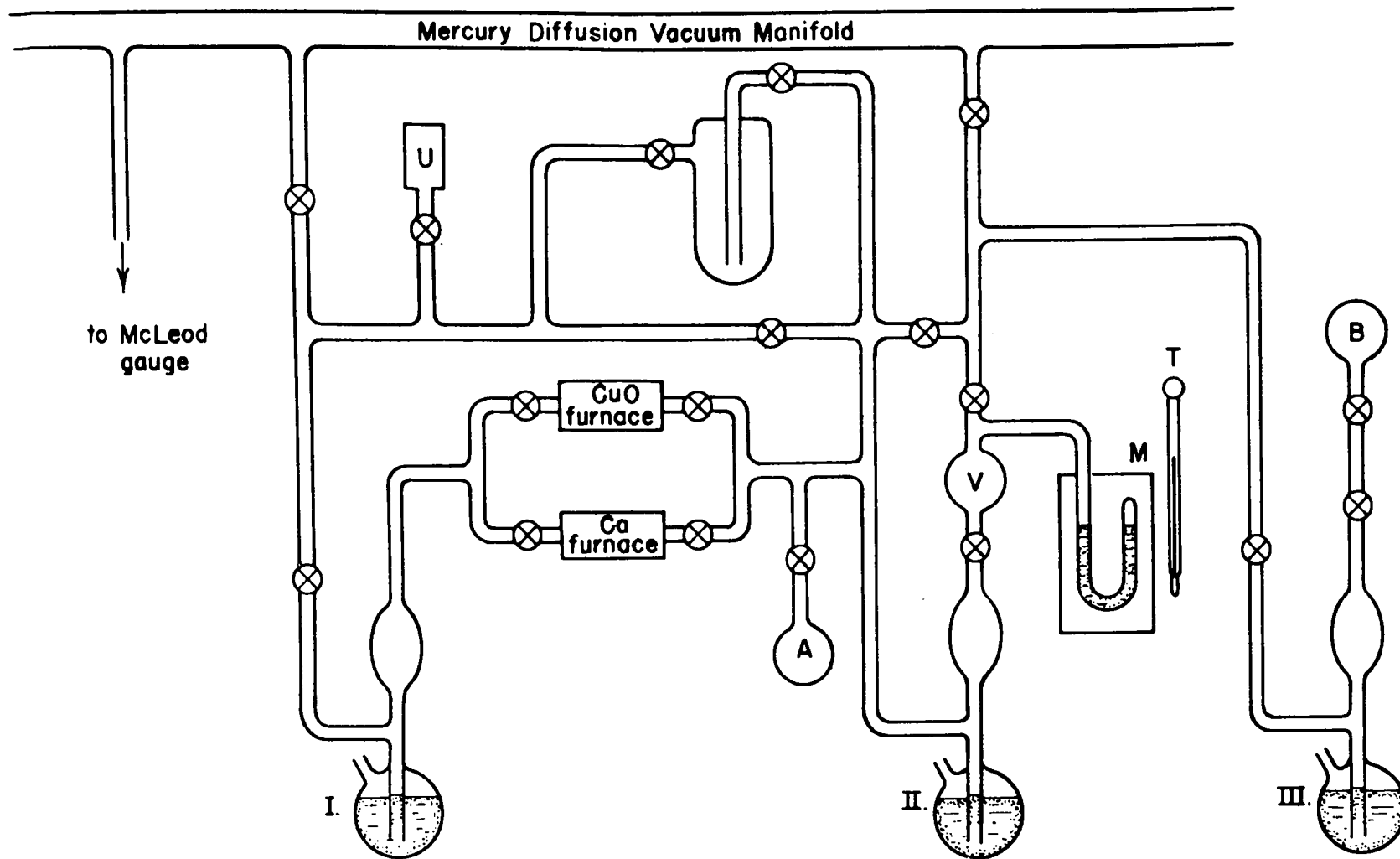
Nylon windows are provided at the entrance and exit ports of the camera when the entire camera is filled with gas for scattering experiments. For the observation of the $\text{He}^3(d,p)\text{He}^4$ reaction a special cradle was constructed so that a cylindrical gas target could be mounted centrally in the camera (see Chapter VI).

CHAPTER IV.

GAS HANDLING

An essential part of this experiment is a means of assuring the purity of the gas which is to be bombarded and of accurately determining the pressure and temperature of the gas in the target at the time the target is filled and also when the gas is recovered, in order that the number of gas atoms per unit volume during the actual bombardment may be precisely known. Fig. 6 shows a schematic diagram of the gas handling system which was used.

The samples of tritium used were made by the $\text{Li}^6(n, \alpha)\text{T}^3$ reaction. The mixture of He^4 and T^3 thus produced can easily be separated by chemical or physio-chemical means. For the sample used the initial separation of the T^3 and He^4 was accomplished at the time the sample was produced by passing a solution of T_2 and H_2 through a palladium valve, the He^4 thus being filtered out of the mixture. Another useful method which can be used to separate hydrogen isotopes from other gases is the formation of uranium hydride, UH_3 , from the mixture of gases by allowing this mixture to come into intimate contact with finely divided uranium metal. This was the actual technique used by the author to purify the tritium gas before bombardment. Heating of the uranium to temperatures of the order of 200° to 600° C. causes the hydrogen isotopes, in this case mainly tritium, to be evolved. The relation between the tritium pressure over



GAS SYSTEM

FIG. 6

uranium hydride and the temperature is given approximately by

$$\log_{10} p = - \frac{4500}{T} + 9.28 \quad 20$$

where p is the pressure in mm Hg and T is the temperature in degrees absolute. It will be observed that at ordinary room temperature, 300°A., the tritium pressure is of the order of 10⁻⁵ mm Hg.

Because the reaction described above is peculiar to hydrogen isotopes this method provides a very convenient method of handling and purifying tritium. Also, since He³ is produced by beta decay of T³ with about a 13 year half life, the uranium furnace gives a simple method of separating the He³ from a sample of T³ which has partially decayed. For these reasons a uranium furnace, indicated as U on the diagram, is included as a part of the gas system.

It is seen that the process of obtaining a pure sample of He³ includes the preparation of a T³ sample. The processes will therefore be described together.

It is conceivable that T³ samples as received at this

20

F. H. Spedding, A. S. Newton, J. C. Warf, O. Johnson, R. W. Nottorf, I. B. Johns, and A. H. Daane, *Nucleonics* 4, No. 1, 4, (Jan. 1949). For further information on the properties of uranium hydride see also A. S. Newton, J. C. Warf, F. H. Spedding, O. Johnson, I. B. Johns, R. W. Nottorf, J. Y. Ayers, R. W. Fisher, and A. Kant, *Nucleonics*, 4, No. 2, 17, (Feb. 1949).

laboratory may contain traces of the gases present in air as contaminants. These would include nitrogen, oxygen, water vapor, carbon dioxide, and the noble gases. Of these gases all except the noble gases are removed by the chemical treatment described below.

Due to the inert nature of the noble gases, however, it is impossible to separate them from the gas sample. If, however, these gases were present in significant amounts they would be detected during the bombardment of the gas sample by observation of the elastically scattered deuterons which they would produce.

The T^3 sample bulb is a glass sphere with two gas leads protruding from it. One of these is a thick walled capillary tube, sealed when the gas is placed in the sample bulb. The second is ordinary tubing about 10 mm in diameter with a capillary seal-off tube inside it. This seal is of the type commonly used in rare gas bulbs, constructed so that it can be broken by the dropping of a steel weight on the seal after the larger tube has been sealed to the gas system.

A tritium sample bulb which has been allowed to decay long enough to produce a worthwhile quantity of He^3 is sealed to the gas system at the point marked A on Fig. 6. Air is then exhausted from the system through the vacuum manifold and the seal tested with a Tesla coil. If there is a leak in the seal its presence will be shown by a bright whitish glow

at the leak, where the spark enters the vacuum system. If no leak is indicated, the seal is further tested by the fact that the system should pump to a sticking vacuum as indicated by the McLeod gauge, corresponding to a pressure of 10^{-6} mm. or less. This test is, of course, made on all seals used during the filling and emptying of a target and the storing of gas in a sample bulb.

When the system is made vacuum tight and pumped to a sticking vacuum, the stopcocks leading to the vacuum manifold are closed and the seal of the tritium bulb is broken by lifting a small cylindrical steel weight, previously placed inside the large tube, with a magnet and allowing it to fall on the capillary seal. The stopcock of the uranium furnace is opened and the tritium allowed to react to completion with the uranium to form uranium hydride. It is usual to observe the rate of reaction by connecting the manometer M to the system and observing the mercury meniscus by means of a cathetometer. The pressure is observed to decrease due to reaction of the tritium with the uranium. After no further decrease in pressure is observed, the gas is allowed to remain in contact with the uranium for two to three hours to insure that equilibrium is attained.

The residual gas in the system, which is He^3 with traces of tritium, is then pumped into a standard

volume, V, by means of Toepler pump II. The pressure and temperature in the standard volume are measured with manometer M and thermometer T; from these measurements the NTP volume of the gas may be computed. The He³ may then be stored in sample bulb B or retained in the gas system and further purified, later to be used in filling a gas target sealed on at B.

To complete the purification of the tritium it is now necessary only to pump on the cold uranium furnace for a few minutes to remove the slight residue of He³. No appreciable amount of tritium is lost by this process, which is repeated just before filling of a gas target with tritium.

Further purification of the He³ is now necessary before it can be used to fill a gas target. This is done in two processes. First the gas is passed over CuO at a temperature of 425°C. and through the liquid air trap, Toepler pump I being used to accomplish the recycling. Here the reaction which takes place is



Traces of tritium are thus removed as tritium water and frozen out in the trap. This treatment also removes traces of water vapor which might be present from other sources. The degree of completion of the reaction is determined by pumping the gas back into the standard volume at intervals. When no decrease in volume is detected between two successive measurements, the

reaction is assumed to be sufficiently complete. The He^3 , being chemically inert and having an extremely low boiling point (3.2_0°A.),²¹ is not affected by this treatment.

Subsequent to being passed through the CuO furnace, the He^3 is passed over metallic Ca at 700°C. , the liquid air trap being shut off from the system and by-passed. This treatment removes oxygen and nitrogen from the sample quantitatively as calcium oxide and calcium nitride respectively. It also removes traces of tritium, deuterium, and hydrogen as calcium hydride. The degree of completion of the reaction is determined as for the CuO treatment.

Finally the gas sample is pumped back into the standard volume and again measured. Ordinarily the purification is done just before the He^3 is to be used for bombardment. Hence the gas is usually transferred to a gas target at B by means of Toepler pump III.

After a bombardment the gas target is sealed onto the system at A and the gas returned to the standard volume, V, to be measured. In every case where He^3 was bombarded the gas was again purified by the same method, in order to ascertain that it had not become contaminated with air. When the gas has been repurified and remeasured in the standard volume, it may be stored in a sample bulb sealed on at B.

21

S. G. Sydoriak, E. R. Grilly, and E. F. Hammel, Phys. Rev. 75, 303 (1949).

In passing it seems worth while to mention the possible health hazard involved in handling tritium. Although nothing is known of the physiological effects of tritium on animal metabolism, a simple calculation shows that certain precautions are necessary.

If the half-life of tritium is taken as thirteen years, it can be shown that the activity is 2.5 curie per cubic centimeter NTP (1 curie = 3.67×10^{10} disintegration/sec). Thus the total source strength of the samples used for bombardment was of the order of 10 curies. The beta particles emitted during the transition to He^3 have as their maximum energy about 18 Kev²² and do not penetrate the walls or windows of an ordinary target as their range is only about 2 mm. in air. However, it is conceivable that they could produce serious effects on living tissue if the tritium came in close proximity, this being especially true in the case of the lungs.

For this reason it is necessary that the gas system be well hooded, in case of accidental breakage of the system. About the only other precaution against breakage to be taken after the gas target is filled with tritium and removed from the system is to stay as far away from it as is convenient.

22

S. C. Curran, J. Angus, and A. L. Cockcroft, Phys. Rev. 76, 853 (1949).

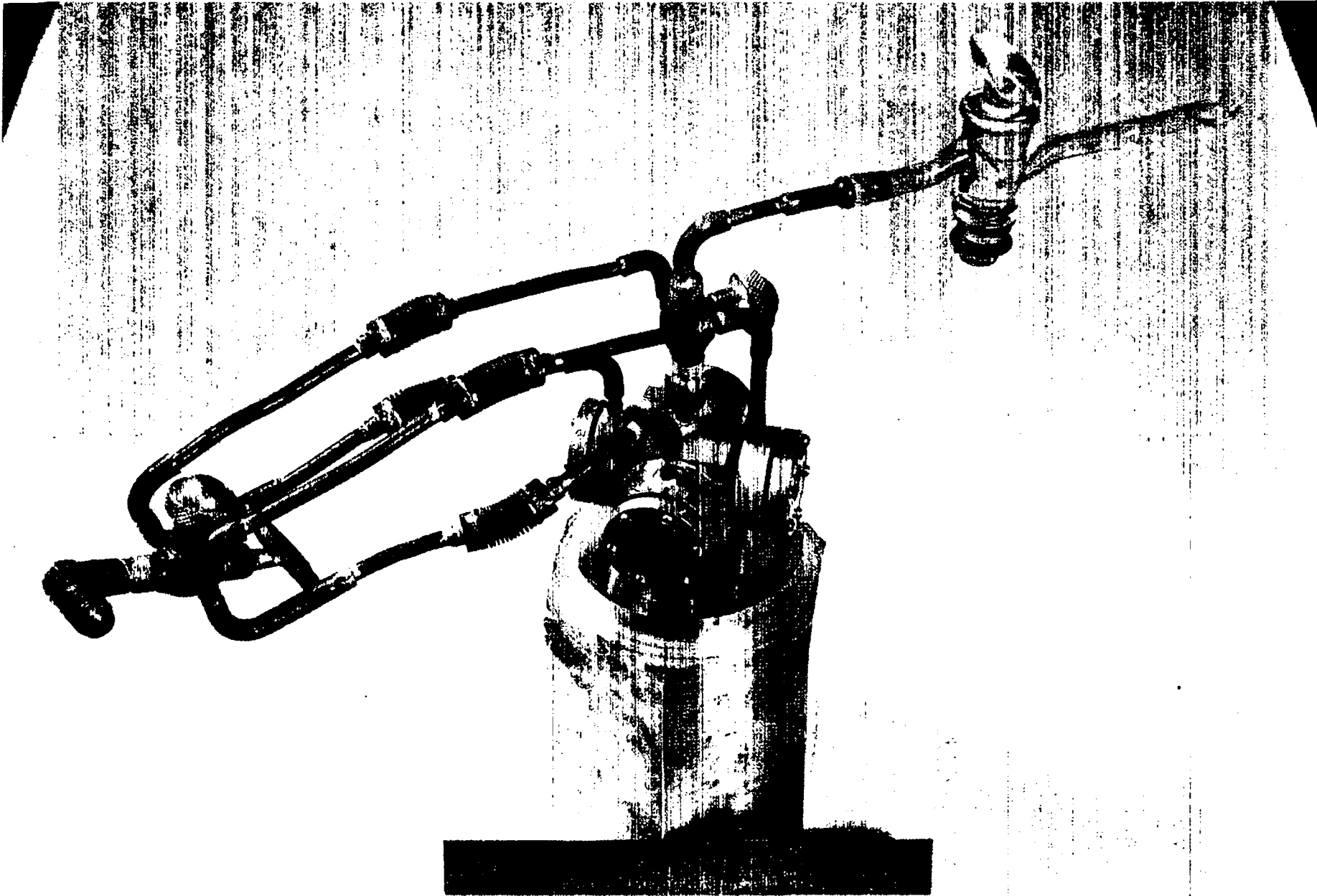
Fortunately no tritium was lost from either of the targets at any time so the problem was in this case a minor one.

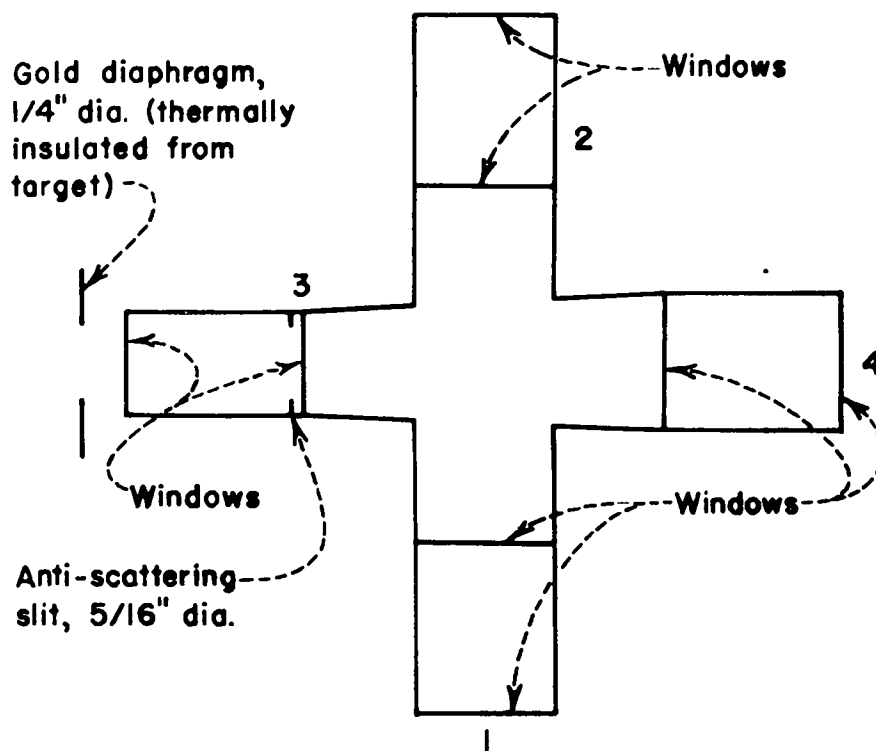
CHAPTER V
GAS TARGETS

To permit the observation of the $\text{He}^3(d,p)\text{He}^4$ reaction it became necessary to construct two somewhat specialized gas targets. In addition to the usual requirements for the design of a gas target two further conditions were imposed because of the nature of the target gas. These were that the volume of the target be minimized, in order that as small a quantity of target gas as possible could be used, and that the greatest possible protection against loss of the target gas be incorporated into the design.

The first of these targets was designed for observation of the $\text{He}^3(d,p)\text{He}^4$ reaction at 90° in laboratory coordinates. This target is shown in Fig. 7 and schematically in Fig. 8. The target body consists of a brass cube $1\frac{1}{4}$ inch on a side through which have been bored two holes whose axes are at right angles to each other. The hole connecting ports 1 and 2 is $1/2$ inch diameter, straight bore. The second hole tapers from a diameter of $3/8$ inch at port 3 to $1/2$ inch at port 4 over the target length of $1\frac{1}{4}$ inch. Double windows are provided at each port and the two outer windows comprise a gas chamber, this being a protective feature which prevents loss of the gas in the event of breakage of one of the inner windows. These four outer chambers were connected together externally and filled with hydrogen gas during a run to a pressure

Figure 7
90° Rare Gas Target





90° RARE GAS TARGET

FIG. 8

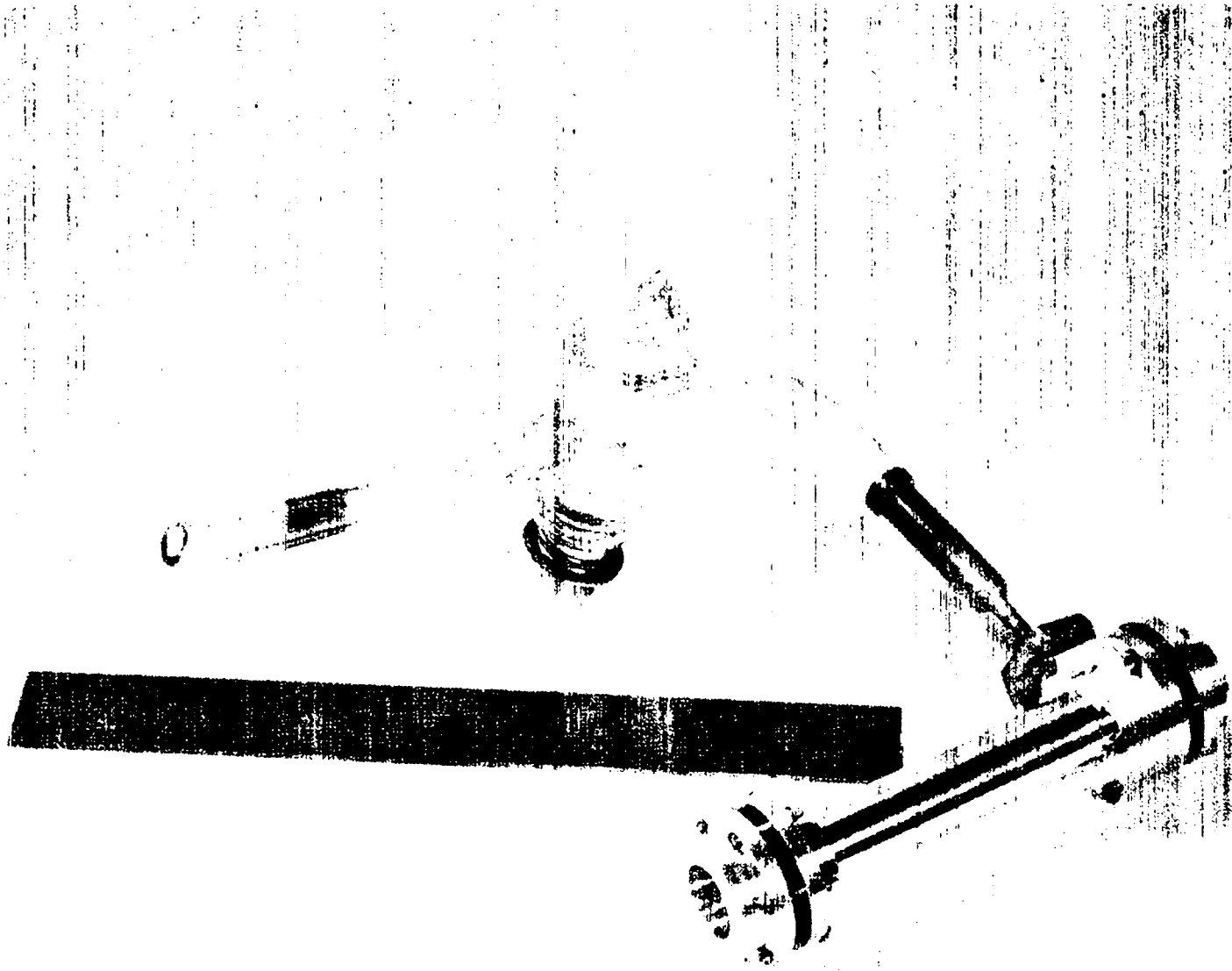
approximately equal to the gas pressure in the central target volume. The gas filling lead for the central target volume is led up through a Hoke bellows valve and connected by means of a Kovar seal to a pyrex glass stopcock. This glass connection was necessary to permit the sealing of the target to the gas filling system during filling and recovery of the gas. Sylphon bellows were provided in the gas leads to the four outer chambers in order to give greater flexibility of these leads during assembly of the target and changing of the windows.

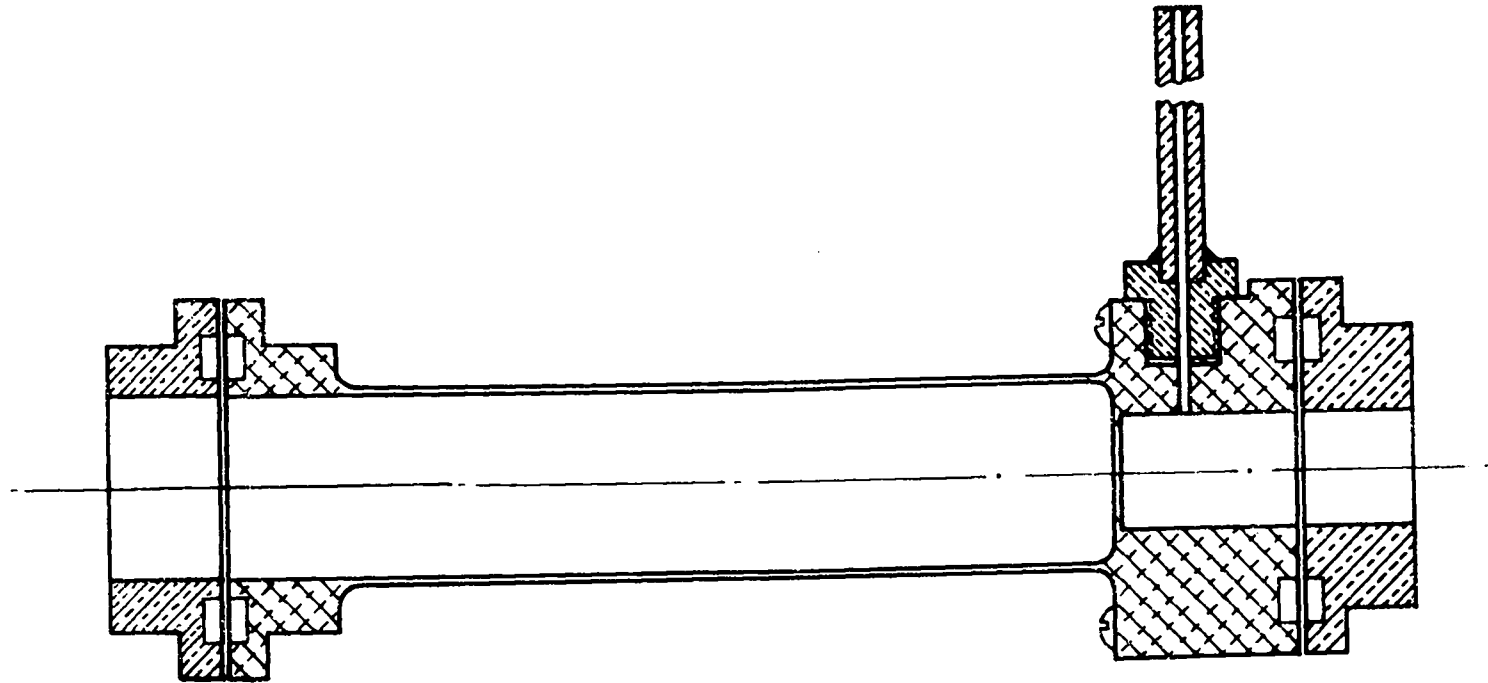
During runs made with this target a water cooled gold diaphragm, thermally insulated from the target, was fitted over port 3. The beam passed through the target in the direction from port 3 to port 4. An anti-scattering slit was provided inside the outer gas chamber on port 3 to remove deuterons scattered from the edges of the gold collimating diaphragm and the outer target window. The taper in the central target body was introduced to insure that the beam did not strike the target walls during its passage through the target. Single plate nuclear cameras and slit assemblies were placed at ports 1 and 2 during a 90° run so that the reaction particles were observed through these ports.

The purpose of the 90° target was to permit the observation of the reaction particles in order that a search could be made for a possible excited state in He^4 and that a preliminary

determination of the differential cross section for the $\text{He}^3(d,p)\text{He}^4$ reaction could be made at this angle. For a determination of the differential cross section over the angular region available in the multiplate camera it was necessary that a second target be constructed. This target is shown in Fig. 9 and schematically in Fig. 10. It consisted simply of a cylindrical dural tube in which the gas was contained. The center section of this tube is $2 \frac{1}{4}$ inch long and was machined to a wall thickness of 0.0050 ± 0.0001 inch. This thin wall section permits the reaction protons of high energy to pass out of the target at angles from 20° to 160° laboratory coordinates. The focused deuteron beam from the cyclotron, collimated by the front collimating tube of the multiplate camera, passed axially through the target in the direction from the end at which the gas target filling lead is connected toward the other end. The end windows of the target were dural, 0.001 inch thick, placed between two rubber gaskets fitted in gasket grooves and drawn up tight by the six gasket screws on either end of the target. The windows of the 90° target were gasketed in exactly the same fashion. Both nylon and dural windows were used in the 90° target. However, it was found to be unnecessary and undesirable (due to the larger air equivalence of the dural) to use the double windows when dural windows were used on the central target chamber of the 90° target. Although provision had been made in the design of the wide angle dural

Figure 9
Wide Angle Dural Gas Target





WIDE ANGLE DURAL GAS TARGET

FIG. 10

target for double end windows with gas chambers corresponding to those on the 90° target, these were omitted in the assembly of the target, since it was believed that the dural windows were strong enough to provide sufficient protection against loss of the gas in the target. The dural windows proved to be satisfactory in this respect.

The methods of alignment and positioning of the wide angle dural target are described in the section on experimental procedure (Chapter VI).

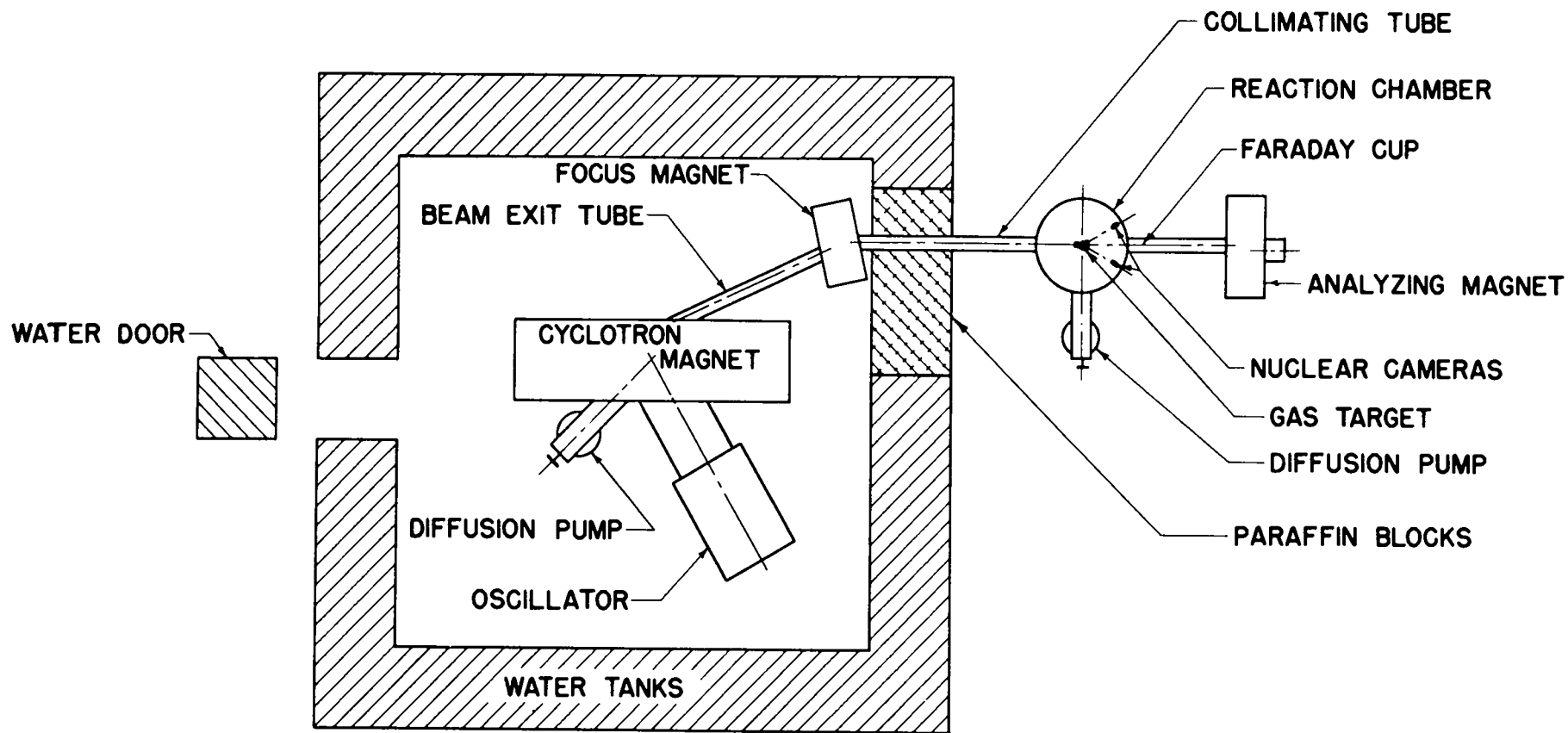
CHAPTER VI
EXPERIMENTAL PROCEDURE

In order to facilitate the conducting of scattering experiments with the 10.8 Mev beam deuterons produced by the Los Alamos cyclotron a system was designed by Curtis, Fowler, and Rosen²³ which focuses a deuteron current of the order of one microampere on a 1/4 inch diameter spot at a distance of about 15 feet from the cyclotron. This arrangement is shown schematically in Figure 11. The fact that the reaction chamber is outside the water tanks of the cyclotron provides a considerable reduction in the neutron and gamma ray background due to reactions in the cyclotron tank.

To provide for the measurement of the total number of deuterons passing through the reaction chamber during an observation, a Faraday cup 9 inches long by 1-3/4 inch diameter is located axially in the center of the tube behind the reaction chamber. To this Faraday cup are secured two Alnico magnets in such a way that the magnets produce a strong transverse magnetic field ($\sim 10^3$ oersted) in the Faraday cup. The purpose of this field is to trap secondary electrons arising when the primary beam strikes the back end of the cup in order that these electrons may not leave the cup and cause

²³
B. R. Curtis, J. L. Fowler, and L. Rosen, Rev. Sci. Inst. 20, 388 (1949).

Figure 11
Cyclotron Schematic



an erroneous measurement of the total charge. The Faraday cup is insulated from ground by means of a lucite washer. In addition the Faraday cup is movable vertically by virtue of a Wilson seal, this arrangement being made so that the primary beam may be allowed to pass through the analyzing magnet and its energy measured by simultaneous measurements of the deflection of the beam and the magnetic field of the analyzing magnet.

The Faraday cup is connected through a low leakage coaxial cable to an electronic current integrator. The beam current striking the Faraday cup charges a condenser in the input circuit of the current integrator which is discharged electronically when the voltage on the condenser reaches a given value. The discharging of the condenser produces a pulse which is fed to a scaler, each pulse indicating that a certain charge has accumulated on the Faraday cup. The current integrator also provides a negative bias of about 120 volts on the Faraday cup which serves to repel secondary electrons produced by the striking of the primary deuteron beam on the back windows of the target or camera assembly which is placed in the chamber.

Calibration of the current integrator is accomplished by connecting, successively, a group of resistances of varying value from the Faraday cup to ground, the current which

flows through these resistors flowing also through a 10,000 ohm standard resistor. Measurement of the voltage across this standard resistor gives a direct measurement of the current. The number of scaler counts produced during a measured time is recorded at each current value. From a measurement of the currents and their respective counting rates one can calculate the absolute charge represented by one count of the scaler. This procedure is repeated over a range of current values in the region of the expected beam current. A plot of current vs. counting rate then permits an accurate evaluation of the integrated beam intensity which passed through the target gas during any given experiment, since the relative beam intensity is monitored by a recording galvanometer throughout the course of each experiment. During a run the beam is also monitored at the control desk of the cyclotron by means of a long-period sensitive galvanometer, through which are fed the discharge pulses from the integrating condenser in the current integrator.

An experiment was done to determine the amount of leakage current due to ionization in the region of the Faraday cup caused by neutrons produced by the striking of the beam on the various diaphragms and on the back of the cup itself. For this purpose a second and smaller Faraday cup was placed immediately behind the camera and just in front of the long

cup, this short cup being used to monitor the beam in the reaction chamber. For a recorded average current of about $0.1 \mu\text{a}$ on the small cup over a seven minute interval, no current integrator counts were observed on the long Faraday cup. Since one current integrator count corresponds to a charge of 1.13×10^{-7} coulomb, the experiment indicates the leakage to be less than 2×10^{-10} ampere. No correction of the results was made for leakage.

Figures 12 and 13 show the general experimental setup. The Wilson seal assembly and coaxial lead for the Faraday cup are visible just to the left of the scattering chamber in Figure 12. The resistance bank for calibration of the current integrator can be seen on top of the analyzing magnet which is at the left in the photograph. To the right of the scattering chamber in the photograph are, in order, an auxiliary diffusion pumping system and a gas filling system.

The experimental procedure is best described in terms of two separate experiments, since the two experiments required completely different target-camera assemblies. The first of these was done using the 90° gas target (see Chapter V). The purposes of this experiment were to determine whether or not the differential cross section for the reaction $\text{H}^3(d,p)\text{H}^4$ was large enough to permit a complete angular determination by the photographic technique, to make an

Figure 12
Reaction Chamber and Auxiliary Equipment

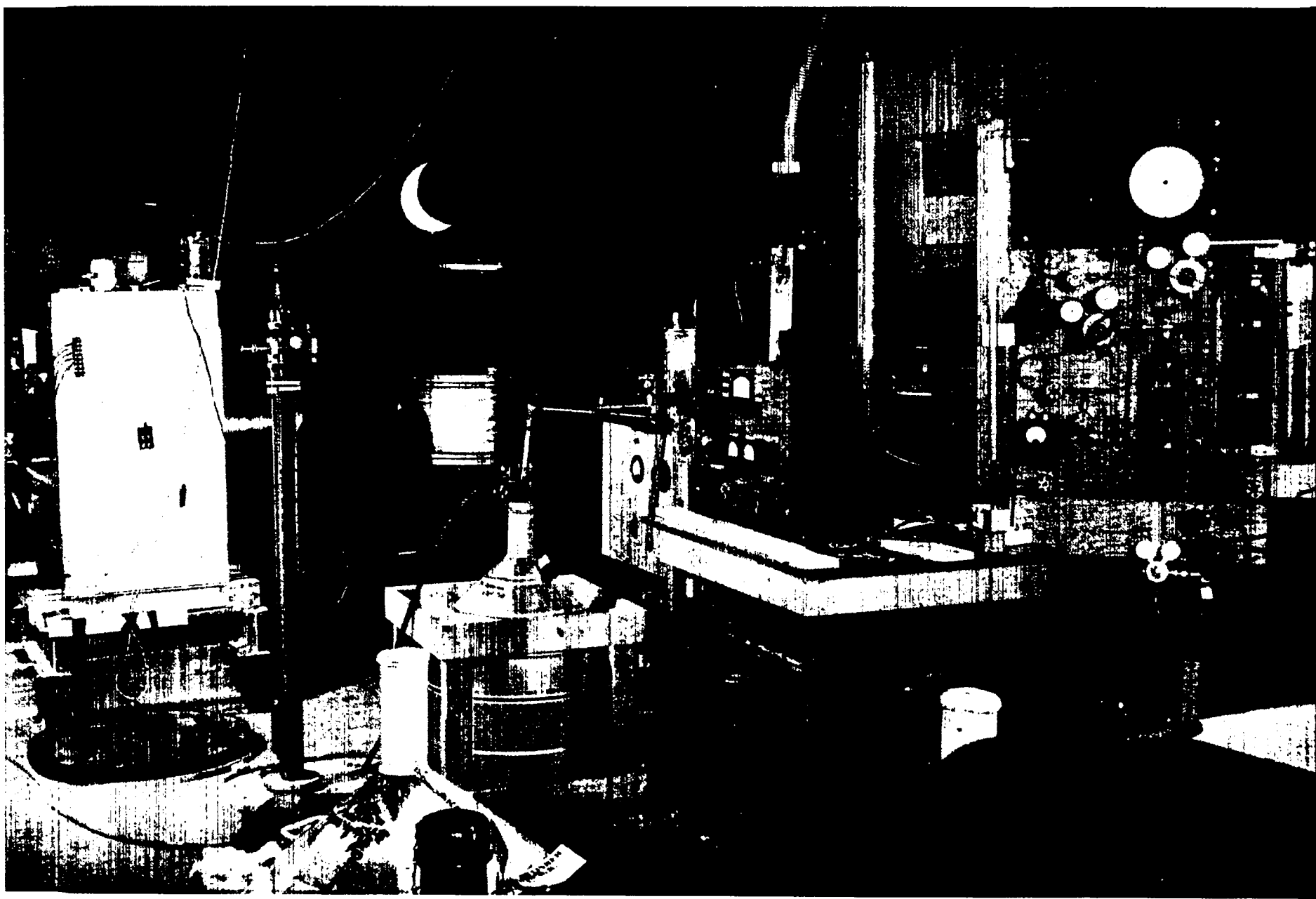
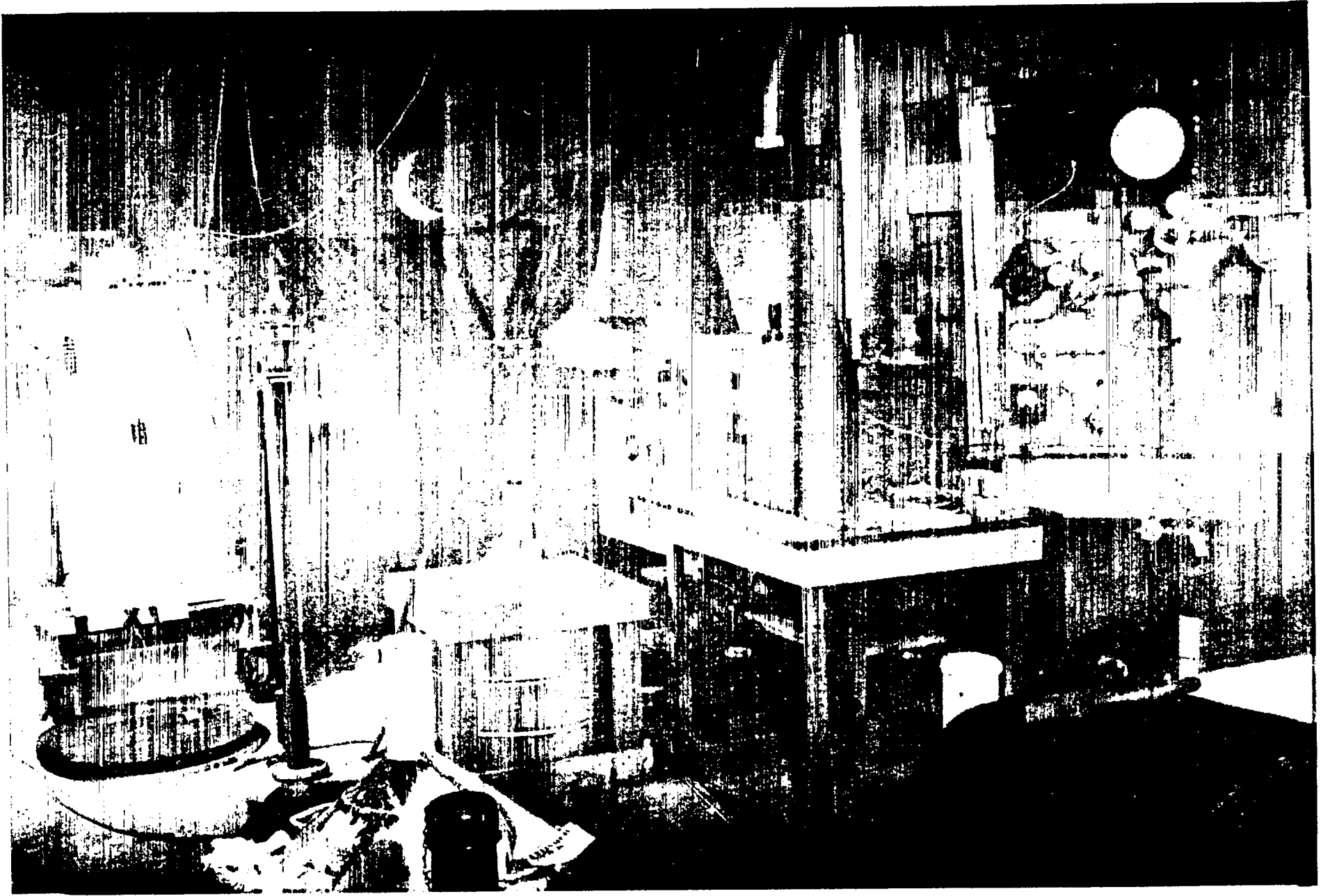
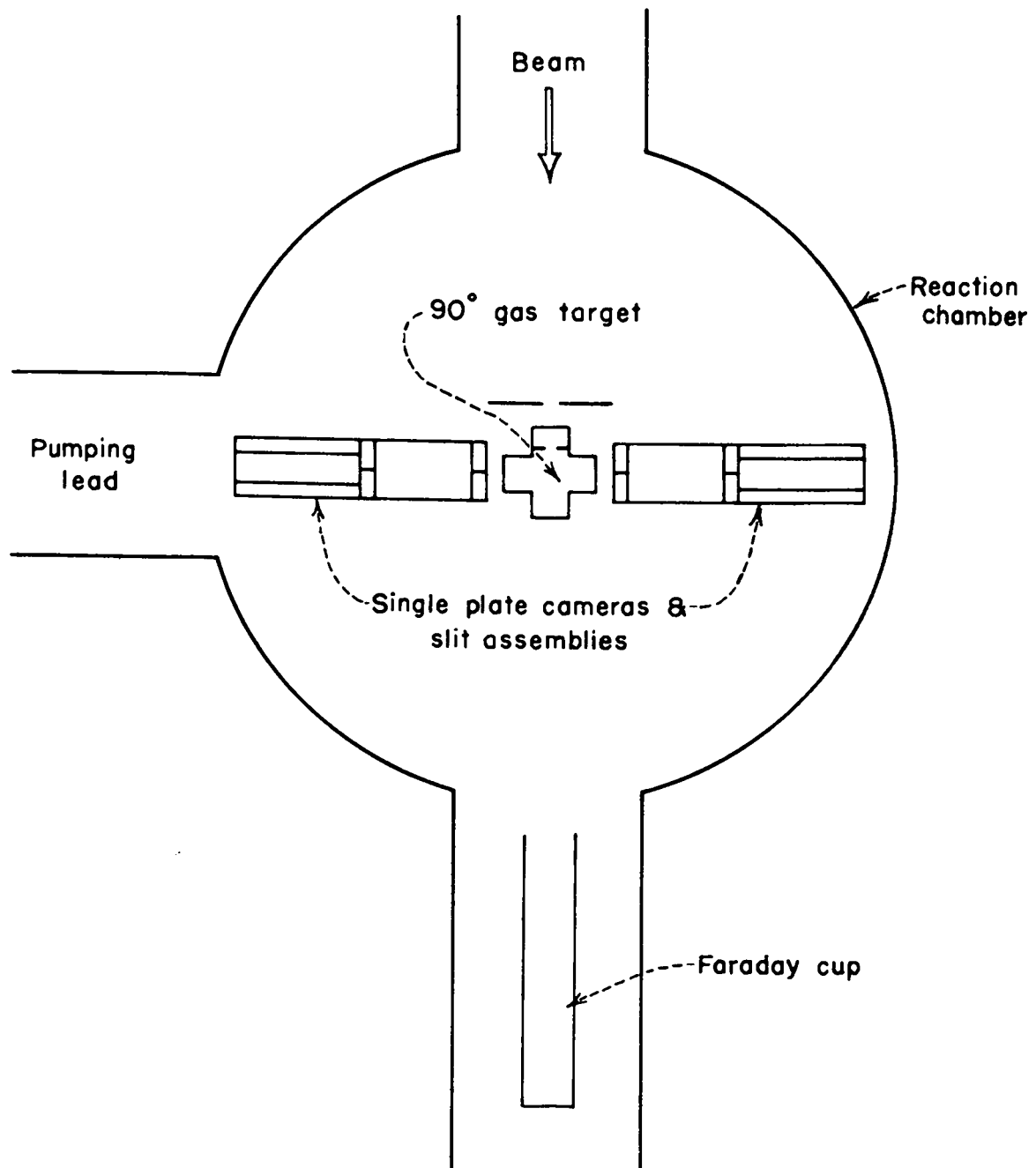


Figure 13
Reaction Chamber and Auxiliary Equipment



accurate measurement of this cross-section at 90° , and to investigate the possible existence of an excited state in the residual He^4 nucleus at an angle of observation of 90° .

The experimental setup is shown schematically in Figure 14. For each of the observations the gas target was placed in a target mount located centrally in the reaction chamber and aligned along the direction of the beam by use of a telescope with which one could sight through the back of the analyzing magnet. The camera assemblies were aligned through the use of a straightedge placed across the top of the scattering chamber and located in direction with plumb bobs dropped to a graduated ring which was mounted on the inside of the reaction chamber. The plates used for all exposures were Ilford emulsion, Type C-2, 200 μ thick. After alignment of the target and camera assemblies, the reaction chamber was covered with the large safety glass disc visible just in front of the analyzing magnet in Figures 12 and 13, the rear port of the analyzing magnet sealed with a similar glass disc, and the reaction chamber pumped down. When a sufficiently low pressure was obtained the cyclotron was started, the focus magnet being turned off until a steady tube beam was obtained. Then the focus magnet was turned on and the target bombarded for a time sufficient to yield the desired number of current integrator counts. In most cases the desired exposure required



GEOMETRY FOR 90° EXPOSURES

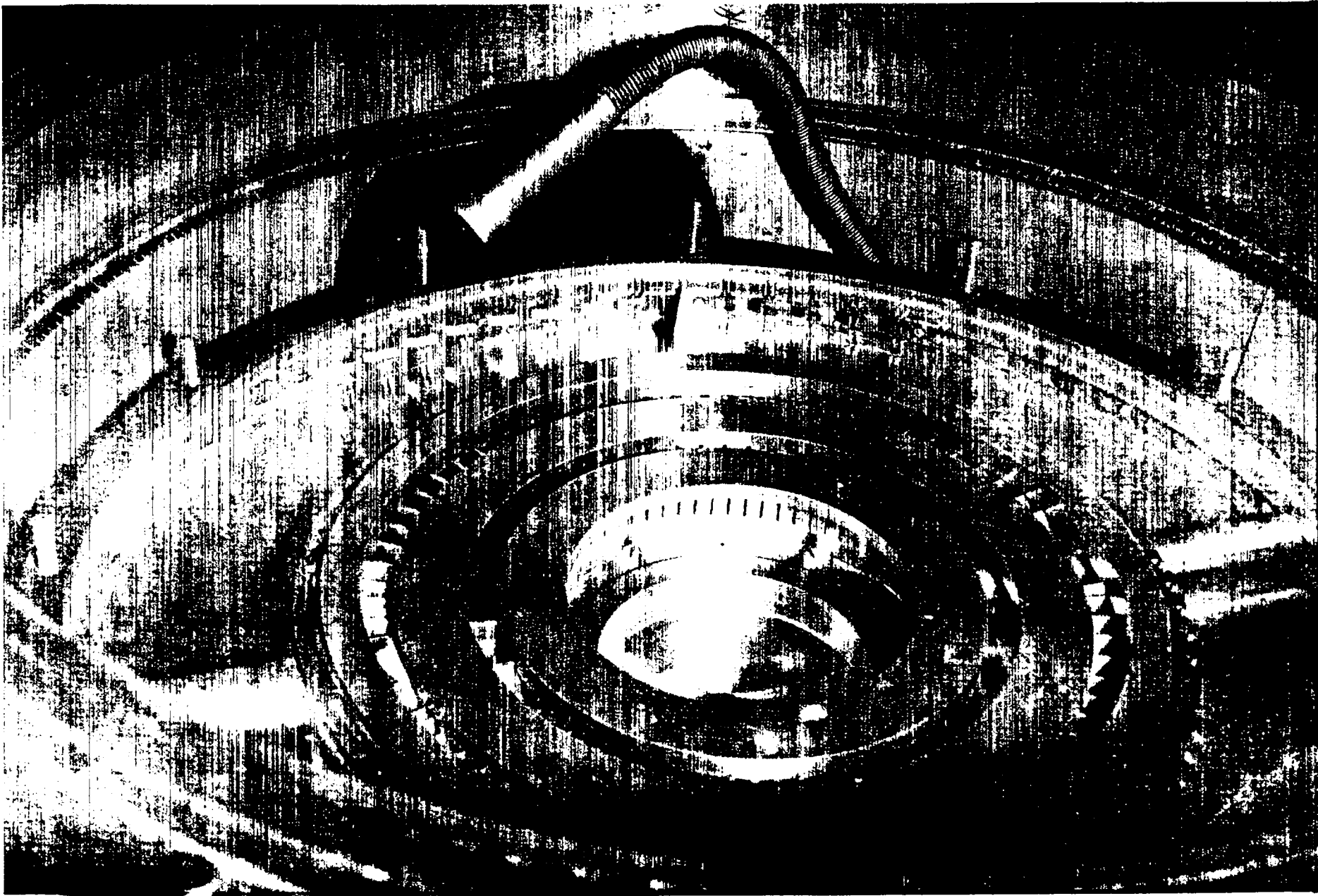
FIG. 14

about 20 minutes, during which time about 100 microcoulombs of charge, or approximately 10^{14} deuterons, passed through the target and into the Faraday cup. After the bombardment air was again admitted into the vacuum system, the camera removed, and the gas from the target recovered.

In order to investigate the possibility of internal scattering of the primary beam in the target and to test the target windows under actual beam conditions, exposures first were made using deuterium as the target gas, the protons from the reaction $D(d,p)T$ being observed. When these experiments were considered to be successful, He^3 and tritium gas were successively introduced into the gas target and exposures made for each gas. By this method values of the differential cross-section for the $He^3(d,p)He^4$ reaction were obtained at 90° . These later served as a check on the results obtained from the multiplate camera insofar as the measurements of gas purity, gas pressure, gas temperature and current integrator calibration are concerned.

The second and more complete experiment of the two was done with the multiplate camera, from which data for the determination of the differential cross-section per unit solid angle for the reaction $He^3(d,p)He^4$ were obtained. The multiplate camera was mounted in the reaction chamber as shown in Figure 15. On account of the necessity for loading

Figure 15
Multiplate Camera in Reaction Chamber



the multiplate camera in place it was necessary to have the dark tent covering the scattering chamber as shown in Figures 12 and 13. In Figure 15 the beam passes from right to left through the center of the camera, the collimating assembly being on the right. The sylphon lead is a pumping tube from the auxiliary diffusion pumping system. Just behind it is visible the tube leading to the large cyclotron diffusion pump. The cradle assembly for the cylindrical wide angle dural gas target is visible in Figures 16 and 17. Due to the fact that the reaction chamber had to remain covered at all times in order to protect the photographic emulsions from light, it was necessary to devise a system for aligning the target in the dark. For this purpose a cylindrical brass bar turned to the proper diameters to fit into the cradle and against the end of the collimating tube was made. By this means the alignment of the cradle assembly could be made very accurately by simply aligning the junction of the brass locating bar with the end of the collimating tube as in Figure 16. This alignment was checked immediately before the target was placed in the cradle and when the target was removed. When the cradle was aligned, it was secured in place with Apiezon-Q wax so that it could not rotate and cause misalignment of the target. The target was then placed in the camera as shown in Figure 17, the camera having previously been loaded with plates from 17.5 degrees to 162.5 degrees

Figure 16

Multiplate Camera with Aligning Bar in Position

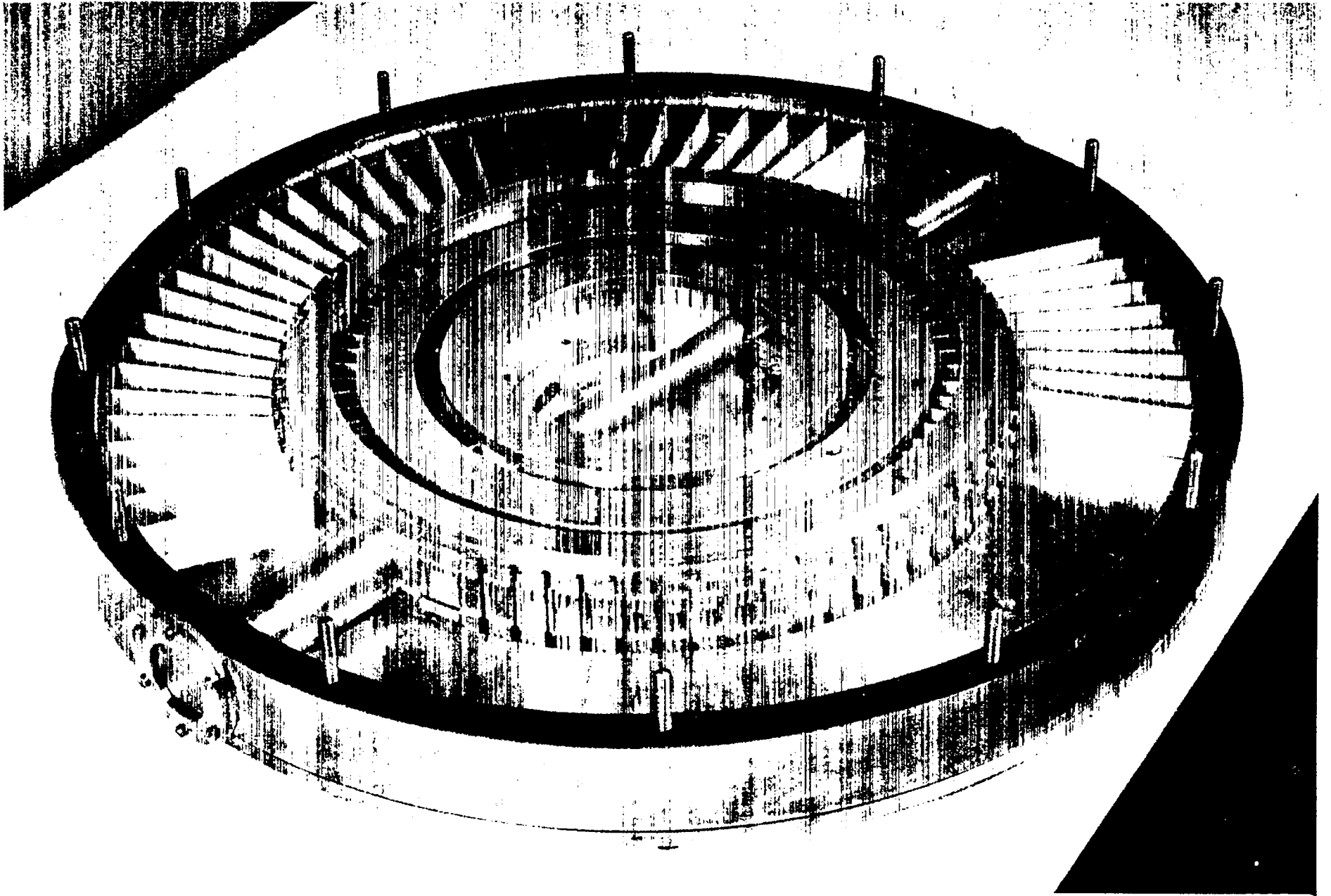
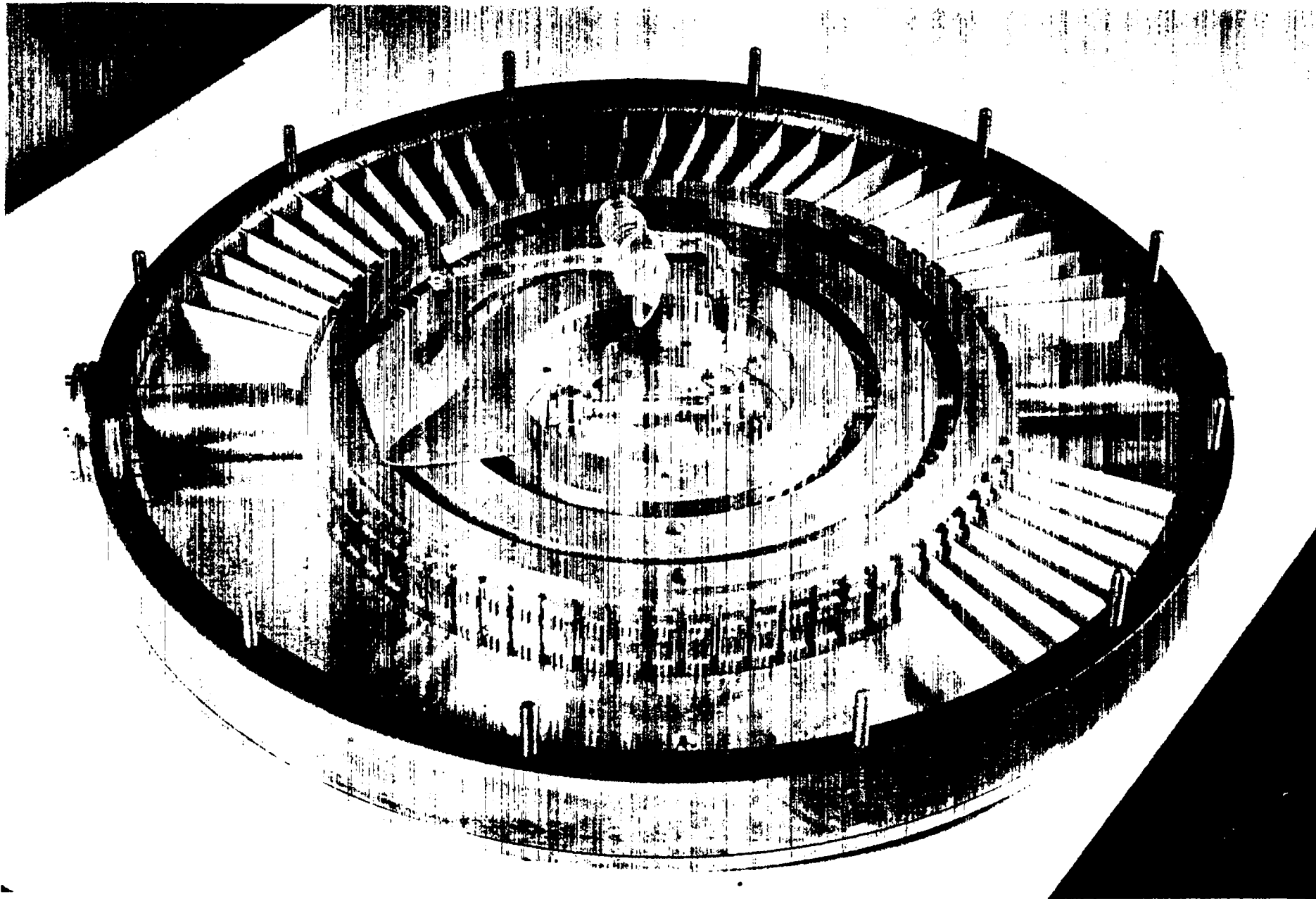


Figure 17

Multiplate Camera with Wide Angle Target in Position



at 2.5 degree intervals in the laboratory system. The laminated glass plate was then placed over the top of the reaction chamber and covered with black cloth. The cyclotron vacuum system, as well as the auxiliary vacuum system, was used to pump down the reaction chamber to a desirable pressure, the subsequent procedure being identical to that for the 90 degree gas target experiment.

An experimental difficulty encountered in the use of the multiplate camera which did not manifest itself in the case of the single plate cameras was some degradation of the cyclotron vacuum due to the water vapor given off by the photographic emulsions. Since it is required that the base pressure in the cyclotron tank be 2.5×10^{-5} mm Hg or less for stable operation, a small amount of water vapor in the vacuum system could have serious effects. It was found that pumping on the scattering chamber for a period of about two hours removed sufficient water vapor so that the above problem presented no serious difficulty.

Once the plates have been exposed in either of the camera setups, all that remains for a determination of the cross-section is a proper analysis of the plates. It is this phase of experiments done by the photographic method which in the past has been most subject to criticism. Doubtless this criticism has been justifiable at times, since for

one thing, the analysis of a plate, if it is not carefully done, could conceivably be a not completely objective procedure. A study of the literature reveals, however, that in cases where the criticism is justified, full advantage has not been taken of this method. A photographic plate contains a great deal more information than is generally recognized. Many more observations may be made on a photographic plate other than the simple counting of a number of tracks; if this is not done, full advantage is not taken of the data available. Let us now see how one takes optimum advantage of the information contained on a photographic plate.

From the geometry of the source of the particles, the two collimating slits, and the photographic plate detector, it is clear that the tracks of the reaction particles as they appear on the plate must start at the surface of the plate and proceed within defined angular limits both in depth and spread on the surface of the plate. This immediately insures that one is only observing tracks originating from the direction of the reaction volume defined by the particular set of slits under consideration. It is equally clear that, due to the fact that each part of the plate does not see the beam with equal efficiency, the density of the tracks along the length of the plate will vary

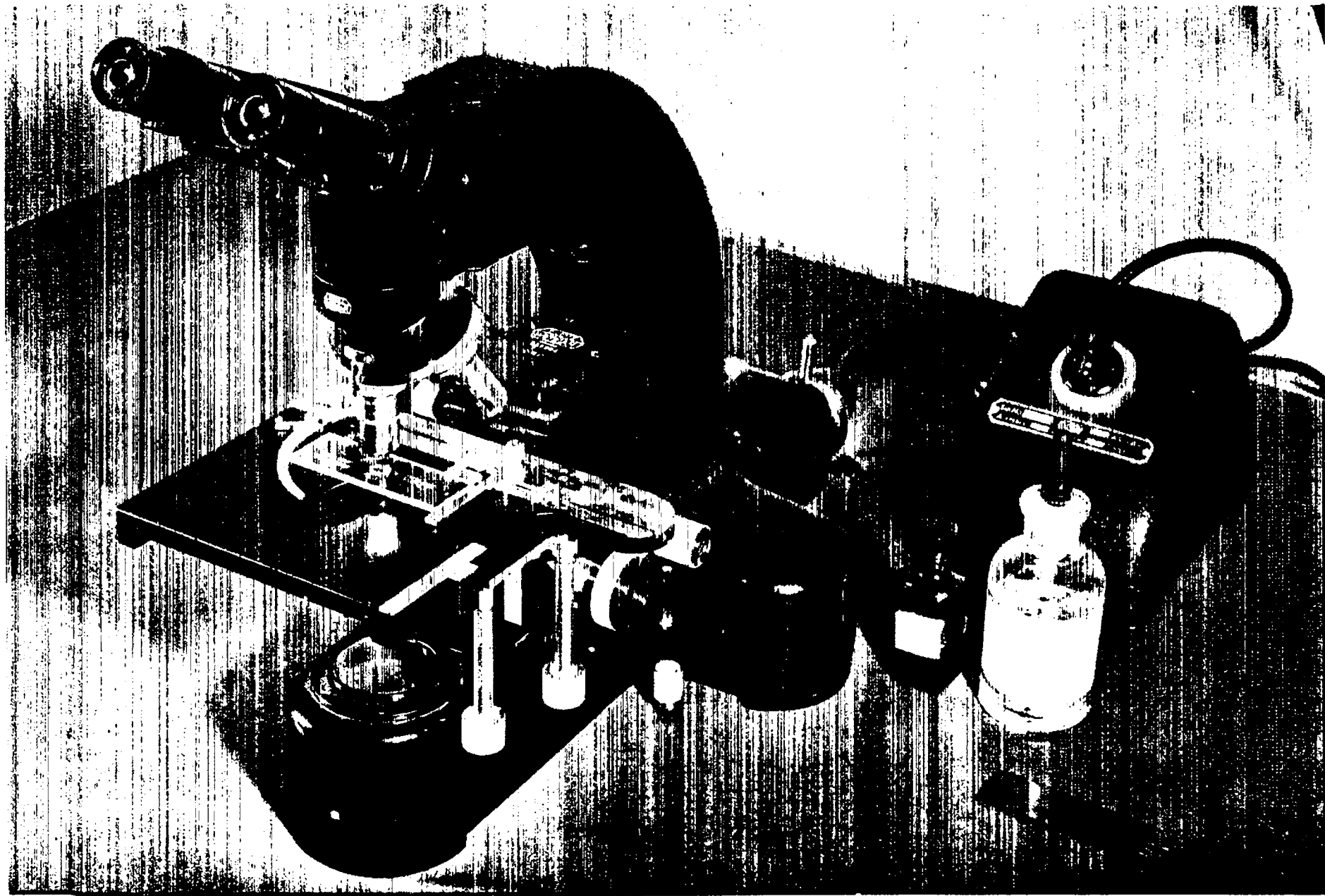
in a manner which can be inferred from the geometry. If, as in the present experiment, the slits are narrow enough, tracks will not be observed at either end of the plate. Thus, if we plot a curve of the density of the tracks along the length of the plate as a function of the length, this curve must have a peak at the position on the plate where the line through the centers of the two slits strikes the plate, and it must go to zero fairly rapidly in a manner determined by the angular resolution of the slits. Some of the reaction particles will be able to penetrate a small distance through the edges of one or the other of the slits. In this process, however, the reaction particle will lose energy and will appear as a shortened track in the emulsion. Slit scattering without penetration is a completely negligible effect. If we are to distinguish between tracks which pass through the two slits without penetration and those which penetrate the slit edges, it is necessary to plot a range vs. number curve for each angular region investigated or even for each individual plate if this seems desirable. Such a curve then permits us to determine precisely which tracks in the swath are produced by the reaction under consideration and pass clearly through the slit system. The track density vs. length curve is also very useful when tracks of low energy are being considered in that it tells whether or not the tracks which are being counted actually proceed from the target volume or are

spurious tracks, due to scattered deuterons from the primary beam or charged particles from neutron induced reactions in the slit edges, for example. Thus, the essentials of analysis of a plate are that the angular directions of the tracks be limited by proper considerations of the geometry of the experiment, that a track density vs. length curve be plotted for the tracks which are being measured, and that a range vs. number curve be obtained. If this is done we can be reasonably certain of obtaining data accurate to within the statistical accuracy of the number of tracks which are counted.

Analysis of the plates used in these experiments was done under magnifications of from 500 to 1000 diameters. The Leitz Ortholux microscope was used in these analyses. One of these microscopes is shown in Fig. 18. A reticule consisting of a large ruled square subdivided into 100 smaller squares, engraved on an optical glass disc, is placed in one of the ocular tubes of the microscope so that the image of the reticule appears in the same plane as the image of the tracks. It is this reticule which determines the width of the swath which is counted, since the observer counts only those tracks which begin within the vertical limits of the reticule as the field is seen in the microscope. Accurate measurement of the width of the swath is accomplished by the use of the stage micrometer, one of which may be seen on the stage of the microscope in Fig. 18. This stage micrometer has engraved on it

Figure 18

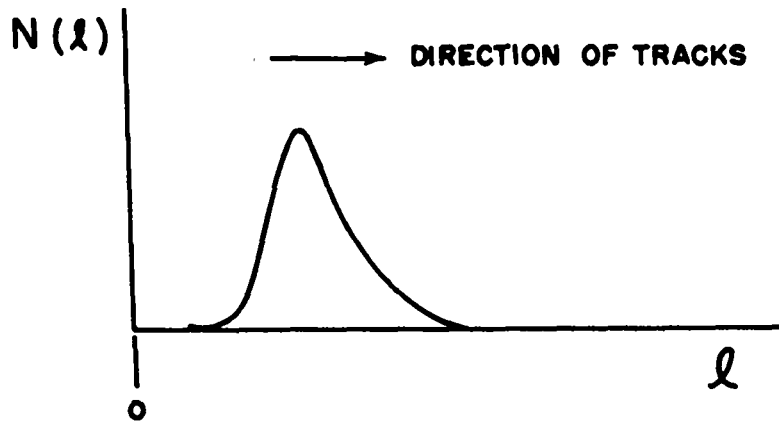
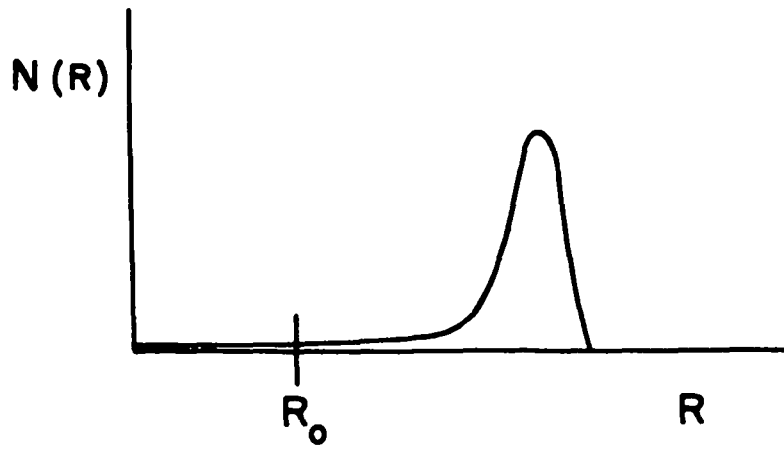
Leitz Ortholux Microscope



a series of lines, ruled 10 microns apart. The overall accuracy of these stage micrometers is about 0.2%. Calibration of the reticule is done by focusing on the stage micrometer and noting the number of 10 micron divisions which the eyepiece reticule covers on the stage micrometer scale. This measurement is repeated about 10 times using different portions of the stage micrometer to make the measurement. The calibration of the reticule also permits the rapid determination of the length of short tracks which fall within the reticule, the length of longer tracks being measured by means of the Vernier scales on the microscope stage.

In order to eliminate subjectivity due to observer bias the data of the present experiment were analyzed by 8 technicians. The analysis required the services of these 8 people working approximately 20 hours per week for 6 weeks. In the analysis of these plates a technician is first asked to measure the length of all tracks in a swath of known width which originate on the surface of the emulsion and proceed within a five degree rectangular pyramid in depth and width on the surface of the plate. From this preliminary analysis two curves may be drawn: a range vs. number curve, and a track density plot. Two such idealized curves are shown in Fig. 19.

The number of tracks represented by the area under the number vs. range curve from zero range to the beginning of



IDEALIZED RANGE VS. NUMBER AND
TRACK DENSITY VS. PLATE LENGTH CURVES

FIG. 19

the peak, when only one peak is present, is in general less than 10% of the number under the peak. After this curve is drawn, the technician is asked to count all tracks which satisfy the proper criteria as to direction and which, in addition, are longer than a certain minimum range, R_0 . The correction for tracks which are of length greater than R_0 but too short to fall in the main peak can be made accurately, since this correction is small and its relative value is known to better than 10% by virtue of the statistics of the range vs. number curve.

A second correction is required when the range of the reaction protons is such that they pass out of the bottom of the emulsion. This is due to the fact that some of these protons will have penetrated the slit edges to a small extent, enough that their ranges are reduced so that they would not fall in the main peak if their true range could be measured. The yield, Y , must therefore be reduced by the proper factor to correct for this effect.

If the material of the slits has a stopping power k relative to air, and if the slits are separated by a distance l , then to a good approximation the ratio of the number of particles degraded in energy by slit penetration to the total number of particles passing through the slits, including those which are degraded, is given by

$$\Delta = \frac{2 X_a}{k l}$$

where X_a is the range of the particles in air (See Appendix III).

It was found that the average effective thickness of the emulsions used at a grazing angle of 6° was 1800 microns. Y was therefore further corrected by the factor

$$\frac{X_a - 1800}{X_a} \Delta$$

for data at angles where the protons passed entirely through the emulsion. This correction was never greater than 2.2%, and was zero at laboratory angles greater than 90° , since practically all of the tracks remained in the emulsion for these angles.

The plot of track density vs. length of the plate serves as a check that all of the tracks being counted come from the target, and shows as well whether or not all of the particles which pass through the slits strike the photographic plate. If a thick absorber is used in front of the plate, the spread may be such that some of the tracks fall off of the plate and a suitable correction may be necessary. However, no data are given for which thick absorbers were used.

Figure 20 illustrates the position of the tracks on a photographic plate which was exposed in the multiplate camera. This plate was at an extreme forward angle and was exposed to deuterons scattered from deuterium gas in the camera. The tracks go toward the end marked -2. This plate is greatly

Figure 20

Plate Exposed in Multiplate Camera Showing
Variation of Track Density with Length.



overexposed and is not suitable for analysis. However, it shows the variation in track density with length along the plate remarkably well. This photograph was made by projecting the plate itself as a negative in an enlarger, which is the reason that the central patch of tracks appears light.

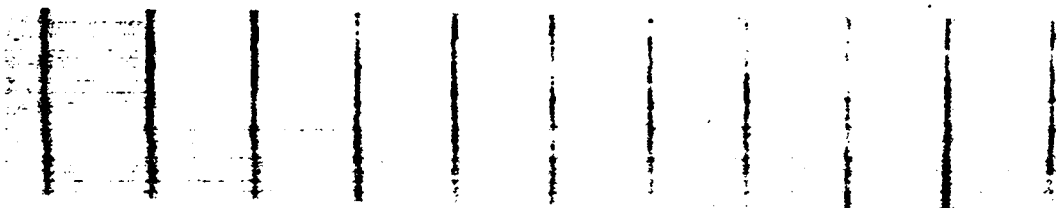
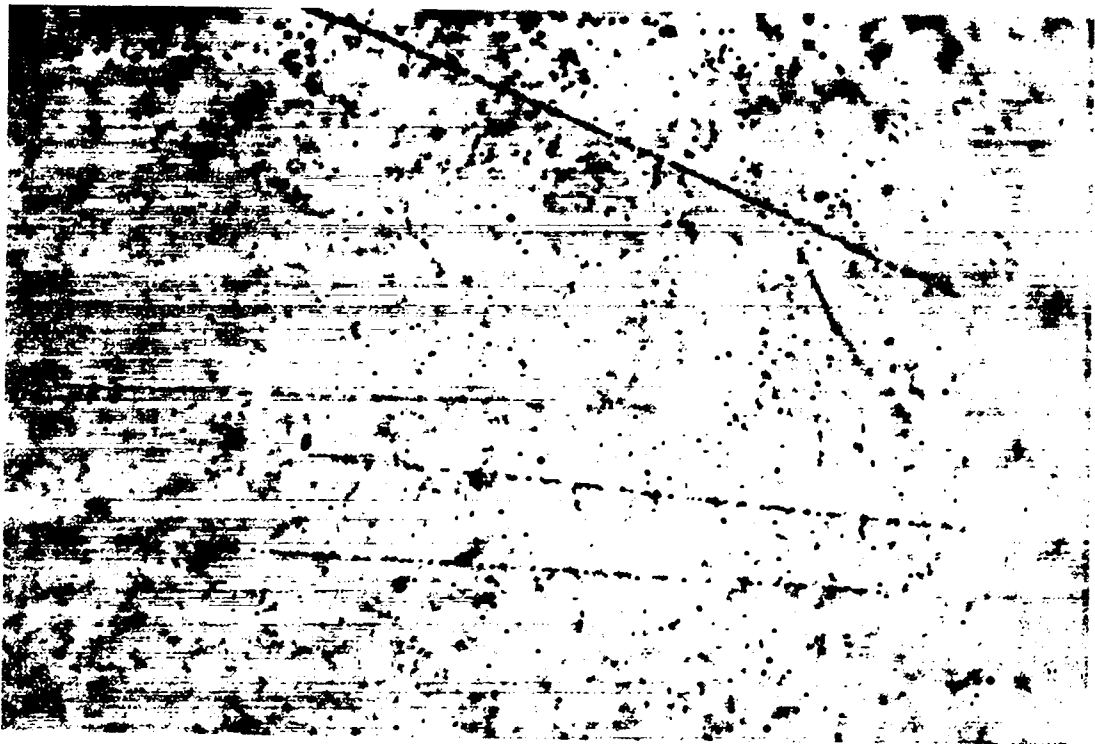
Figure 21 is a composite of three photographs made with the Vickers projection microscope. The top photograph shows the surface of the emulsion of a plate exposed at 45° laboratory system in the multiplate camera. The long, tenuous tracks are the high energy protons from the $\text{He}^3(d,p)\text{He}^4$ reaction. The shorter tracks are deuterons which have been scattered elastically from He^3 . All tracks go from right to left in the picture.

The lower photograph shows the protons from the same reaction at a laboratory angle of 120° . Note that the deuteron tracks do not appear. The upper track is due to a degraded proton which penetrated the edge of one of the slits. Since it makes an angle greater than 5° with the longitudinal axis of the plate, it would not have been counted in the analysis of the plate. Actually the total length of this degraded track was about 300 microns so that it would not have been counted for this reason also.

The series of lines at the bottom of Figure 21 is a section of a stage micrometer, photographed at the same magnification as was used for the pictures above. The spacing

Figure 21

Composite Photomicrograph of Tracks at 45° and 120° ,
with Stage Micrometer at the same magnification.



between lines is 10 microns, the magnification being 1350 diameters.

According to Critchfield's formula the differential cross section per unit solid angle for a given reaction is

$$\sigma(\theta) = \frac{Y}{N n_0 I}$$

where $I = \frac{4abwf}{L l \sin \theta}$

$$f = 1 - \frac{a^2 + b^2}{2l^2} - \frac{P a^2 + Q b^2}{3l^2} \cot \alpha + \frac{P^2 a^2 + Q^2 b^2}{3l^2}$$

$$P = \frac{m(\cot \alpha - \cot \theta)}{L}$$

$$Q = \frac{(m+l)(\cot \alpha - \cot \theta)}{L}$$

In the discussion above we have shown how the quantity Y , the corrected value for the number of tracks observed in a swath of known width, is determined. The factor I contains quantities which are determined completely by the geometry of the experiment, as for instance the separation and widths of the slits, the swath width and other factors which can be measured directly. Let us now consider the method of determination of the quantities N and n_0 .

The calibration of the electronic current integrator has been described earlier in this chapter. There was shown the method by which one obtains an absolute calibration in terms of the amount of charge collected on the Faraday cup per scaling pulse produced by the current integrator. If the number of pulses produced by the current integrator is recorded on a scaling circuit during a particular run, the total integrated charge will be known. Therefore all that is necessary to compute N is a knowledge of the charge per deuteron. Since the cyclotron produces an atomic beam of deuterons, this charge is simply e , the electronic charge. Thus, N may be computed by dividing the total charge accumulated by the charge per particle, e .

The determination of N by a charge measurement assumes that the beam is composed entirely of singly charged atomic deuterium ions. It is not, of course, entirely certain that all deuterons which strike the Faraday cup are charged or even

that the beam is not in part composed of singly charged deuterium molecules. This possibility seems remote in the face of certain experimental evidence, however. First, the cyclotron is by nature a mass spectrograph and will accelerate only ions having the e/m for which it is tuned. This precludes acceleration of all ions except D^{2+} and He^{4++} . The beam is "analyzed" by the focus magnet, in that particles lacking the proper e/m will not be deflected toward the Faraday cup. Recombination must therefore occur in the interval of the passage of the deuterons from the focus magnet to the Faraday cup if any error in the measurement is to be incurred.

When the energy of the beam is measured by the magnetic deflection method, the beam is again effectively analyzed. If as much as 10% (or possibly less) of the total beam were uncharged or singly charged deuterium molecules, this fact would be made evident by the appearance of a second spot on the fluorescent screen on which the deflection of the deuteron beam is measured. This effect is not observed. Since the deuteron beam travels the order of twice as far to the fluorescent screen as to the Faraday cup, the chance of recombinations occurring is further reduced.

Another check on the accuracy of the current integrator was made by members of the Los Alamos cyclotron group.²⁴

²⁴

K. W. Erickson, J. L. Fowler, and E. J. Stovall, Jr.
Phys. Rev. 76, 1141 (1949).

In this experiment the heating effect of the deuteron beam on a gold and copper block was measured, the beam being monitored by observation of the He^3 particles produced by the $\text{D(d,n)\text{He}^3}$ reaction. The energy measurement of the beam entered into the calculations as well. As a result of this experiment the probable error assigned to the current integrator measurements was 2.5%, which is the value used in this report.

The possibility of the presence of He^{4++} in the beam is also precluded by the above arguments, since the energy of an alpha particle accelerated by the cyclotron would be 20 Mev. This larger energy would show its effect in the heating of the gold and copper block if He^4 were present in the beam. In addition, it is known that the deuterium gas which is used to supply the ion source of the cyclotron contains the order of 1% impurities, principally hydrogen, nitrogen, and oxygen. The possible maximum contamination with He^4 is probably much less than 0.1%. This would introduce an error negligible compared with other experimental errors. The possibility of He from the atmosphere entering the cyclotron tank, appearing in the arc source, and being accelerated seems equally remote.

In the formula for the cross section n_0 represents the number of target nuclei per unit volume. This quantity may be computed using the universal gas law, if the pressure and temperature at the time of filling the target are known.

Since the target is sealed at the time of its filling, changes in temperature do not affect the number of particles per unit volume. Due to the fact that only a limited quantity of gas was available in the case of He^3 and tritium fillings of the target, and since it was desired to use all of the gas in the target rather than as a part of a pressure measuring system, a less direct method was chosen for the measurement of the quantity n_0 .

In this method it was first necessary to measure accurately the volume of the target. To make this measurement the target was filled with He^4 to a pressure approximately that to be used in the target when it was filled with He^3 or tritium. This filling was done with a mercury manometer connected to the system in order that the pressure of the He^4 in the gas target could be measured. After filling the target the stopcock on the filling lead was closed and the remainder of the system evacuated. Then the gas in the target was transferred to a standard volume by means of a Toepler pump and the pressure of the He^4 in the standard volume measured (see Chapter IV). The temperatures of the gas in the target at the time of filling and in the standard volume were also recorded. Application of the universal gas law then permitted the computation of the volume of the gas target up to and including the bore of the stopcock.

During the filling of the target with either He^3 or tritium

the gas sample was placed in the same standard volume and its pressure and temperature measured. The volume of the sample then was reduced to NTP conditions. It is clear that n_0 is then given by the expression

$$n_0 = \frac{K A v}{V_s V_t}$$

where n_0 is the number of atoms per cc, K is the number of atoms per molecule, A is Avogadro's number, $V_s = 22.4$ liters = volume of a standard mole of gas, v_g is the NTP volume of the gas sample, and V_t is the target volume.

Since the geometry of the multiplate camera is accurately and rigidly fixed one may safely assume that, for any given run, the relative values of the differential cross sections must of necessity be reproducible within the statistical accuracy of the measurements, and this was found to be the case. There remains, however, the possibility of making errors in the determinations of the quantities N and n_0 defined above. In order to check on these quantities the cross section obtained at 90° with the small target was compared with the corresponding cross section obtained with the multiplate camera. This also served as an internal check on the effect of scattering by the walls of the target used with the large camera.

The energy of the cyclotron beam was measured immediately prior to and following the experiment and determined the range

of protons and deuterons scattered by the deuterons of the primary beam. This energy was found to be 10.7 Mev before the He^3 and T experiments and 10.95 Mev after these experiments. These values must, of course, be corrected for energy loss in the target windows used in various experiments. The average value, 10.8 Mev, agrees well with the observed range of the protons from the $\text{He}^3(d,p)\text{He}^4$ reaction at the angles where the protons were stopped in the emulsion.

CHAPTER VII

DIFFERENTIAL CROSS-SECTION OF THE REACTION $\text{He}^3(d,p)\text{He}^4$

The data obtained in this experiment are summarized in Figure 22, which shows the differential cross section for the reaction $\text{He}^3(d,p)\text{He}^4$ in the center of mass system as a function of center of mass angle for a bombarding energy of 10.2 Mev. Since the behavior of the curve near 0° and 180° is not known, it is not possible to give an accurate value for the total cross-section. The axial symmetry of the reaction makes the integral for the total cross-section.

$$\sigma_T = 2\pi \int_0^\pi \sigma(\Omega) \sin \Omega \, d\Omega$$

It is seen that the effect of $\sin \Omega$ is to make variations near the end of the curve relatively less important in the integral. If a reasonable guess is made for the shape of the ends of the curve, integration at 10° intervals by the trapezoidal rule gives $\sigma_T = 43$ millibarns; however, this value may be incorrect by as much as 20%.

No tracks were observed on the plates of the various background runs (H^3 and He^4 target gases) which satisfied the proper angular criteria and were of a length sufficient to fall in the range of the proton peaks for the $\text{He}^3(d,p)\text{He}^4$ reaction. This indicates that tracks counted as protons for the He^3 runs were due entirely to the $\text{He}^3(d,p)\text{He}^4$ reaction.

Figure 22

Differential Cross Section of the Reaction
 $\text{He}^3(d,p)\text{He}^4$ at 10.2 Mev Bombarding Energy.

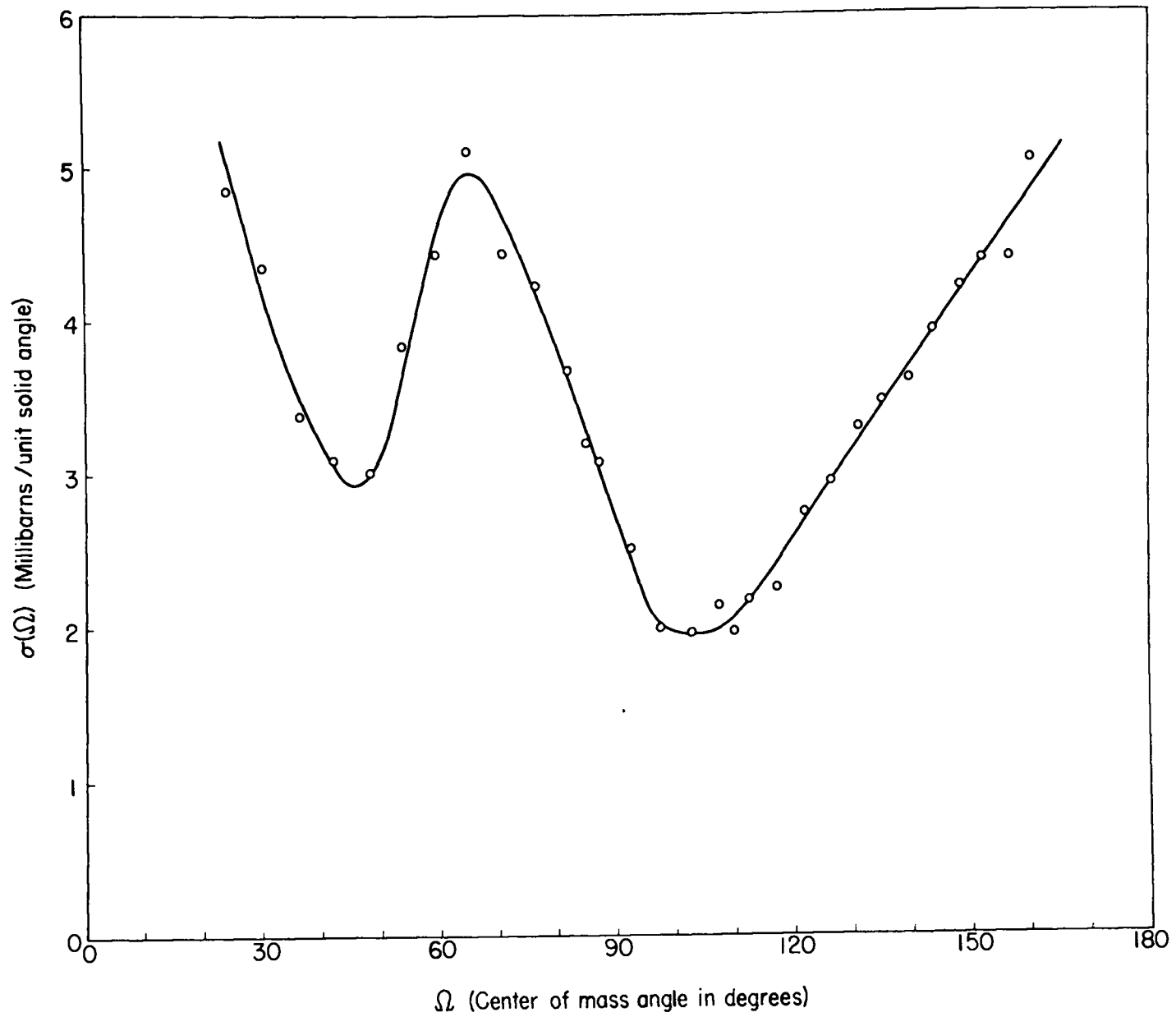
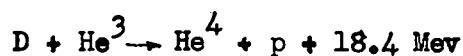


FIG. 22

Typical range analyses and track density distributions for laboratory angles of 60° and 135° are shown in Figure 23. These may be compared with the idealized curves of Figure 19. It may be noted that the background tracks amount only to a few percent of the total number of tracks in the peak. Part of this background may be due to other reactions which may occur when He^3 interacts with deuterons, as discussed below. It is important that the track density curve goes to zero well within the limits of the plate length, as shown in Figure 23.

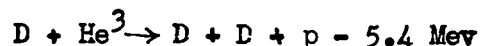
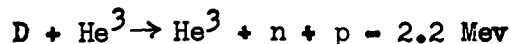
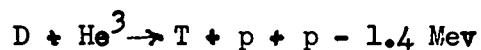
The track lengths as plotted on the range vs. number curves are as measured on the microscope stage vernier, uncorrected for the shortening effect of the penetration of the tracks into the emulsion. These lengths are therefore $R \cos \alpha$ (see Chapter II and Appendix II), where R is the true range of the tracks in the emulsion.

Besides the exoergic reaction

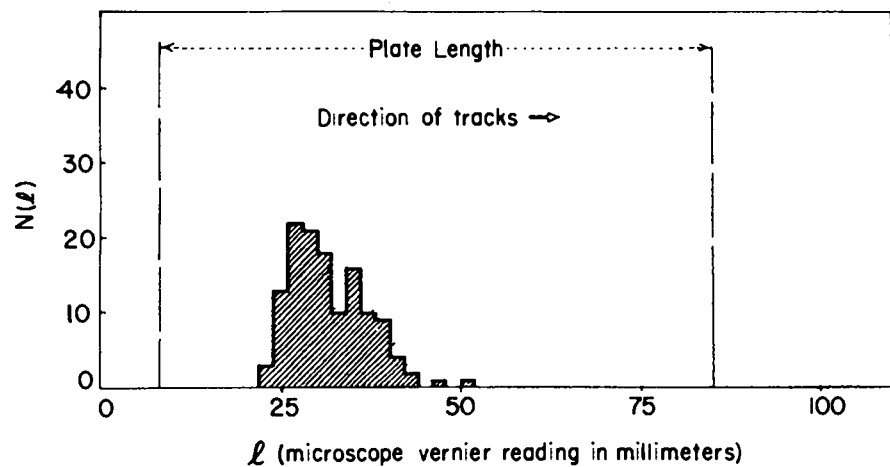
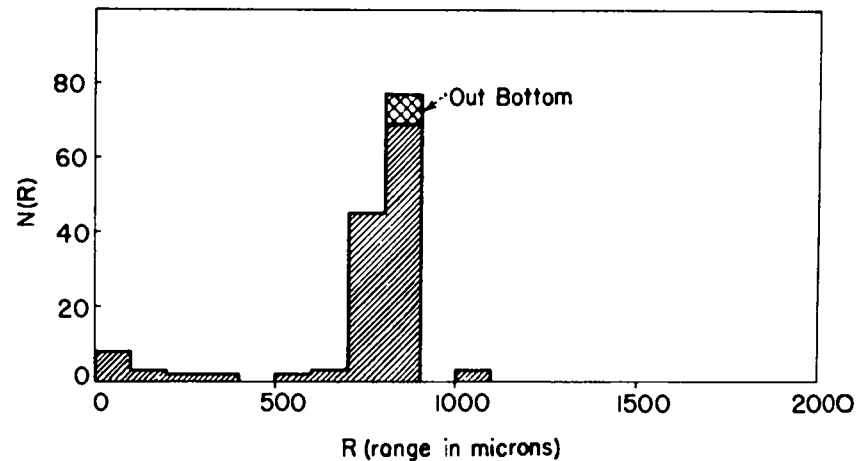
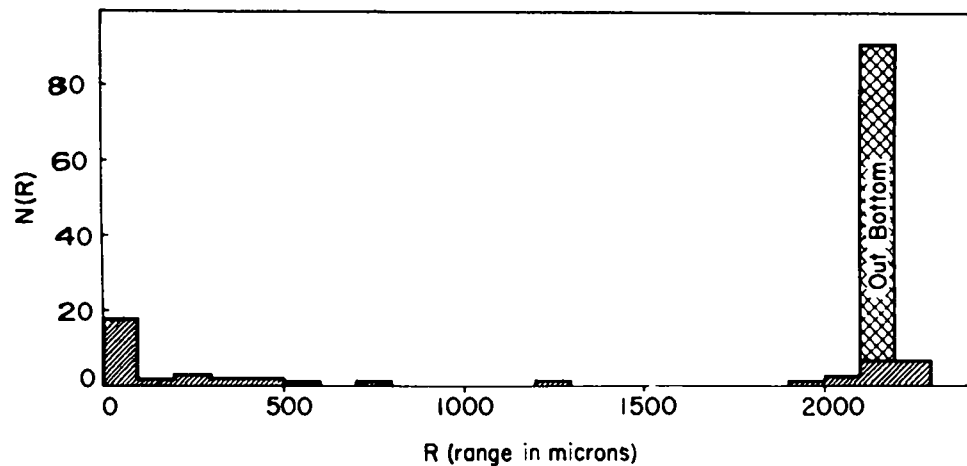


it is conceivable that any or all of three other possible reactions may occur when He^3 is bombarded with 10 Mev deuterons.

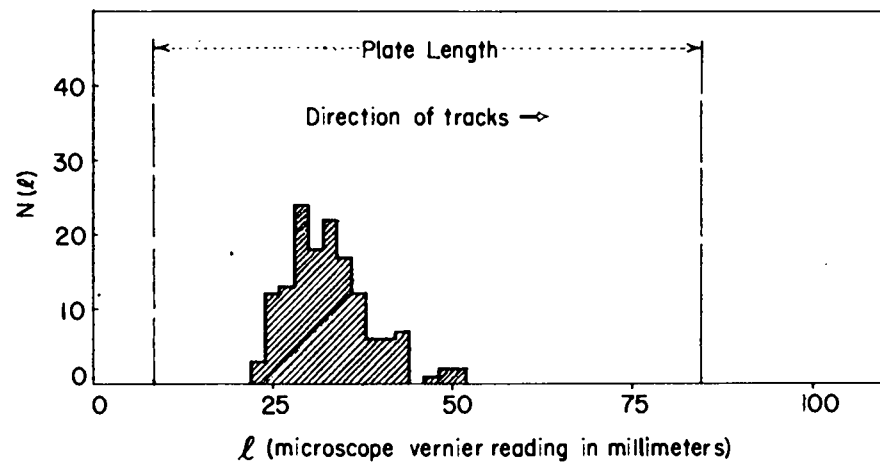
These are



all of which are endoergic. All are energetically possible at



$\phi=60^\circ$, 130 tracks



$\phi=135^\circ$, 144 tracks

Typical Range vs. Number and Track Density vs. Plate Length Plots

FIG. 23

this bombarding energy, since the kinetic energy of the center of mass system is only 4 Mev. Since these are three-body disintegrations there would be no definite correlation between angle and energy for any of the reaction products, making it difficult to determine which, if any, of these reactions might occur. Even if the reactions go, their cross-sections would reasonably be expected to be much smaller than that of the exoergic reaction. It is significant, however, that the possibility of these reactions exists and that they might therefore contribute to the background of low energy particles observed. In no case would any of the particles have enough energy to become a part of the proton peaks on which the measurement of the differential cross-section of the $\text{He}^3(d,p)\text{He}^4$ reaction is based.

Values of the cross-section are tabulated in Table A, together with the corresponding laboratory angle and the differential cross-section in the laboratory system. Table B gives the yield per micron swath width for some typical angles of observation and indicates the order of magnitude of the corrections applied to correct for background and slit penetration. Table C shows the computation of N , the integrated deuteron flux, for one set of data. In Table D the calculation of n_0 , the number of reaction centers/cm³, is shown for the wide angle dural gas target. This calculation is essentially the same for the 90° target, except for the difference in target volumes. Table E gives the important geometrical dimensions of the multiplate camera.

The values of the cross-sections at 90° measured with the single plate cameras and the multiplate cameras are 1.87 and 1.96 millibarns, respectively, in the center of mass system. The 4.7% difference is well within the overlapping errors of the two measurements. This constitutes an excellent internal check of the consistency of the data.

On the average, 954 tracks were counted for each point on the curve, giving an average statistical accuracy of 3.2%. The smallest number of tracks counted at one point was 769 (at 85° lab) and the largest 1137 (at 70° lab). Other errors in the various quantities occurring in the cross-section formula are estimated to be as follows:

Y (excluding statistical error)	2.0%
a,b	0.5%
w	0.1%
L,l	0.1%
N	2.5%
n_0	1.0%
	<hr/>
r.m.s. measurement error	3.5%

The factor f in the cross-section formula is very nearly unity, and its value is computed to better than 0.1%.

The errors listed above, except that for Y, enter only into the absolute error for the cross-section. That is, the relative values of the cross section given by the curve should be

accurate within the r.m.s. error due to the statistical and interpretation errors in Y, which is 3.8%.

The total r.m.s probable error for the cross-section curve is estimated to be 4.7%, based on the average probable statistical error of each point and the r.m.s measurement error as shown above.

At the end of a series of scattering experiments the position of the darkened spot on the rear window of the camera was measured and found to be displaced 0.098 inch from the center line of the camera toward the left looking in the direction of the beam. This represents an average position of the deuteron beam in the camera over a period of about two weeks and does not necessarily mean that the beam was in this position for the $\text{He}^3(d,p)\text{He}^4$ experiment. The angle represented by this displacement of the beam over the diameter of the camera is 0.28° . Since the angular resolution of the slit systems is 1.73° and since the spread of the deuteron beam is limited only to 1.2° total width by collimating slits in the tube between the focus magnet and the scattering chamber (see Figure 11), an angular variation of 0.28° would not be resolved in the cross-section measurement.

For this reason no direct correction has been made to the angular measurements or to the values of the differential cross-section given in Table A. However, since ϕ enters into the

cross-section formula as $\sin \phi$, and into the conversion into center of mass coordinates in the factor $\frac{I}{I} \left(\frac{r}{\phi} \right)$, it is necessary to investigate the effect of a variation in the angle of observation on the computed cross-section values. (The notation here is that of Appendix I.)

The correction in $\sin \phi$ will amount to 1.4% for $\phi = 20^\circ$ and 0.001% at $\phi = 90^\circ$. Since $\frac{I}{I} \left(\frac{r}{\phi} \right)$ varies very slowly with ϕ (see Appendix I) the second correction is negligible for all ϕ . $\frac{I}{I} \left(\frac{r}{\phi} \right)$ is as well a function of the bombarding energy, E_0 , and varies the order of 0.3% for a variation of E_0 of 0.1 Mev in the vicinity of 0° and 180° . Near 90° lab this variation is zero. In order to take into account these possible sources of error, the overall probable error of the curve must be increased to 4.9%.

The error in the cross-section measurements caused from Rutherford scattering of the reaction protons by the walls of the cylindrical target can only be appreciable in angular regions where the second derivative of the cross-section curve is large in the laboratory system. This effect was computed for the minimum at 40° lab and found to be of the order of 0.1% at this angle. This error is negligible compared to other experimental errors. A second effect of Rutherford scattering by the target walls is to decrease the effective angular resolution of the measurements. This decrease in resolving power varies with

the angle of observation, since the scattering is a function of the energy of the protons. It amounts to an increase in the angle of resolution of the order of 2° or less for all angles of observation. Taking into account the resolution of the slit systems in the multiplate camera and the spread of the beam, it is estimated that variations of the cross-section over angular regions of 3.5° or less would not have been resolved in these measurements.

TABLE A

Measured Cross-Sections as Function of Angle
 in Laboratory and Center of Mass Systems
 at 10.2 Mev Bombarding Energy

ϕ	$\sigma(\phi)$	Ω	$\sigma(\Omega)$
20	6.88	24.3	4.85
25	6.09	30.2	4.35
30	4.66	36.3	3.38
35	4.19	42.0	3.09
40	4.01	48.1	3.02
45	5.01	53.6	3.84
50	5.63	59.7	4.44
55	6.31	65.0	5.11
60	5.32	71.0	4.44
65	4.93	76.7	4.23
70	4.14	82.0	3.68
72.5	3.55	85.0	3.20
75	3.36	87.3	3.08
80	2.64	92.5	2.51
85	2.02	97.4	1.99
90	1.92	102.7	1.96
95	2.02	107.2	2.14
97.5	1.83	109.7	1.97
100	1.98	112.5	2.18
105	1.97	117.1	2.25
110	2.33	121.9	2.75
115	2.41	126.4	2.95
120	2.61	131.0	3.30
125	2.66	135.1	3.47
130	2.68	139.7	3.61
135	2.84	143.5	3.93
140	2.96	148.1	4.21
145	3.02	151.9	4.39
150	2.96	156.3	4.40
155	3.34	160.0	5.05

Angles in degrees; cross-sections in Millibarns/unit solid angle.

TABLE B

CORRECTIONS FOR SLIT PENETRATION

ϕ (Degrees)	$\frac{Y}{W}$ (Uncorrected) <u>No. Tracks</u> Micron Swath Width	R_o (Micron)	Slit Penetration from Range- Number Curve %	Additional Slit Penetration Corrected (Calculated) %	$\frac{Y}{W}$ (Corrected) <u>No. Tracks</u> Micron Swath Width
30	0.707	1000	0.8	1.8	0.689
45	1.142	600	7.2	1.3	1.046
60	0.926	1400	1.0	0.9	0.908
90	0.299	600	6.6	0	0.281
120	0.449	600	1.2	0	0.444
150	0.915	300	4.6	0	0.873

TABLE C

Current Integrator Calibration:

I ($\mu a.$)	0.1767	0.1297	0.0909	0.0641
Counting Rate (Counts/Min)	97.5	71.0	49.0	33.5

$$\text{Average Counting Rate For Run} = 32.0 \frac{\text{Counts}}{\text{Min}} = 0.533 \frac{\text{Counts}}{\text{Sec}}$$

From Plot Of Current Integrator Calibration,

$$I = 0.605 \mu a. \text{ for } 32.0 \frac{\text{Counts}}{\text{Min}}$$

Then

$$0.533 \text{ Count} = 0.0605 \mu a \text{ sec} = 0.0605 \mu \text{Coul}$$

$$1 \text{ Count} = 0.113 \mu \text{Coul}$$

$$\text{No Counts For Run} = 1280$$

$$q = \text{Total Charge} = 1280 \times 0.113 \mu \text{Coul} = 144.6 \mu \text{Coul}$$

$$N = \frac{q}{e} = \frac{144.6 \mu \text{Coul}}{1.602 \cdot 10^{-13} \frac{\mu \text{Coul}}{\text{Deuteron}}} = 9.03 \cdot 10^{14} \text{ Deuterons}$$

TABLE D

NTP Volumes of Gases for Various Runs

Run No.	Vol (NTP cm ³)	Gas	Target	Windows
1	4.84	He ³	90°	Nylon
2	5.18	87% T ₂ - H ₂	90°	Nylon
3	5.81	He ³	90°	Dural
4	5.34	87% T ₂ - H ₂	90°	Dural
5	7.29	He ³	Wide Angle	Dural
6	7.29	72% T ₂ - H ₂	Wide Angle	Dural

Volume of 90° Target = 7.18 cm³

Volume of Wide Angle Target = 11.03 cm³

For Run 5

$$N_0 = \frac{6.023 \cdot 10^{23} \text{ Nuclei}}{2.24 \cdot 10^4 \text{ cm}^3} \cdot \frac{7.29 \text{ cm}^3}{11.03 \text{ cm}^3}$$

$$N_0 = 1.777 \cdot 10^{19} \frac{\text{Nuclei}}{\text{cm}^3}$$

TABLE E

Multiplate Camera Geometry

$$a = b = 0.0225 \text{ inch}$$

$$n = 2.997 \text{ inch}$$

$$l = 2.972 \text{ inch}$$

	$\alpha = 6^\circ$	$\alpha = 11^\circ 46'$
L	7.378	7.520
m	1.409	1.551

For Angles of Observation Which Are Integral Multiples of 5° , $\alpha = 6^\circ$; For Multiples of 2.5° , $\alpha = 11^\circ 46'$.

CHAPTER VIII

RESULTS OF SEARCH FOR EXCITED STATE IN He^4

If an excited state in the residual He^4 nucleus in the $\text{He}^3(d,p)\text{He}^4$ reaction exists within the energy limits detectable in this experiment, the effect of this excited state should be to produce a low energy group of protons. A range analysis of various plates has been made for tracks of low range at favorable angles of observation in order to investigate this possibility. For comparison with the D-He^3 interaction, deuteron bombardments of T_2 and He^4 were made under the same conditions as used for the He^3 observations, and range analyses were made for the low energy particles resulting from these interactions as well.

Figure 24 shows the range distribution resulting from the D-He^4 bombardment at 90° with nylon windows. The peak of the curve is at 21 microns. Since the air equivalent of the target windows, target gas, and camera windows for this run was 6.4 ± 0.5 cm, the energy of this group, which consists of deuterons scattered by He^4 , appears to be 3.3 Mev as computed from the range-energy relations. For this exposure double nylon windows having a total air equivalence of 9.6 cm were used in the beam ports of the 90° target and the energy of the deuteron beam was reduced to 10.0 Mev. The energy of 10.0 Mev deuterons scattered elastically from He^4 at 90° lab is calculated to be 3.3 Mev, in agreement with the value given above.

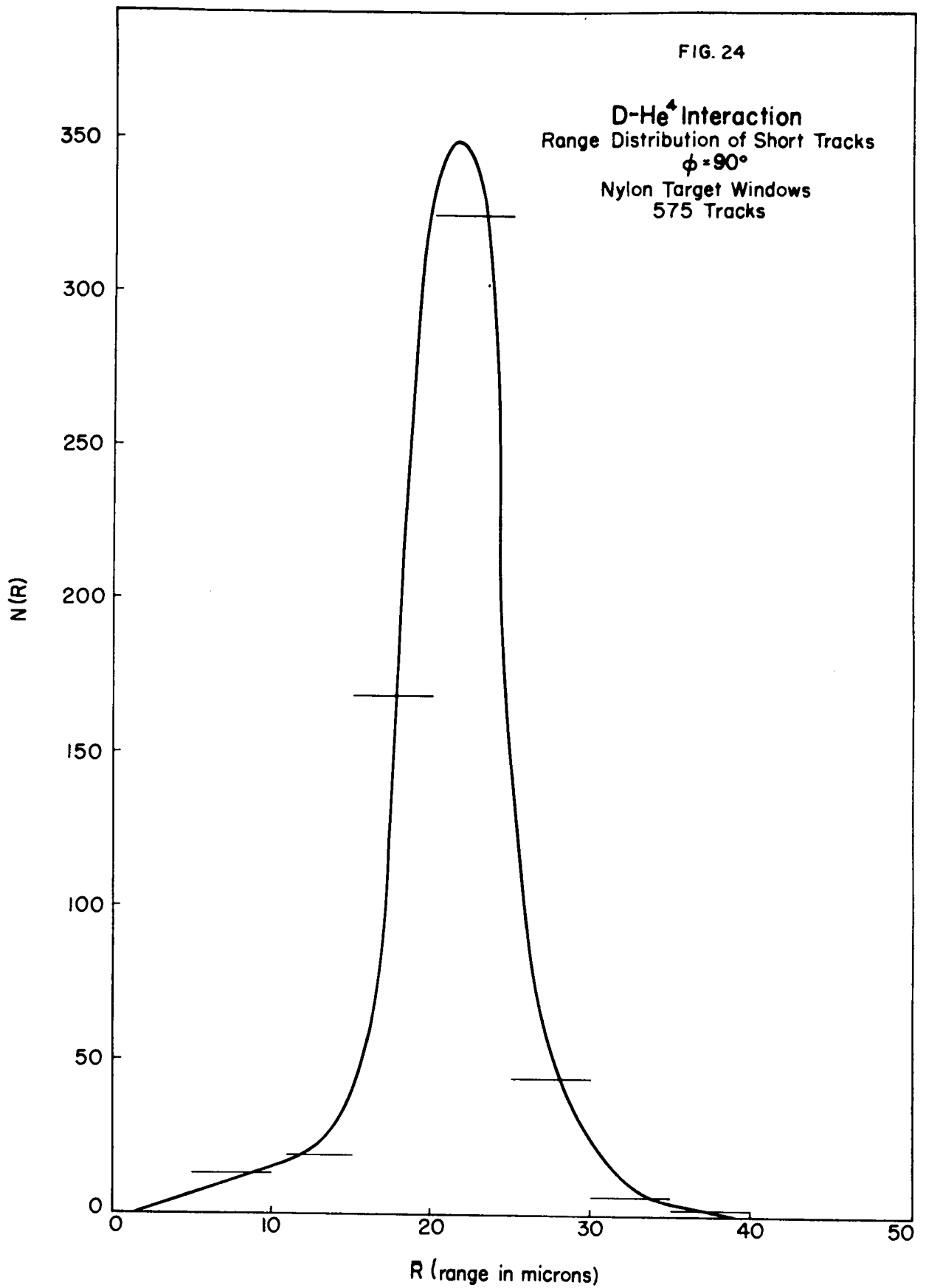
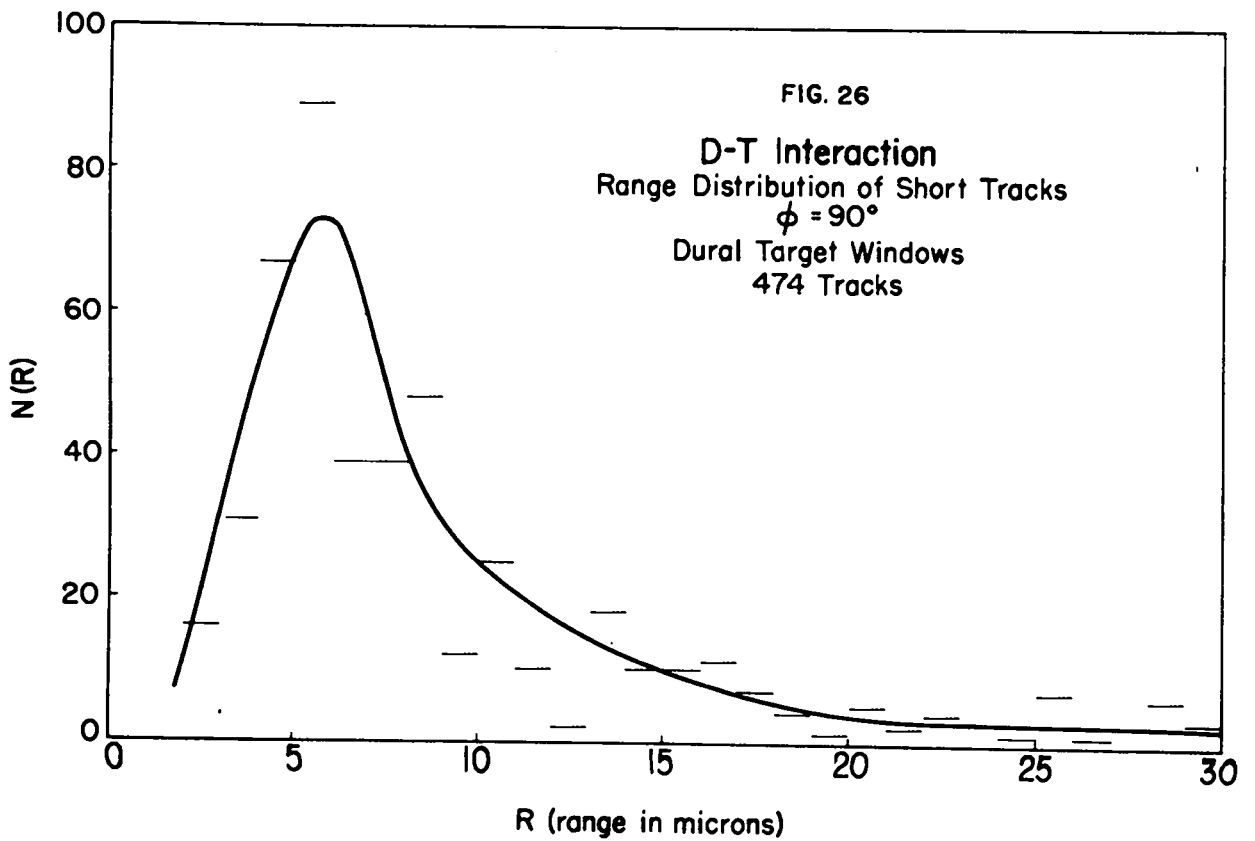
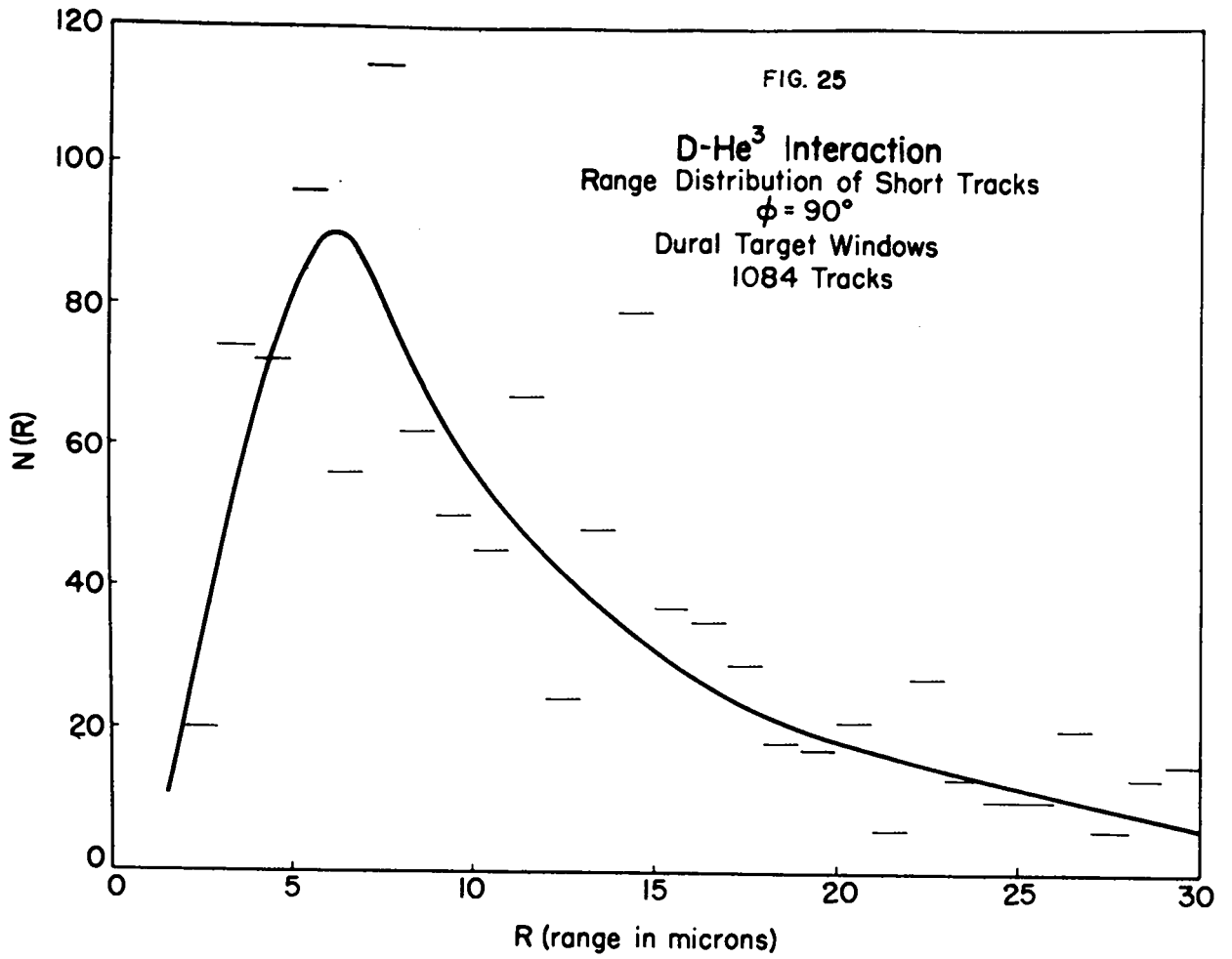


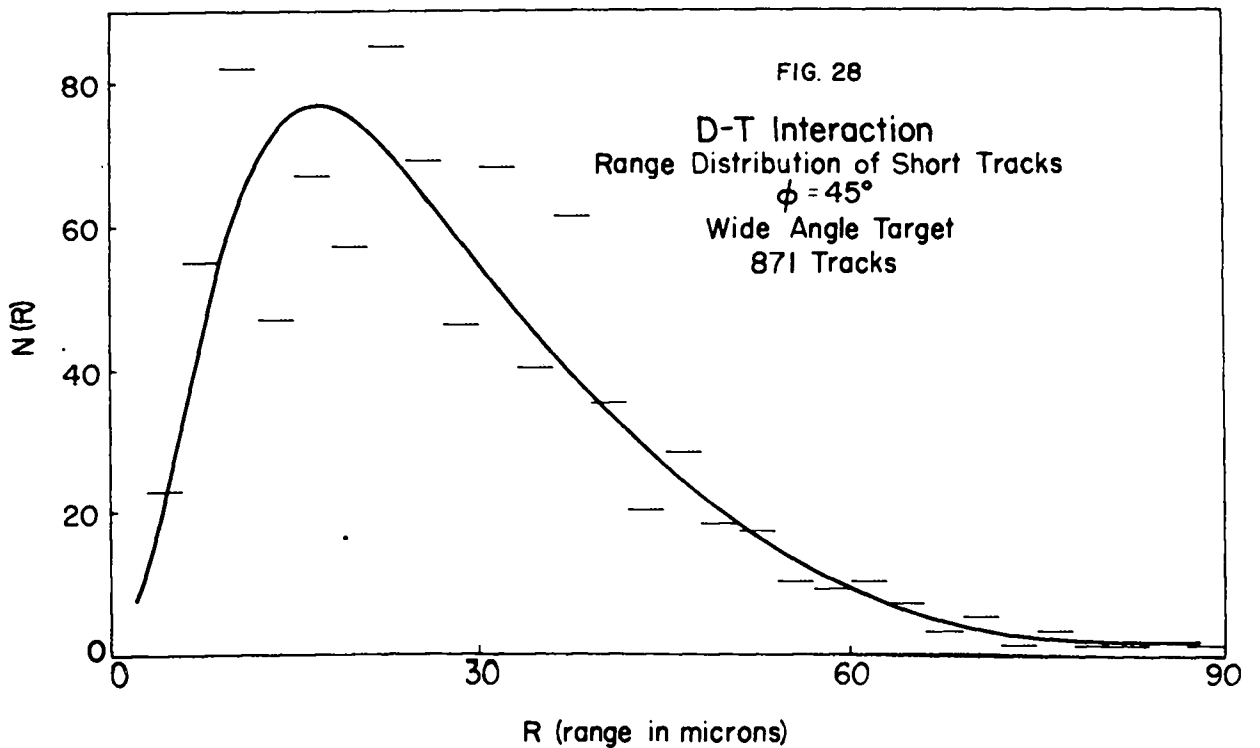
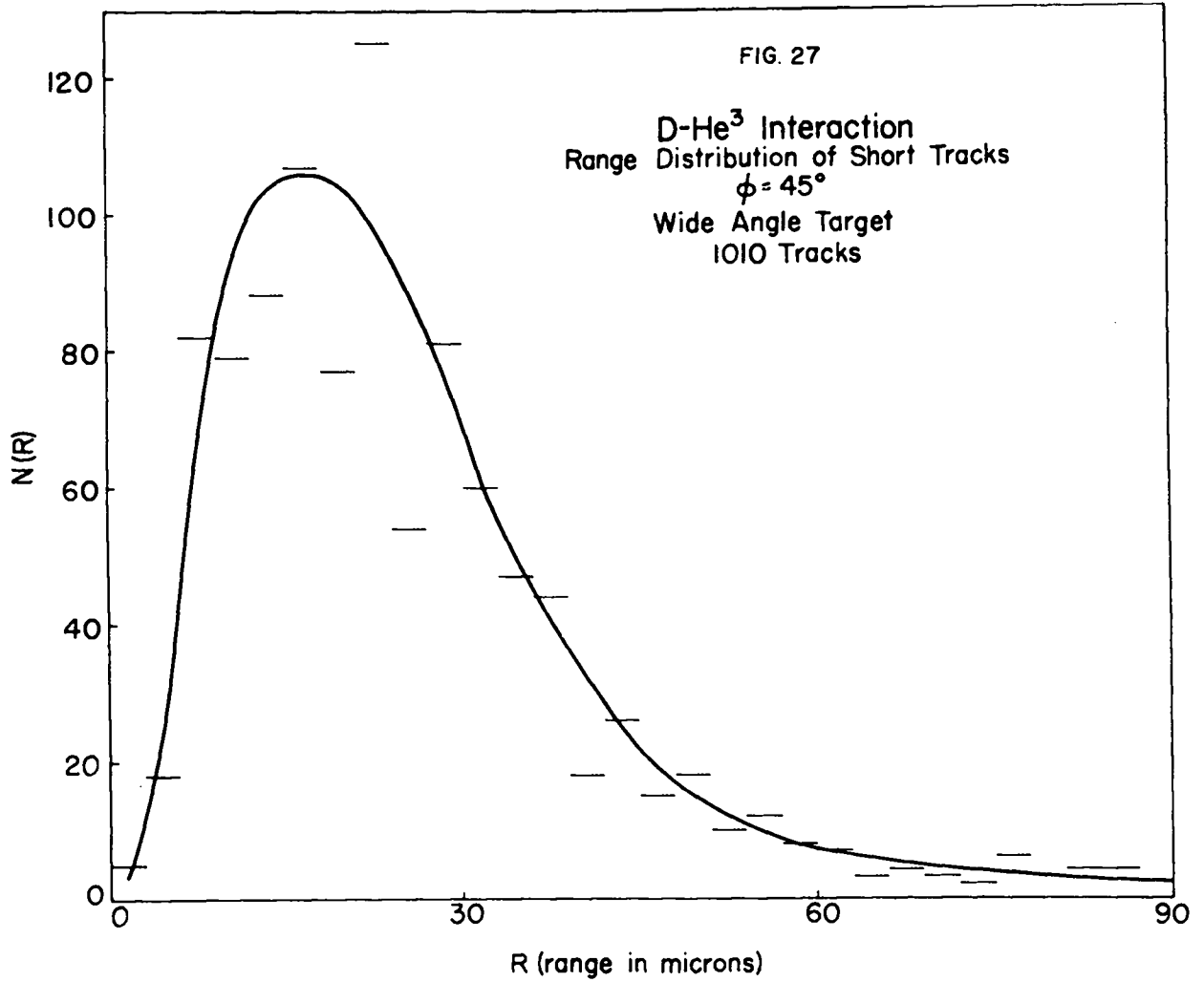
Figure 25 shows the range distribution of short tracks resulting from the $D\text{-He}^3$ interaction observed at 90° in laboratory coordinates. This plot is to be compared with Figure 26, the range distribution of short tracks from the $D\text{-T}$ interaction. Single dural windows were used in the 90° target for both runs. This gave a reduction in the total air equivalent between the reaction volume and the photographic plate, the total being 5.5 cm air. The bombarding energy for this run was 10.4 Mev. It may be noted that straggling is greatly increased for these exposures, due to the reduced particle energy. It is pertinent that the number of tracks in the range 0-4 microns is probably too small since the detection efficiency of photographic plates for tracks of this length is rather low. For this reason it seems likely that the distribution of tracks observed on these two runs represents the tail of the peak of elastically scattered deuterons. This reasoning is further borne out by the fact that the ratio of the low energy peak to the long range proton peak is 1:3; whereas one would expect the cross-section for $D\text{-He}^3$ scattering to be as large, and probably larger by a factor of at least ten, than the $\text{He}^3(d,p)\text{He}^4$ reaction cross-section.

If a group of low energy protons is produced from the $\text{He}^3(d,p)\text{He}^4$ reaction at the present bombarding energy, it should be observable as an irregularity in the $D\text{-He}^3$ range distribution



curve as compared with the D-T range distribution curve. No irregularity is observed. If, however, a proton group were present having a range of 20 microns and a magnitude one third as great as that of the observed number of scattered deuterons, it would have been detected. Such a group would correspond to a proton energy of 2.2 Mev and an excited level in the He^4 nucleus of 20.9 Mev. It therefore seems reasonable to conclude from these data that the formation of a residual excited He^4 nucleus from the $\text{He}^3(d,p)\text{He}^4$ reaction for a level of excitation up to 20.9 Mev. does not occur with a cross-section as great as $\frac{1}{9}$ of the cross-section for the primary $\text{He}^3(d,p)\text{He}^4$ reaction at 90° laboratory coordinates. This upper limit for the cross-section thus is about 0.2 millibarns unit solid angle (cm and lab) at 90° Lab (102.7 $^\circ$ cm).

Figures 27 and 28 show the range distributions of short tracks from the D- He^3 and D-T interactions, respectively, at an angle of observation of 45° , laboratory coordinates. At this angle the air equivalence of the 0.005 inch dural wall is 31.5 cm and the bombarding energy was 10.2 Mev. Again no significant difference in the range distributions is apparent. The ratio of the number of tracks in the low energy peak to those in the high energy proton peak is about 10:1 for this analysis. The slight asymmetry of the curve indicates that the entire peak of elastically scattered deuterons is not included in Figures 27



and 28. The low counting efficiency for particles of very low range would again explain this feature.

From these results one can say with reasonable certainty that a proton group at 45 microns having a magnitude $\frac{1}{3}$ as great as that of the elastically scattered deuteron peak would have been detected. This range infers a low energy proton group at 5.6 Mev, and an excited level in He^4 at 20.3 Mev.

Hence, we conclude that the cross-section for the production of an excited He^4 nucleus in the $\text{He}^3(d,p)\text{He}^4$ reaction at 45° lab (53.6° cm) is less than three times that of the cross-section for the primary reaction for an excitation energy of 20.3 Mev. or less. This cross-section would be less than 11.5 millibarns/unit solid angle in the center of mass system.

For a low energy group at 60 microns residual range it appears likely that a peak of magnitude one tenth of that of the scattered deuteron peak would have been detected. This group would have had an initial energy of 5.7 Mev. and would indicate the existence of an excited state in He^4 at 20.2 Mev. It follows that the cross-section for the excitation of the He^4 nucleus to a level of energy less than 20.2 Mev. at an angle of observation of 45° lab (53.6° cm) is not greater than the cross-section for the primary reaction, 3.84 millibarns/unit solid angle in the center of mass system.

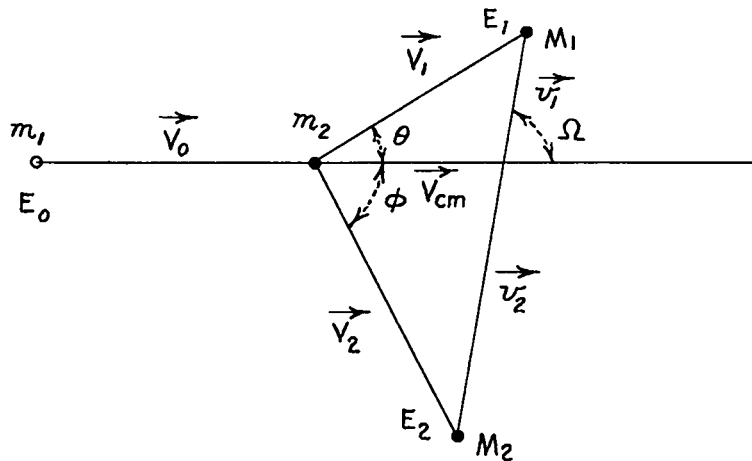
The estimated probable error in the energy values of the upper limits of an excited state in He^4 is $\pm 2\%$, based on the possible fluctuations of beam energy and errors of measurement of the beam energy, as well as possible variation of the thickness of the various target windows.

Finally, it should be noted that the evidence presented here is not conclusive in one respect; namely, that selection rules may prevent the reaction from proceeding in such a way as to leave an excited He^4 nucleus for this reaction, while allowing such an excited state to be observed in other reactions. There is also the possibility that the excited level lies above the threshold of detection for this experiment. For this reason it would be desirable to repeat the experiment using a monoergic source of deuterons of energy of the order of 15 Mev, so that a higher detection threshold could be obtained.

APPENDIX I

COLLISION MECHANICS OF NUCLEAR REACTIONS*

Let a particle of mass m_1 , velocity v_0 , and energy E_0 be incident on a particle of mass m_2 , stationary in the laboratory system. A reaction may occur, having associated with it an energy Q . Q is taken positive if the reaction is exoergic. Subsequently two particles M_1 and M_2 emerge at angles θ and ϕ , with velocities V_1 and V_2 and energies E_1 and E_2 , respectively, in the laboratory system. The situation is shown below:



* The notation of this section is that of B. Carlson, M. Goldstein, L. Rosen, and D. Sweeney, LA-723, January, 1949.

If a reaction occurs, mass is not conserved. The change in total mass is so slight, however, that we may neglect it for these calculations, and take

$$m_1 + m_2 = M_1 + M_2$$

For the comparison of differential cross sections observed at different bombarding energies (E_0), it is convenient to transform to a common system of coordinates in which the center of mass of the system of particles is at rest.

Since the momentum of the system before collision is the same in center of mass coordinates and in laboratory coordinates we have

$$m_1 \vec{v}_0 = (m_1 + m_2) \vec{v}_{cm} \tag{1}$$

$$\vec{v}_{cm} = \frac{m_1}{m_1 + m_2} \vec{v}_0$$

Hence m_2 must have the velocity $-\vec{v}_{cm}$ and m_1 the velocity $\vec{v}_0 - \vec{v}_{cm}$ in the center of mass system. In the center of mass system the principles of conservation of momentum and energy lead to the following:

$$M_1 \vec{v}_1 + M_2 \vec{v}_2 = 0 \tag{2}$$

$$\begin{aligned}
 \frac{M_1 v_1^2}{2} + \frac{M_2 v_2^2}{2} &= E_0 + Q - \frac{(m_1 + m_2)}{2} \left(\frac{m_1}{m_1 + m_2} v_0 \right)^2 \\
 &= E_0 \left(1 - \frac{m_1}{m_1 + m_2} \right) + Q \quad (2) \\
 &= E_0 \frac{m_2}{m_1 + m_2} + Q
 \end{aligned}$$

Substituting for v_2 from (2) and solving for v_1^2 , we obtain

$$v_1^2 = \frac{2}{M_1} \left(\frac{M_2}{M_1 + M_2} \right) \left(E_0 \frac{m_2}{m_1 + m_2} + Q \right) \quad (3)$$

Applying the law of cosines, we have

$$V_1^2 = v_1^2 + v_{cm}^2 - 2 v_1 v_{cm} \cos(\pi - \Omega) \quad (4)$$

Now setting

$$\begin{aligned}
 E_1 &= \frac{M_1 v_1^2}{2} = \text{energy of } M_1 \text{ in the laboratory system} \\
 E_T &= E_0 + Q
 \end{aligned}$$

And substituting from (1), (2), (3), and (4) to obtain an expression for $\frac{E_1}{E_T}$, we have

$$\begin{aligned} \frac{E_1}{E_T} &= \frac{M_2 m_2}{(M_1 + M_2)^2} \left(1 + \frac{m_1}{m_2} \frac{Q}{E_T} \right) \\ &+ \frac{m_1 M_1}{(M_1 + M_2)^2} \left(1 - \frac{Q}{E_T} \right) \\ &+ \frac{2}{(M_1 + M_2)^2} \sqrt{m_1 M_1 m_2 M_2 \left(1 - \frac{Q}{E_T} \right) \left(1 + \frac{m_1}{m_2} \frac{Q}{E_T} \right)} \cos \Omega \end{aligned} \quad (5)$$

By a similar process, we obtain an expression for $\frac{E_2}{E_T}$, where E_2 is the kinetic energy of M_2 in the laboratory system

$$\begin{aligned} \frac{E_2}{E_T} &= \frac{m_2 M_1}{(M_1 + M_2)^2} \left(1 + \frac{m_1}{m_2} \frac{Q}{E_T} \right) \\ &+ \frac{m_1 M_2}{(M_1 + M_2)^2} \left(1 - \frac{Q}{E_T} \right) \\ &- \frac{2}{(M_1 + M_2)^2} \sqrt{m_1 M_1 m_2 M_2 \left(1 - \frac{Q}{E_T} \right) \left(1 + \frac{m_1}{m_2} \frac{Q}{E_T} \right)} \cos \Omega \end{aligned} \quad (6)$$

These expressions can be greatly simplified by definition of the following parameters:

$$A_1 = \frac{m_1 M_1}{(M_1 + M_2)^2} \left(1 - \frac{Q}{E_T} \right) \quad (7)$$

$$A_2 = \frac{m_1 M_2}{(M_1 + M_2)^2} \left(1 - \frac{Q}{E_T} \right)$$

$$B_1 = \frac{m_2 M_2}{(M_1 + M_2)^2} \left(1 + \frac{m_1}{m_2} \frac{Q}{E_T} \right)$$

$$B_2 = \frac{m_2 M_1}{(M_1 + M_2)^2} \left(1 + \frac{m_1}{m_2} \frac{Q}{E_T} \right)$$

(5) and (6) then become

$$\frac{E_1}{E_T} = A_1 + B_1 + 2\sqrt{A_1 B_1} \cos \Omega \quad (8)$$

$$\frac{E_2}{E_T} = A_2 + B_2 - 2\sqrt{A_2 B_2} \cos \Omega \quad (9)$$

it follows from (3) and (7) that

$$v_1 = \sqrt{\frac{2 E_T B_1}{M_1}} \quad (10)$$

and similarly

$$v_2 = \sqrt{\frac{2 E_T B_2}{M_2}} \quad (11)$$

$$v_{cm} = \sqrt{\frac{2E_T}{M_1}} A_1 = \sqrt{\frac{2E_T}{M_2}} A_2 \quad (12)$$

To obtain relations between Ω , θ , and ϕ we use equations (10), (11), and (12), together with

$$V_1 = \sqrt{\frac{2E_1}{M_1}} \quad (13)$$

$$V_2 = \sqrt{\frac{2E_2}{M_2}} \quad (14)$$

And apply the law of sines to the appropriate triangles.

$$\frac{\sin \theta}{v_1} = \frac{\sin \Omega}{V_1} \quad (15)$$

$$\frac{\sin \phi}{v_2} = \frac{\sin \Omega}{V_2} \quad (16)$$

whence

$$\sin \theta = \sqrt{\frac{E_1}{E_1/E_T}} \sin \Omega \quad (17)$$

$$\sin \phi = \sqrt{\frac{B_2}{E_2/\epsilon_T}} \sin \Omega \quad (18)$$

From (17) and (18)

$$\sin \Omega = \sqrt{\frac{E_1/\epsilon_T}{B_1}} \sin \theta = \sqrt{\frac{E_2/\epsilon_T}{B_2}} \sin \phi \quad (19)$$

$$\sin \theta = \sqrt{\frac{B_1}{B_2} \frac{E_2/\epsilon_T}{E_1/\epsilon_T}} \sin \phi \quad (20)$$

and since $E_T = E_1 + E_2$

$$\sin \theta = \sqrt{\frac{M_2}{M_2} \frac{E_2/\epsilon_T}{(1 - E_2/\epsilon_T)}} \sin \phi \quad (21)$$

$$\sin \theta = \sqrt{\frac{M_2}{M_1} \frac{(1 - E_1/\epsilon_T)}{E_1/\epsilon_T}} \sin \phi \quad (22)$$

In order to eliminate Ω in expressions (8) and (9) for $\frac{E_1}{E_T}$ and $\frac{E_2}{E_T}$, it is necessary to substitute from (17) and (18)

$$\cos \Omega = \sqrt{1 - \frac{B_1}{E_1/E_T} \sin^2 \theta} \quad (23)$$

$$\cos \Omega = \sqrt{1 - \frac{B_2}{E_2/E_T} \sin^2 \phi} \quad (24)$$

in (8) and (9) and solve the resulting quadratic equations in $\frac{E_1}{E_T}$ and $\frac{E_2}{E_T}$.

The results are

$$\frac{E_1}{E_T} = A_1 (\cos \theta \pm \sqrt{\frac{B_1}{A_1} - \sin^2 \theta})^2 \quad (25)$$

$$\frac{E_2}{E_T} = A_2 (\cos \phi \pm \sqrt{\frac{B_2}{A_2} - \sin^2 \phi})^2 \quad (26)$$

Both signs apply when $A_1 > B_1$ in which case these expressions give the energies of the fast and slow components of the reaction particles. For $A_1 \leq B_1$ only the positive sign is applicable.

The relative intensities of the reaction particles in the two coordinate systems are inversely proportional to the corresponding elements of solid angle. That is,

$$\frac{I(\Omega)}{I(\theta)} = \frac{2\pi \sin\theta d\theta}{2\pi \sin\Omega d\Omega} = \frac{\sin\theta d\theta}{\sin\Omega d\Omega}$$

and

$$\frac{I(\Omega)}{I(\phi)} = \frac{\sin\phi d\phi}{\sin\Omega d\Omega}$$

In order to obtain expressions for these ratios we first note from the figure that

$$v_{cm} = V_1 \cos\theta - v_1 \cos\Omega$$

$$v_{cm} = V_2 \cos\phi + v_2 \cos\Omega$$

Using (10), (11), (12), (13), and (14), we have

$$\sqrt{\frac{2E_T}{M_1}} A_1 = \sqrt{\frac{2E_1}{M_1}} \cos \theta - \sqrt{\frac{2E_T}{M_1}} B_1 \cos \Omega \quad (27)$$

AND

$$\sqrt{\frac{2E_T}{M_2}} A_2 = \sqrt{\frac{2E_2}{M_2}} \cos \phi + \sqrt{\frac{2E_T}{M_2}} B_2 \cos \Omega \quad (28)$$

Solving for $\cos \Omega$ in each equation,

$$\cos \Omega = \sqrt{\frac{E_1/E_T}{B_1}} \cos \theta - \sqrt{\frac{A_1}{B_1}} \quad (29)$$

$$\cos \Omega = -\sqrt{\frac{E_2/E_T}{B_2}} \cos \phi + \sqrt{\frac{A_2}{B_2}} \quad (30)$$

Now differentiating (29) with respect to Ω , considering $\frac{E_1}{E_T}$ as a function of Ω ,

$$\begin{aligned}
 -\sin \Omega &= -\sin \theta \frac{d\theta}{d\Omega} \left(\frac{E_1}{E_T}\right)^{\frac{1}{2}} (B_1)^{-\frac{1}{2}} \\
 &+ \frac{1}{2} \left(\frac{E_1}{E_T} B_1\right)^{-\frac{1}{2}} \frac{d E_1/E_T}{d \Omega} \cos \theta
 \end{aligned}$$

From (8)

$$\frac{d E_1/E_T}{d \Omega} = -2\sqrt{A_1 B_1} \sin \Omega$$

Substituting and rearranging terms we have

$$\frac{\sin \theta d\theta}{\sin \Omega d\Omega} = \frac{B_1^{\frac{1}{2}} \left[\left(\frac{E_1}{E_T}\right)^{\frac{1}{2}} - A_1^{\frac{1}{2}} \cos \theta \right]}{E_1/E_T}$$

From (25),

$$\left(\frac{E_1}{E_T}\right)^{\frac{1}{2}} = A_1^{\frac{1}{2}} \left[\cos \theta + \sqrt{\frac{B_1}{A_1} - \sin^2 \theta} \right]$$

and

$$\frac{I(\Omega)}{I(\theta)} = \frac{\sqrt{A_1 B_1} \sqrt{\frac{B_1}{A_1} - \sin^2 \theta}}{E_1/E_T} \quad (31)$$

From (30), (9), and (26), similarly, we obtain

$$\frac{I(\Omega)}{I(\phi)} = \frac{\sqrt{A_2 B_2} \sqrt{\frac{B_2}{A_2} - \sin^2 \phi}}{E_2/E_T} \quad (32)$$

In the investigation of the excited state of He^4 , it was convenient to have an expression for the energy of the excited state in terms of the bombarding energy, the Q of the primary reaction, and the energy at which low energy protons could be detected. This expression was derived from

$$\frac{E_2}{E_T} = A_2 \left(\cos \phi + \sqrt{\frac{B_2}{A_2} - \sin^2 \phi} \right)^2 \quad (26)$$

By means of the substitutions

$$Q^* = Q - E^*$$

$$E_T = E_0 + Q^*$$

Where E^* is the energy of a detectable excited state.

The expressions are:

For $\phi = 90^\circ$

- 133 -

$$E^* = Q - \frac{5E_2 - 2E_0}{4}$$

For $\phi = 45^\circ$

$$E^* = Q - \frac{5E_2 - 2E_0 - 2\sqrt{E_2 E_0}}{4}$$

APPENDIX II

DERIVATION OF CRITCHFIELD FORMULA

The following computation of the quantity I, defined in Chapter II, is due to Dr. C. L. Critchfield, Professor of Physics at the University of Minnesota and Consultant to the University of California, Los Alamos Scientific Laboratory.

As shown in Chapter II

$$d^2 I = \frac{w dx dy \sin \phi}{R^2}$$

where w is the width of a swath lengthwise down the plate and the other quantities are as shown on Figure 29.

It is convenient to transform to coordinates in the planes of the slits for the integration, since these coordinates have independent limits. Let these coordinates, ξ and η , be the distance from the axis of the slits at which R passes the first and second slits, as shown on Figure 29.

Then the following relations hold:

$$\begin{aligned} \sin(\phi - \alpha) &= \frac{\xi - \eta}{\sqrt{R^2 + (\xi - \eta)^2}} ; \cos(\phi - \alpha) = \frac{R}{\sqrt{R^2 + (\xi - \eta)^2}} \\ \sin \phi &= \sin [(\phi - \alpha) + \alpha] \\ &= \frac{(\xi - \eta) \cos \alpha + R \sin \alpha}{\sqrt{R^2 + (\xi - \eta)^2}} \end{aligned}$$

$$\frac{R}{L - y \cos \theta - x \cos \alpha} = \frac{\sqrt{l^2 + (\xi - \eta)^2}}{l}$$

$$\frac{y \sin \theta - \xi}{n - y \cos \theta} = \frac{\xi - \eta}{l} = \frac{x \sin \alpha + \eta}{m - x \cos \alpha}$$

whence

$$y = \frac{n(\xi - \eta) + l\xi}{l \sin \theta + (\xi - \eta) \cos \theta}; \quad x = \frac{m(\xi - \eta) - l\eta}{l \sin \alpha + (\xi - \eta) \cos \alpha}$$

$$\frac{\partial y}{\partial \xi} = \frac{n + l - y \cos \theta}{l \sin \theta + (\xi - \eta) \cos \theta} \quad \frac{\partial x}{\partial \xi} = \frac{m - x \cos \alpha}{l \sin \alpha + (\xi - \eta) \cos \alpha}$$

$$\frac{\partial y}{\partial \eta} = \frac{-n + y \cos \theta}{l \sin \theta + (\xi - \eta) \cos \theta} \quad \frac{\partial x}{\partial \eta} = \frac{-(m + l) + x \cos \alpha}{l \sin \alpha + (\xi - \eta) \cos \alpha}$$

$$\frac{\partial(x, y)}{\partial(\xi, \eta)} = \frac{\begin{vmatrix} n + l - y \cos \theta & m - x \cos \alpha \\ -n + y \cos \theta & -(m + l) + x \cos \alpha \end{vmatrix}}{[l \sin \theta + (\xi - \eta) \cos \theta][l \sin \alpha + (\xi - \eta) \cos \alpha]}$$

$$\frac{\partial(x, y)}{\partial(\xi, \eta)} = \frac{-l[L - y \cos \theta - x \cos \alpha]}{[l \sin \theta + (\xi - \eta) \cos \theta][l \sin \alpha + (\xi - \eta) \cos \alpha]}$$

substituting

$$\begin{aligned} d^2 I &= \frac{w \sin \phi}{R^2} \left| \frac{\partial(x, y)}{\partial(\xi, \eta)} \right| d\xi d\eta \\ &= \frac{w l^3 [(\xi - \eta) \cos \alpha + l \sin \alpha]}{[l^2 + (\xi - \eta)^2]^{3/2} [L - y \cos \theta - x \cos \alpha]} \\ &\quad \cdot \frac{d\xi d\eta}{[l \sin \theta + (\xi - \eta) \cos \theta][l \sin \alpha + (\xi - \eta) \cos \alpha]} \end{aligned}$$

Let the denominator be $[l^2 + (\xi - \eta)^2]^{\frac{3}{2}}$ X, and substitute in X for x and y; then

$$X = L \sin \theta \sin \alpha \left(l + (\xi - \eta) \cot \alpha + \frac{m(\xi - \eta) - \eta l}{L} [\cot \theta - \cot \alpha] \right)$$

and

$$d^2 I = \frac{w l^2}{L \sin \theta [l^2 + (\xi - \eta)^2]^{\frac{3}{2}}} \cdot \frac{[l + (\xi - \eta) \cot \alpha] d\xi d\eta}{\left\{ l + (\xi - \eta) \cot \alpha + \frac{m(\xi - \eta) - \eta l}{L} [\cot \theta - \cot \alpha] \right\}}$$

now set

$$P = \frac{m [\cot \alpha - \cot \theta]}{L} \quad Q = \frac{(m + l) [\cot \alpha - \cot \theta]}{L}$$

and divide numerator and denominator by l^3 , to obtain

$$d^2 I = \frac{w d\xi d\eta}{L l \sin \theta \left[1 + \left(\frac{\xi - \eta}{l} \right)^2 \right]^{\frac{3}{2}}} \cdot \frac{1}{1 - \frac{P\xi - Q\eta}{l + (\xi - \eta) \cot \alpha}}$$

expanding,

$$d^2 I = \frac{w d\xi d\eta}{L l \sin \theta} \left\{ \left[1 - \frac{\xi - \eta}{l} + \frac{(\xi - \eta)^2}{2l^2} + \dots \right] \left[1 + \frac{P\xi - Q\eta}{l + (\xi - \eta) \cot \alpha} + \left(\frac{P\xi - Q\eta}{l + (\xi - \eta) \cot \alpha} \right)^2 + \dots \right] \right\}$$

$$d^2I = \frac{w d \xi d \eta}{L l \sin \theta} \left\{ \left[1 - \frac{3}{2} \left(\frac{\xi - \eta}{l} \right)^2 + \dots \right] \left[1 + \left(\frac{P \xi - Q \eta}{l} \right) \left(1 - \frac{\xi - \eta}{l} \cot \alpha + \dots \right) \right. \right. \\ \left. \left. + \left(\frac{P \xi - Q \eta}{l} \right)^2 \left(1 - 2 \frac{\xi - \eta}{l} \cot \alpha + \dots \right) \right] \right\}$$

Retaining only second order terms in ξ and η

$$d^2I = \frac{w d \xi d \eta}{L l \sin \theta} \left\{ 1 - \frac{3}{2} \left(\frac{\xi - \eta}{l} \right)^2 + \frac{P \xi - Q \eta}{l + (\xi - \eta) \cot \alpha} + \left(\frac{P \xi - Q \eta}{l} \right)^2 \right\}$$

$$d^2I = \frac{w d \xi d \eta}{L l \sin \theta} \left\{ 1 - \frac{3}{2} \left(\frac{\xi - \eta}{l} \right)^2 + \frac{P \xi - Q \eta}{l} - \frac{(P \xi - Q \eta)(\xi - \eta) \cot \alpha}{l} \right. \\ \left. + \left(\frac{P \xi - Q \eta}{l} \right)^2 \right\}$$

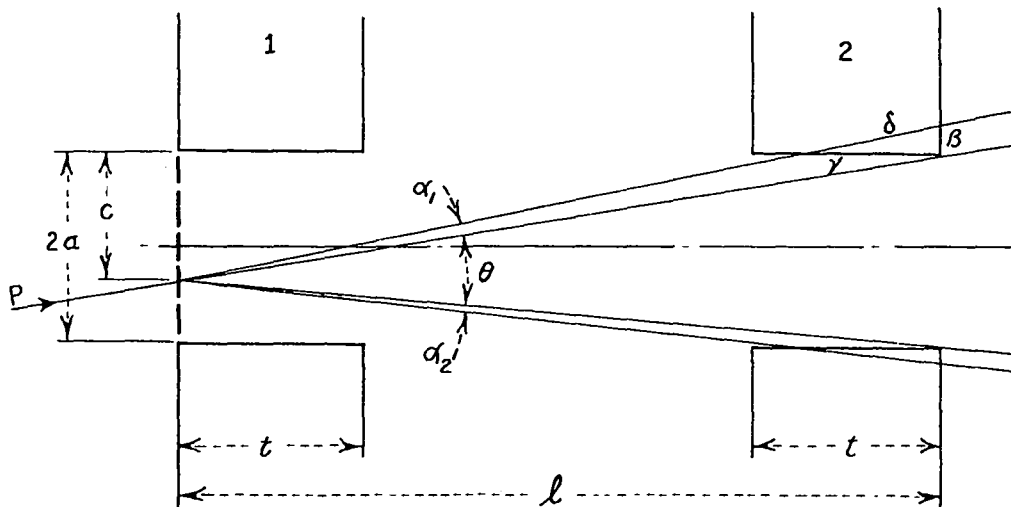
Integrating ξ from $-a$ to $+a$ and η from $-b$ to $+b$,

$$I = \frac{4abw}{L l \sin \theta} \left\{ 1 - \frac{a^2 + b^2}{2l^2} - \frac{Pa^2 + Qb^2}{3l^2} \cot \alpha + \frac{P^2 a^2 + Q^2 b^2}{3l^2} \right\}$$

APPENDIX III

CORRECTION FOR SLIT PENETRATION

Consider two slits, axially aligned, of material having a stopping power K relative to air. Let their half-width be a and their separation be l , as shown.



We wish to compute the number of particles in a beam collimated by the slits which penetrate the slit edges relative to the total number of particles in the beam. Let the source of particles be a line source in a plane perpendicular to the lengths of the slits, as was the case in the experiment described there. The problem reduces to a simple one in probability, for we have the following alternatives:

- A. A particle may miss both slits completely.

- B. A particle may miss the first slit edge and penetrate the second, or vice versa.
- C. A particle, traveling diagonally, may penetrate both slit edges to some extent.

Let the range of the particle in air be X , and the thickness t of the slits be such that $X < Kt$, i.e., the particle cannot penetrate a slit directly.

Now consider P , the path of A particle which misses one edge of Slit 1 by a distance C . Since its direction is random, it may either penetrate the edge of Slit 2, strike Slit 2 so that it is stopped, or miss Slit 2 completely. If it is stopped, it is of no further interest. To compute the relative probabilities of penetration and passage without penetration, we have merely to calculate the angles which permit the occurrence of these processes.

From the Figure we have

$$\frac{c + \beta}{l} = \frac{\beta}{r}$$

Whence, if $\beta \ll c$

$$r = \frac{\beta l}{c}$$

Particles may penetrate the slit for $K\delta < X$

where δ is given by

$$\delta = (\beta^2 + r^2)^{\frac{1}{2}} = \beta \left(1 + \frac{l^2}{(c + \beta)^2} \right)^{\frac{1}{2}}$$

or, if $c + \beta \ll l$

$$S = \frac{\beta l}{c + \beta}$$

The maximum value of S is $S_0 = \frac{x}{\kappa}$,

corresponding to the greatest permissible value of α .

Substituting, we have

$$\beta_0 = \frac{c x}{\kappa l - x}$$

and

$$\alpha_1 = \frac{\beta}{l} = \frac{c x}{l(\kappa l - x)}$$

For particles which penetrate the opposite edge of Slit 2, a similar procedure gives

$$\alpha_2 = \frac{(2a - c) x}{l(\kappa l - x)}$$

Now the angle through which the particles may pass without slit penetration is clearly

$$\theta = \frac{2a}{l}$$

The ratio of particles which penetrate one edge of Slit 2 to the total number (penetrations + free passages) is thus

$$\begin{aligned} R &= \frac{\alpha_1 + \alpha_2}{\alpha_1 + \alpha_2 + \theta} \\ &= \frac{\frac{2ax}{l(\kappa l - x)}}{\frac{2ax}{l(\kappa l - x)} + \frac{2a}{l}} \\ &= \frac{x}{\kappa l} \end{aligned}$$

Since this process can occur in the reciprocal manner, i.e., penetration of the edge of Slit 1 and free passage through Slit 2, the correction to be applied is

$$\Delta = 2R = \frac{2X}{kL}$$

From the foregoing it is clear that Process C, the penetration of both slit edges, is of second order compared to Δ .

In this derivation we have assumed

$$\beta \ll c$$

and

$$c + \beta \ll L, \text{ which assumptions should}$$

now be investigated.

The greatest value of β is

$$\beta_0 = \frac{cX}{kL - X}$$

For the highest energy protons observed $X \cong 700 \text{ cm.}$
 $k = 4 \cdot 10^3$ for brass, the material of the slits, and
 $L \cong 3 \text{ in.} = 7.5 \text{ cm.}$

Then

$$\frac{\beta_0}{c} = \frac{700}{2.93 \cdot 10^4} \cong 0.024$$

Similarly, for the maximum value of

$$c = 2a = 4.5 \cdot 10^{-2} \text{ in.}, \beta_0 = 1.08 \cdot 10^{-3} \text{ in. AND}$$

$$\frac{c + \beta_0}{L} = 0.015$$

Since the total slit penetration correction is only 4.7% for the highest energy particles observed, and since only the fraction $\frac{X_e - 1800}{X_e}$ of this correction is applied to the results (See Chapter VI) it is clear that the errors introduced by the above assumptions are negligible, i.e., the order of 0.02%.

APPENDIX IV

FABRICATION OF MULTIPLATE CAMERA

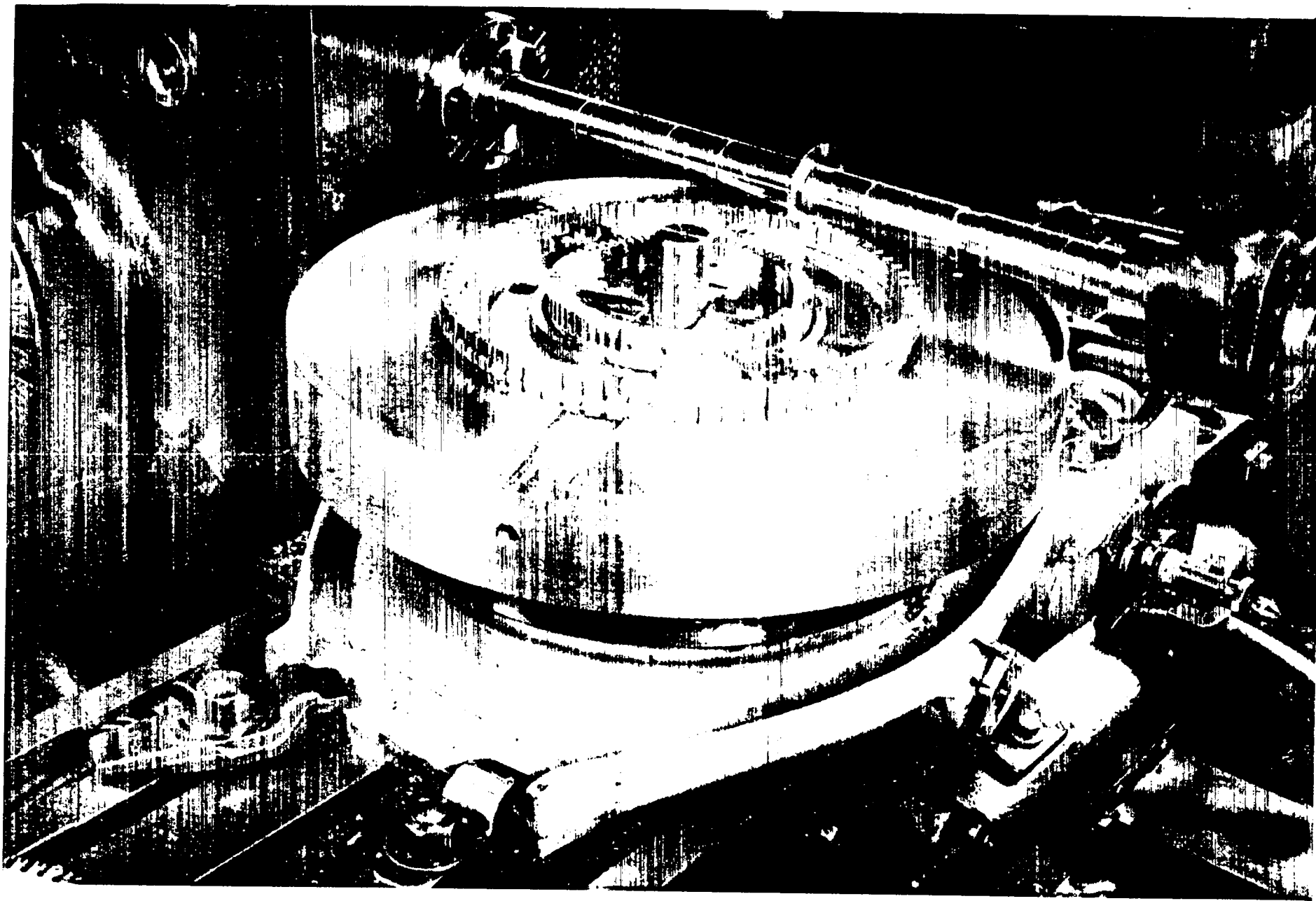
Previously it has been stated that the results obtained with the multiplate camera are accurate essentially within the statistics of the counting of each plate exposed. Some justification of these remarks is needed, since the statement depends on the accuracy and care with which the camera was constructed.

In anticipation of the construction of the camera, a new rotary dividing table for use with the various machines was acquired. According to machine checks, this dividing table was capable of angular measurement within an accuracy of 10 seconds of arc. No play was detectable in the mechanism of the dividing table, either before or after its use.

A steel jig, machined to the dimensions of the bottom of the camera, was used to locate the slit systems and outer ring of the camera body during the machining operations in which angular measurements were required. The slit rings themselves were located in angular position on the jig through the use of dowel holes and toolmaker's dowels, identical positioning being provided in the camera body itself.

The reaction beam defining slits were cut with a rotary saw on a milling machine, as shown in Figure 30. The saw was measured before and after this operation and found to

Figure 30
Cutting of Slits of Multiplate Camera



be 0.0450 inch wide for both measurements. In order to insure that the slits were not wedge shaped, due to wobbling of the saw, the mill table was raised and lowered during the cutting of each slit. The slits were measured with a feeler gauge which was checked accurately with a micrometer to be 0.0450 inch. This dimension was a tight slip fit in the slits. Had there been more than 0.0002 inch clearance of the feeler gauge in the slits, it is believed that this fact would have been detected. Therefore, for the determination of an absolute cross section the slit widths are taken as $0.0450 \begin{matrix} + 0.0002 \\ - 0.0000 \end{matrix}$ inch. It is important to note however, that the method by which the slits were cut insures a very high probability that they are of uniform size. For this reason it is felt that the variation in slit width which might cause errors in the relative values of cross section determined over the entire angular region available is less than 0.1% and therefore negligible compared to the statistical accuracy ordinarily obtained.

The middle ring of anti-scattering slits was cut in an identical manner with a larger saw (0.051 inch wide). After assembly of the camera the alignment of the slit systems was checked by insertion of a parallel bar of the same width as the reaction beam defining slits into the two slits. No interference of the anti-scattering slits was detected, and, in fact, clearance on either side of the parallel was

observable.

The centers of the slit systems and the location of the primary beam collimating tube were determined through the use of the same dowels which located the slit rings. These measurements are estimated to be accurate within 0.0005 inch.

Boring of the ports for the passage of the deuteron beam was the final operation in the fabrication. This was done with the slit rings in place in the camera, so that the receiving holes for the beam collimating tube in each slit ring would be concentric.

Most of the machining operations on the multiplate camera were done by Mr. R. W. Kania, under the supervision of Mr. H. C. Brockman, V Shop Foreman for the Los Alamos Laboratory. Their very valuable work is deeply appreciated, since it is obvious that this entire experiment would have been practically impossible without this fine piece of apparatus.

BIBLIOGRAPHY

- Baker, C. P., M. G. Holloway, L. D. P. King, and R. E. Schreiber, "The Cross Section for the Reaction $20(230,240)10$ " LAMS-2 (1943)(declassified).
- Bethe, H. A. and R. F. Bacher, "Nuclear Physics. A. Stationary States of Nuclei", Rev. Mod. Phys. 8, 147 (1936).
- Coon, J. H. and R. A. Nobles, "Disintegration of He^3 and N^{14} by Thermal Neutrons", Phys. Rev. 75, 1358 (1949).
- Crane, H. R., L. A. Delsasso, W. A. Fowler, and C. C. Lauritsen, "Gamma-Rays from Nitrogen Bombarded with Deuterons", Phys. Rev. 48, 100 (1935).
- Crane, H. R., L. A. Delsasso, W. A. Fowler, and C. C. Lauritsen, "Cloud Chamber Studies of the Gamma-Radiation from Lithium Bombarded with Protons", Phys. Rev. 48, 125 (1935).
- Curran, S. C., J. Angus, and A. L. Cockcroft, "The Beta-Spectrum of Tritium", Phys. Rev. 76, 853 (1949).
- Curtis, B. R., J. L. Fowler, and L. Rosen, "Instrumentation for Nuclear Studies with Externally Focused Deuteron Beam from Ten-Mev Cyclotron", Rev. Sci. Inst. 20, 388 (1949).
- Erickson, K. W., J. L. Fowler, and E. J. Stovall, Jr., "Cross Section as a Function of Angle for the $\text{D}(d,n)\text{He}^3$ Reaction for Ten-Mev Bombarding Deuterons", Phys. Rev. 76, 1141 (1949).
- Feenberg, E., "Does the Alpha-Particle Possess Excited States?", Phys. Rev. 49, 328 (1936).
- Goldstein, L., "On the Two Inverse Reactions $\text{H}^3(p,n)\text{He}^3$ and $\text{He}^3(n,p)\text{H}^3$ ", Declassified Los Alamos Report LADC-539 (December, 1947).
- Hatton, J. and G. Preston, "Long-Range Protons from the $\text{He}^3(d,p)$ Reaction", Nature 164, 143 (1949).
- King, L. D. P. and L. Goldstein, "The Total Cross Section of the He^3 Nucleus for Slow Neutrons", Phys. Rev. 75, 1366 (1949).
- Kinoshita, S., "The Photographic Action of the Alpha-Particles Emitted from Radioactive Substances", Proc. Roy. Soc. 83A, 432 (1910).

- Lattes, C. M. G., D. H. Fowler, and P. Cser, "Range-Energy Relation for Protons and Alpha-Particles in the New Ilford 'Nuclear Research' Emulsions", Nature 159, 301 (1947).
- Newton, A. S., J. C. Warf, F. H. Spedding, O. Johnson, I. B. Johns, R. W. Nottorf, J. Y. Ayers, R. W. Fisher, and A. Kant, "Uranium Hydride II", Nucleonics 4, No. 2, 17 (Feb. 1949).
- Powell, C. F., A. N. May, J. Chadwick, and T. G. Pickavance, "Excited States of Stable Nuclei", Nature 145, 893 (1940).
- Powell, C. F. and G. P. S. Occhialini, Nuclear Physics in Photographs, Oxford: The Clarendon Press, 1947.
- Reinganum, M., "Streuung und Photographische Wirkung der -Strahlen", Physik. Zeits. 12, 1076 (1911).
- Rosen, L., F. K. Tallmadge, and J. H. Williams, "Range Distribution of the Charged Particles from the D-D Reactions for Ten-Mev Deuterons: Differential Elastic Scattering Cross Section at 40 Degrees, 60 Degrees, and 80 Degrees in the Center of Mass System", Phys. Rev. 76, 1283 1949.
- Shapiro, M. M., "Tracks of Nuclear Particles in Photographic Emulsions", Rev. Mod. Phys. 13, 58 (1941).
- Spedding, F. H., A. S. Newton, J. C. Warf, O. Johnson, R. W. Nottorf, I. B. Johns, and A. H. Doane, "Uranium Hydride I", Nucleonics 4, No. 1, 4 (January 1949).
- Sydoriak, S. G., E. R. Grilly, and E. F. Hammel, "Condensation of Pure He³ and Its Vapor Pressures between 1.2° and Its Critical Point", Phys. Rev. 75, 303 (1949).
- Webb, J. H., "Photographic Plates for Use in Nuclear Physics", Phys. Rev. 74, 511 (1948).
- Wilkins, T. R., "The Response of Photographic Materials to Atomic Particles", J. App. Phys. 11, 35 (1940).

DOCUMENT ROOM

REC. FROM Eng-1

DATE 3-21-50

REC. NO. REC. _____